# DENGUE VIRUS AND WEST NILE VIRUS PROTEASE INHIBITORS

A Dissertation by

Sridhar Aravapalli

Master of Science, Osmania University, India, 1998

Submitted to the Department of Chemistry
and the faculty of the Graduate School of
Wichita State University
in partial fulfillment of
the requirements for the degree of
Doctor of Philosophy

May 2013

**DENGUE VIRUS AND WEST NILE VIRUS PROTEASE INHIBITORS**

The following faculty members have examined the final copy of this thesis for form and content, and recommend that it be accepted in partial fulfillment of the requirement for the degree of Doctor of Philosophy with a major in Chemistry.

_____
William C. Groutas, Committee Chair

_____
Erach R. Talaty, Committee Member

_____
James G. Bann, Committee Member

_____
Douglas S. English, Committee Member

_____
Lop-Hing Ho, Committee Member

Accepted for the College of Liberal Arts and Sciences

_____

Ron Matson, Interim Dean

Accepted for the Graduate School

_____

Abu Masud, Interim Dean

## DEDICATION

To my parents, all of my family members,
near and dear friends

## ACKNOWLEDGEMENTS

I would like to express my sincere gratitude to my advisor, Dr. William C. Groutas, for his invaluable guidance, unparalleled training, motivation, and support throughout my graduate studies and research at Wichita State University.

I would also like to thank my committee members, Dr. Erach R. Talaty, Dr. James G. Bann, Dr. Douglas S. English, Dr. Lop-Hing Ho for their advice and support during my graduate studies.

I am thankful to Dr. R. Padmanabhan and his research group at Georgetown University Medical Center for performing biochemical studies on Dengue virus and West Nile virus inhibitors. I would also like to thank Dr. Gerald H. Lushington at University of Kansas for his help with computational studies. I am grateful to Dr. Dengfeng Dou, Guijia He, and Yi Li for their help, guidance, and support especially during my early days of graduate studies. I also like to acknowledge our research group members, Sivakoteswara Rao Mandadapu, Kok Chuan Tiew, Mallikarjuna Reddy Gunnam, Pathum Weerawarna, Anushka Chathuranga, and Roxanne Adeline Z. Uy, and in particular Dr. Kevin R. Alliston for their help.

Foremost, I am greatly indebted to my wonderful parents, all of my other family members for their love, care, wishes, and support and special thanks goes to my brother for the inspiration, and insightful guidance and advice. Without them my dream of pursing doctoral studies would not have come true.

I am also grateful to all of my near and dear friends for their support and help.

## ABSTRACT

Dengue virus and West Nile virus are important mosquito-borne pathogens of *Flaviviridae* family affecting millions of people worldwide and causing a severe global health care threat. However, currently there are no approved effective antiviral drugs or vaccines available for the treatment of virus infection. This thesis describes the design, synthesis and discovery of two novel classes of reversible competitive inhibitors of Dengue Virus and West Nile Virus NS2B/NS3 protease. Structure-activity relationship studies have led to the identification of a low micromolar hit, which will be used in a hit-to-lead campaign to generate lead compounds that display superior ADMET and PK characteristics.

## TABLE OF CONTENTS

**Chapter** **Page**

## TABLE OF CONTENTS (continued)

**Chapter** **Page**

## LIST OF FIGURES

**Figure** **Page**

## LIST OF FIGURES (continued)

**Figure** **Page**

## LIST OF FIGURES (continued)

**Figure** **Page**

## LIST OF TABLES

## LIST OF SCHEMES

**Scheme** **Page**

## LIST OF ABBREVATIONS

| | |
|---|---|
| Arg | Arginine |
| Asp | Aspartic acid |
| Bz | Benzoyl |
| C | Capsid |
| CDC | Center for Disease Control |
| $CDCl_3$ | Deuterated chloroform |
| CDI | Carbonyldiimidazole |
| $CF_3CH_2OH$ | Trifluoroethanol |
| CHAPS | 3-[(3-cholamidopropyl)dimethylammonio]-1-propanesulfonate |
| $CuSO_4.5H_2O$ | Copper(II) sulfate pentahydrate |
| DENV | Dengue Virus |
| DHF | Dengue Hemorrhagic Fever |
| DMSO | Dimethyl Sulfoxide |
| dsRNA | Double Stranded Ribonucleic Acid |
| DSS | Dengue Shock Syndrome |
| E | Envelope |
| EtOAc | Ethyl Acetate |
| His | His |
| HCl | Hydrochloric Acid |
| $H_2O$ | Water |
| Lys | Lys |
| MeOH | Methanol |
| $NaN_3$ | Sodium azide |

## LIST OF ABBREVATIONS (continued)

| | |
|---|---|
| $NaHCO_3$ | Sodium bicarbonate |
| NaOH | Sodium Hydroxide |
| NMR | Nuclear Magnetic Resonance |
| NS | Non-structural protein |
| prM | Membrane Precursor |
| Ser | Ser |
| ssRNA | Single Stranded Ribonucleic Acid |
| t-butyl | Tertiary butyl |
| TFA | Trifluoroacetic acid |
| THF | Tetrahydrofuran |
| TLC | Thin Layer Chromatography |
| WHO | World Health Organization |
| WNV | West Nile Virus |

# Chapter 1

# INTRODUCTION

## 1.1 Significance

Dengue virus (DENV) and West Nile virus (WNV) have emerged as important mosquito-borne viral pathogens affecting humans [1]. According to the World Health Organization, approximately 2.5 billion people worldwide, *i.e.,* 40% of the world's population, is at risk of Dengue infection, predominantly in tropical and subtropical regions [2, 3]. An estimated 50 million infections occur annually, with about 5 million clinical hospitalizations of severe dengue and 22,000 fatalities, primarily in children [2, 3]. Since its first occurrence in Africa, it was spread to Southeast Asia, the Pacific, and the Americas (Figure 1.1) [2]. Dengue virus has been endemic in more than 100 countries and today it is considered to be the most important mosquito-borne pathogen affecting humans next to malaria [4, 5]. The recent emergence of DENV with several infections in Texas, Hawaii, and most recently in Florida shows the growing threat of disease in the United States [6]. The global spread of DENV is thought to be due to increased urbanization, population growth, climate change, lack of effective vector control, migration, and increased international travel [7].

The closely related WNV was also originated in Africa and is endemic in parts of Africa, Middle East, Europe, Asia and Australia [8]. It caused a sporadic outbreak in New York in 1999, since then it was spread rapidly to the North-American continent, Central-America, and finally to South America [8, 9]. Since 1999, the United States

Center for Disease Control (CDC) has reported over 20,000 infections in humans and more than 1000 fatalities, and in the year 2003 the infections peaked with 9862 human cases and 264 deaths [8, 10]. The most recent outbreak of WNV in the United States with 5,128 cases and 229 deaths in the year 2012 alone is the highest number of human infections reported since 2003 [11]. WNV infection also caused significant mortality in horses, wild and domestic birds [8]. In view of the recent outbreak, and growing reemergence of WNV, and increase in the epidemics of DENV in North America, the United States National Institutes of Health has raised concerns that these infections represent a potential threat to the United States [4].


**Figure 1.1. Geographic distribution of Dengue [12].**

## 1.2 Incidence

The incidence of Dengue infection has been increasing significantly over the past 50 years and at an especially alarming rate in the last two decades (Figure 1.2) [13]. The number of cases reported to WHO and the countries affected for the period 2004-2007 alone are almost double the number for the period 1990-1999 [14]. In 2002, 1 million cases are reported in the Americas alone [3]. The high incidence rate and disease severity of dengue is posing a threat to global health care and causing a severe economic burden especially in tropics, for example $ 2 billion annually just from eight countries [6].

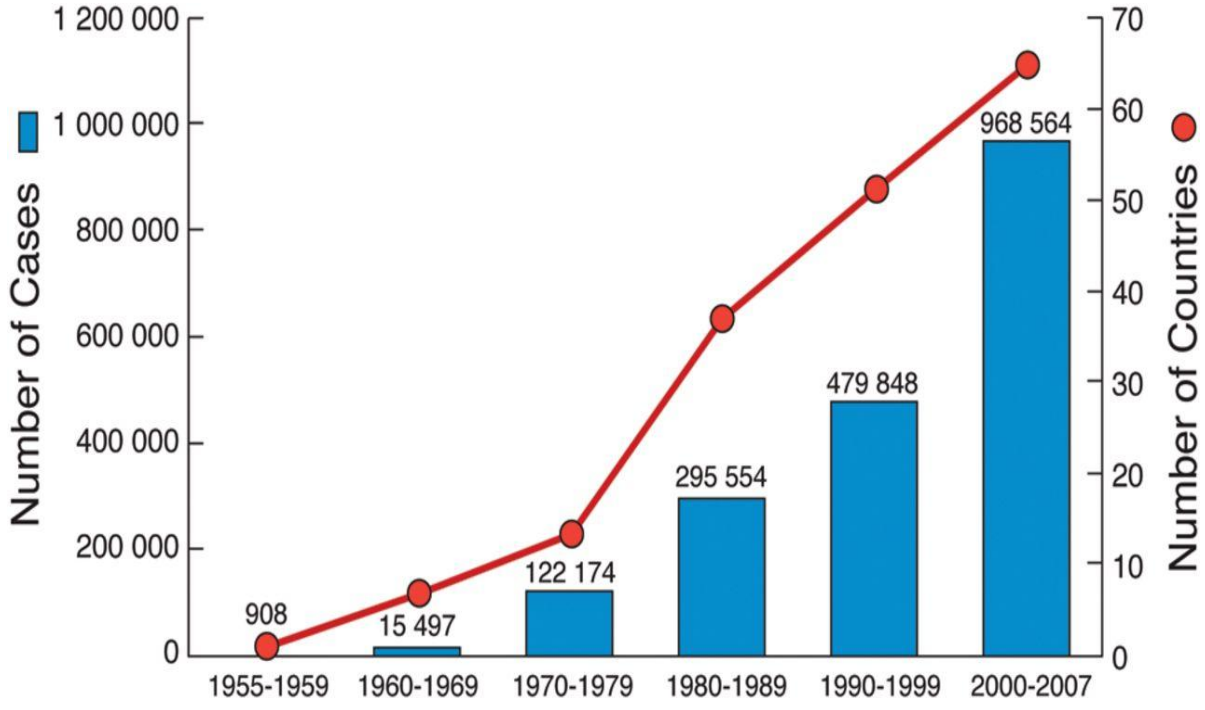


**Figure 1.2. The rising incidence of dengue [14].**

## 1.3 Disease

DENV infection in humans causes mild dengue fever (DF). The symptoms are typically flu-like such as high fever, chills, retro-ocular pain, nausea, severe headache, typical rash, myalgia, and arthralgia ("break-bone fever") [4, 7]. About 3-6% of Dengue infections progress to more severe and life-threatening dengue hemorrhagic fever (DHF) and dengue shock syndrome (DSS) [15]. The disease includes plasma leakage in different serous cavities, including pleural, pericardial, and peritoneal cavities, characterized by petechiae, hemoconcentration, and hypoproteinemia [5]. This can lead to shock and death if not treated appropriately.

WNV infections in humans are mainly asymptomatic [8, 16]. Twenty percent of infections develop mild febrile illness, associated with headache, chills, diaphoresis and lymphadenopathy [17]. This can lead to severe fever known as 'West Nile Fever' [8, 17]. Five percent of the symptomatic infections further develop neuroinvasive diseases such as meningitis and encephalitis, and poliomyelitis-like disease [8]. Around 10% of neuroinvasive disease cases are fatal and the survivors are likely to suffer from long-term cognitive and neurological complications [16].

## 1.4 Transmission

DENV transmission cycle consists of human-mosquito-human [18]. DENV is transmitted to humans by the bite of mosquito vector of the species *Aedes aegypti*, while the other vectors, *Aedes albopictus* and *Aedes polynesiensis* were also reported in the recent outbreaks [18, 19]. The *Aedes aegypti* is an urban habitat and breeds mainly in artificial containers. It is a day time feeder with peak biting periods is early

mornings and evenings. The anticoagulant present in the saliva of mosquito prevents the host's blood clotting. Once introduced, the virus enters an incubation stage of 3-14 days; thereafter a person would experience mild febrile illness which may go from 2-10 days. During this period the viruses circulate in the peripheral blood. If the mosquito bites this viremic person, it becomes infected and subsequently transmits to another uninfected human host after an extrinsic incubation period of approximately 10 days [18]. WNV is transmitted by Culex mosquitoes from avian reservoir to humans, horses, and other vertebrate hosts [8, 17].

### 1.5 Treatment

Currently there is no effective licensed vaccine or antiviral therapy available for the treatment or prevention of DENV/WNV infection [8, 13, 20]. At present the treatment is only supportive care [2, 8]. The management of DF involves the use of antipyretics such as paracetamol (acetaminophen) and the DHF involves the maintenance of the body fluid [2, 13].

### 1.6 Characteristics

DENV/WNV belong to the *Flavivirus* genus of the *Flaviviridae* family, which also includes *Hepacivirus*, and *Pestivirus* genera [1, 19]. The family *Flaviviridae* has around 70 viruses, which are mainly transmitted by mosquito or ticks [1]. The note-worthy members that are responsible for significant morbidity and mortality in humans and animals include Yellow Fever Virus (YFV), Hepatitis C Virus (HCV), Japanese encephalitis (JEV), Tick-borne encephalitis (TEBV), St Louis Encephalitis (SLE), and

Murray Valley Encephalitis (MVE) [1, 19]. DENV exists in four different antigenically distinct serotypes (DENV 1-4), with each serotype shares around 65% of the genome and causes similar syndromes in humans. Infection with one serotype does not provide immunity against others but rather enhances the likelihood of developing life-threatening DHF or DHS upon infection with another serotype by mechanism such as antibody-mediated enhancement (ADE) [7, 19]. Only one serotype exists for WNV.

## 1.7 Virion and Genome

DENV/WNV virions are icosahedral particles of ~50 nM diameter [3]. The virion is comprised of a nucleocapsid made of viral genomic RNA and capsid protein C, enveloped by a lipid bilayer formed by envelope and membrane proteins (Figure 1.3) [4, 5, 21]. The DENV/WNV virus genome (Figure 1.4) consists of single–stranded positive–sense RNA which is approximately 11 kb in length, that has a single open reading frame flanked by 5' – and 3' –untranslated regions (UTRs) that are essential for transcription, replication and virion assembly [4, 5, 21]. The UTRs have type 1 cap on its 5' end, but the 3' end lacks poly-A tail [4, 21].

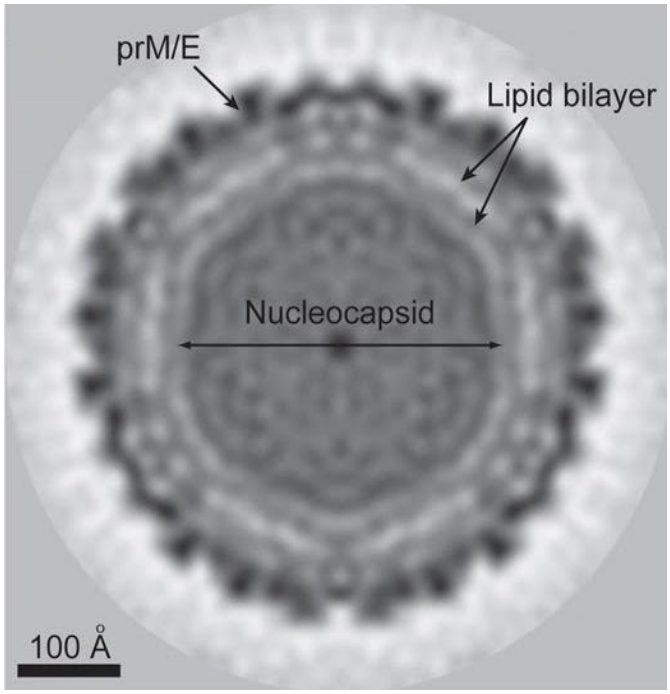


**Figure 1.3. Virion [22].**

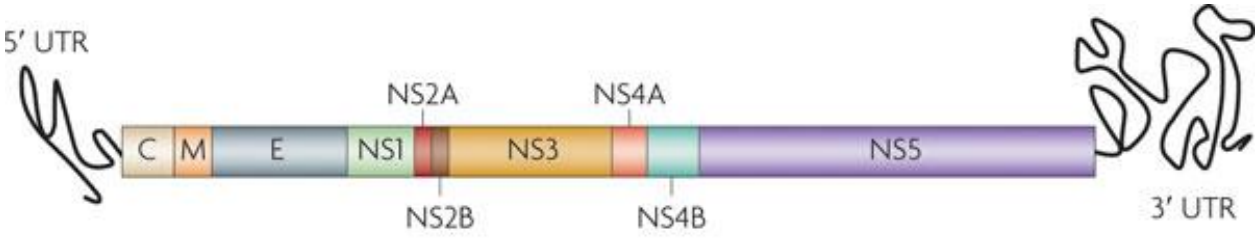


**Figure 1.4. Flavivirus Genome [3].**

The viral genome encodes three structural proteins – the capsid (C), pre-membrane (prM), and envelope (E), at the 5' end and seven non-structural proteins (NS1, NS2A, NS2B, NS3, NS4A, NS4B, and NS5) at the 3' end [4, 5, 21]. The genome

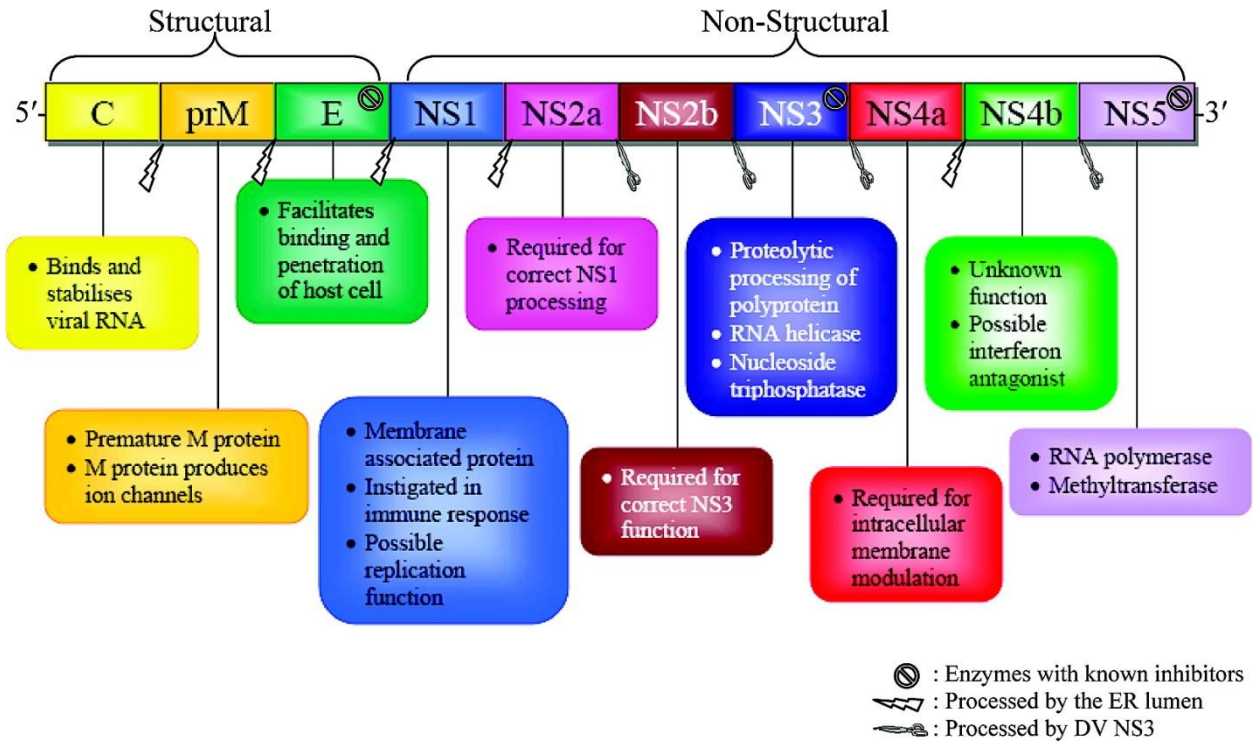


**Figure 1.5. Viral Polyprotein [23].**

is directly translated into a single polyprotein (Figure 1.5) that is co- and post-translationally processed by host and viral proteases to produce the 10 individual functional proteins [21]. The structural proteins are involved in the viral particle

formation and the non-structural proteins take part in the replication and expression, assembly, release, and evasion of immune response [4, 5, 21].

## 1.8 Life Cycle

### 1.8.1 Receptor Binding, Viral Entry, Fusion

The first step in the life cycle (Figure 1.6) involves the attachment of virus to the host cell surface through the interaction of the E protein domain III with the receptor [16, 24, 25, 26]. The primary receptors for DENV are DC-SIGN (dendritic-cell-specific ICAM-grabbing non-integrin), GRP78/BiP (glucose-regulating protein 78), and CD14-associated molecules [25]. The virion enters the host cell by receptor-mediated endocytosis *via* clathrin coated pits [27]. Following viral entry into the cell, the pH changes taking place in the endosome induce an irreversible trimerization of the E glycoproteins leading to the fusion between the viral and endosomal membranes, thereby releasing the nucleocapsid into the cytoplasm, where it dissociates into the capsid protein and RNA [24, 25, 26, 27].

### 1.8.2 Replication

The viral RNA genome in *Flaviviruses* acts as a mRNA and is directly translated into a single polyprotein [26]. The viral induced membranous structures and the rough endoplasmic reticulum (RER) form continuous structures known as convoluted membranes/paracrystalline arrays (CM/PC), where the polyprotein processing is believed to take place [24, 27].

The polyprotein is cleaved co- and post-translationally by host and viral proteases [21]. The host signal peptidase present in the ER cleaves at C–prM, prM–E, E–NS1 and NS4A–NS4B junctions and cleavage at the NS1-NS2A takes place by an unknown

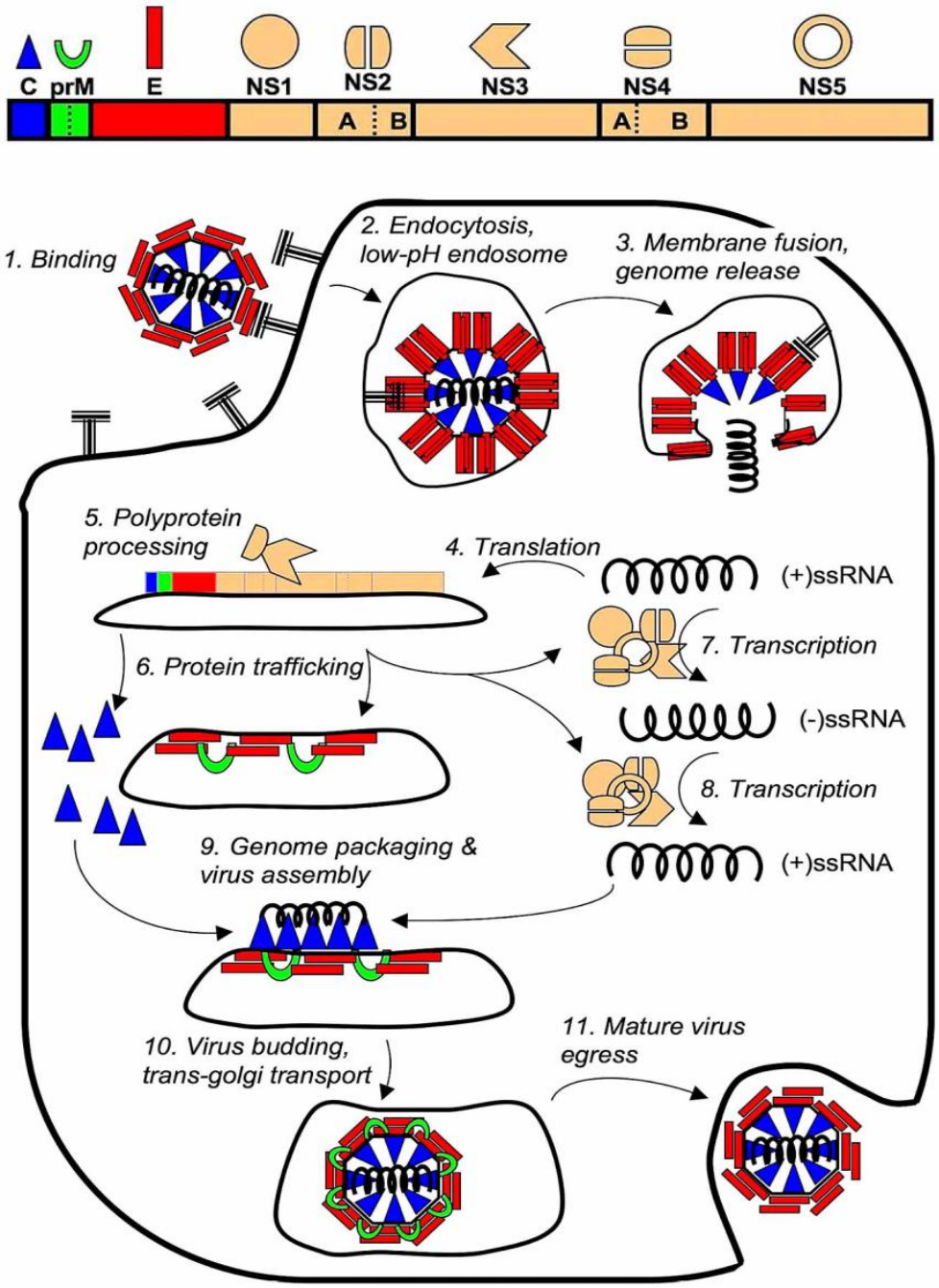


**Figure 1.6. Viral Life Cycle [4].**

protease of the ER [4, 5]. The viral serine protease (NS2B/NS3pro) performs the cleavages at NS2A–NS2B, NS2B–NS3, NS3–NS4A and NS4B–NS5 junctions and also cleaves internal sites within C, NS2A, NS3, and NS4A [4, 5, 24]. Viral replication takes place in the RER and in the Golgi-derived membranes called vesicle packets (VP) [24]. Viral replication is catalyzed by a replication complex comprised of NS5, NS3, NS1, NS2A, NS4A and NS4B, which transcribes the (+)-strand viral genomic RNA into a complementary (-)-strand RNA, which is then copied back into (+)-strand [21]. Thus a transient dsRNA intermediate is formed and then separates into individual strands for further rounds of replication [26]. The newly synthesized viral RNA extrudes into the intermembrane space of the double-membrane VPs, from which it exits into the cytoplasm by an unknown mechanism [24].

### 1.8.3 Assembly, Maturation, and Release

After replication, the viral RNA particles are coated with capsid protein in the lumen of the rough ER, which is the first step in the virion assembly [24]. The nucleocapsid is then enveloped by lipid bilayer (formed by hetero-dimeric complex of prM and E proteins) as it buds into the lumen of the rough ER to form a non-infectious immature virus particle [21, 24]. These virions undergo maturation in the trans-Golgi network, where the host protease, furin, cleaves the prM protein into mature protein M and the pr segment [24]. The resulting mature, infectious virions are transported to the cell surface by secretory pathway, which are finally exited from the host cell by exocytosis [24, 25].

## 1.9 Viral Proteases as Potential Drug Targets

Viral proteases represent an important pharmaceutical target in the discovery of antiviral therapeutics [28]. The studies from the past 20 years exemplify that viruses encode essential proteases, which are central to many structural and functional processes such as viral entry into the cells, viral replication, processing of large precursor proteins to generate mature active proteins [28, 29]. The catalytic activity of these viral proteases is also needed to produce infectious virions [29]. Knowing the processing site sequence, catalytic mechanism, and substrate binding interactions of the viral proteases, it is possible to envision the development of potent protease inhibitors [29]. The breadth of success of protease inhibitors for HIV-1 infection with nine protease inhibitors currently approved by the FDA and several more in clinical trials has demonstrated that viral proteases are considered to be valid molecular targets for the development of antiviral drugs [28, 29, 30, 31]. This approach has been extended to other pathogenic viruses like HCV, SARS, Cytomegalovirus, T-cell lymphotropic virus, and Picornavirus [29, 30]. There are several protease inhibitors of HCV and HRV currently in clinical trials [29, 30, 32, 33]. The high success of HCV NS3 protease inhibitors not only encouraged others to develop antiviral therapeutics against similar protease (NS2B/NS3pro) for DENV/WNV but has also provided further proof-of-concept that NS2B/NS3pro is a valid, established drug target for the development of protease inhibitors [32, 33]. Hence it is imperative to know the structural details of the enzyme active site, substrate specificity, substrate-binding interactions, and catalytic mechanism in the design, and development of potent inhibitors.

### 1.9.1 NS2B/NS3 protease (NS2B/NS3pro)

NS3 protein is a 69 kDa, 618 amino acid length multi-functional protein with distinct activities [26]. The N-terminal domain (1-185) of NS3 along with NS2B co-factor has a protease activity. The C-terminal domain has NTPase [34], helicase [35], and RTPase (RNA triphosphatase) [36] activities. NTPase/helicase activity is needed for unwinding the double-stranded RNA in viral replication [24]. RTPase activity is required for RNA capping [24]. NS3 protease of DENV and WNV share a significant (41%) amino acid sequence homology, and 65-74% within all four DENV serotypes [37]. Mutational studies have revealed that full length NS3 is required to produce optimal activity of all enzymatic activities [16].

NS2B is an ER-resident integral membrane protein consisting of three hydrophobic domains and a conserved hydrophilic domain [24]. The hydrophobic sequence of NS2B is essential for co-translational insertion of the protease cofactor into ER membranes for efficient cleavage of the NS2B/NS3 junction [24]. The central hydrophilic domain of NS2B spanning 49-95 residues (CF40) fuses with 1-169 amino-acids of NS3 protein *via* a flexible linker ($Gly_4$-Ser-$Gly_4$) to form a proteolytic core [26] , referred to as “NS2B/NS3pro”, [38, 39, 40] which has a trypsin like serine protease activity with a catalytic triad of His51, Asp75, and Ser135. NS2B thus plays a pivotal role in the formation of protease active site in association with NS3 and also provides stability to it. NS2B/NS3pro has been implicated in viral replication and polyprotein processing [16].

### 1.9.2 Structure Perspectives of DENV/WNV NS2B/NS3pro

The X-ray crystal structure of WNV protease has been solved with either peptide-based inhibitors or protein inhibitors or ligand free structures [41, 42] and very recently the X-ray crystal structure of DENV-3 NS2B/NS3pro bound to a peptide inhibitor (Benzoyl-Norleucine-Lys-Arg-Arg-aldehyde) (Figure 1.7) and the serine-protease inhibitor, aprotinin (bovine pancreatic trypsin inhibitor) (Figure 1.8) have been solved [43]. Like in WNV structures [16], it was shown for the first time that the NS2B region in

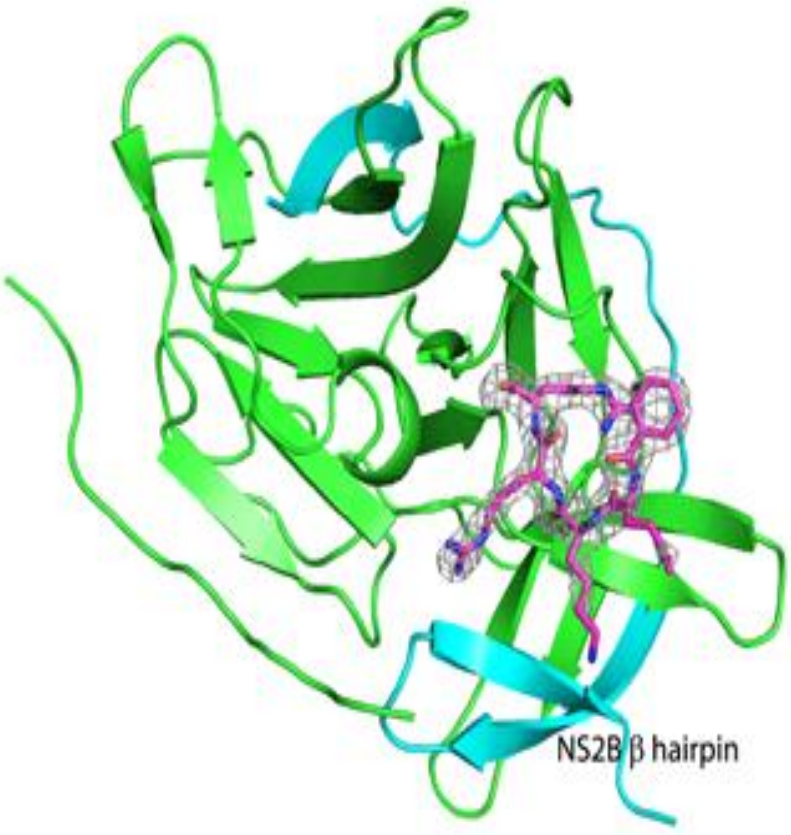


**Figure 1.7. Cartoon representation of the structure of DENV-3 protease bound to Bz-NleLysArgArg-H. NS3 in green, NS2B in blue, Bz-NleLysArgArg-H is shown in stick representation [43].**

DENV also forms an ordered $\beta$ hairpin that wraps around the NS3 core to form an active, closed conformation that is not observed in ligand free structures [43, 44]. This suggests that the $\beta$ hairpin is part of the active site and plays a crucial role in the

**Figure 1.8 Cartoon representation of the structure of DENV-3 protease (NS3 in purple, NS2B in orange) bound to aprotinin (yellow) [43].**

catalytic activity as it directly participates in the substrate binding interactions during proteolysis [43, 44], until then it was not known for certain. The ligand bound crystal structure of an enzyme is extremely important as it provides structural insights for the rational design of enzyme-specific inhibitors.

### 1.9.3 Substrate Specificity and Substrate-binding Interactions

The development of potent and specific enzyme inhibitors necessitates a deeper understanding of solution structure of the **substrate-binding pocket** and the **residues** involved in **substrate binding** [16].

To accomplish proteolysis, a peptide substrate or inhibitor has to be bound within the enzyme active site cleft. Usually an active site (catalytic site) of a protease is comprised of a series of subsites or pockets (Figure 1.9) that interact with a substrate or inhibitor by various non-covalent forces like H-bonds, ion-ion and cation- interactions, van der Waal's, hydrophobic [45]. Amino acid residues to the left of the scissile bond (that is cleaved bond) are numbered P1 (for peptide1), P2, P3, etc., with numbering increasing in the direction of the N-terminal residue of the substrate or inhibitor [45]. Residues to the right of the scissile bond are numbered P1', P2', etc. The corresponding complementary regions of the active site, i.e., subsites/pockets are numbered S1, S2,….and S1', S2', etc. S1 is called the *primary specificity site* and P1 is the primary

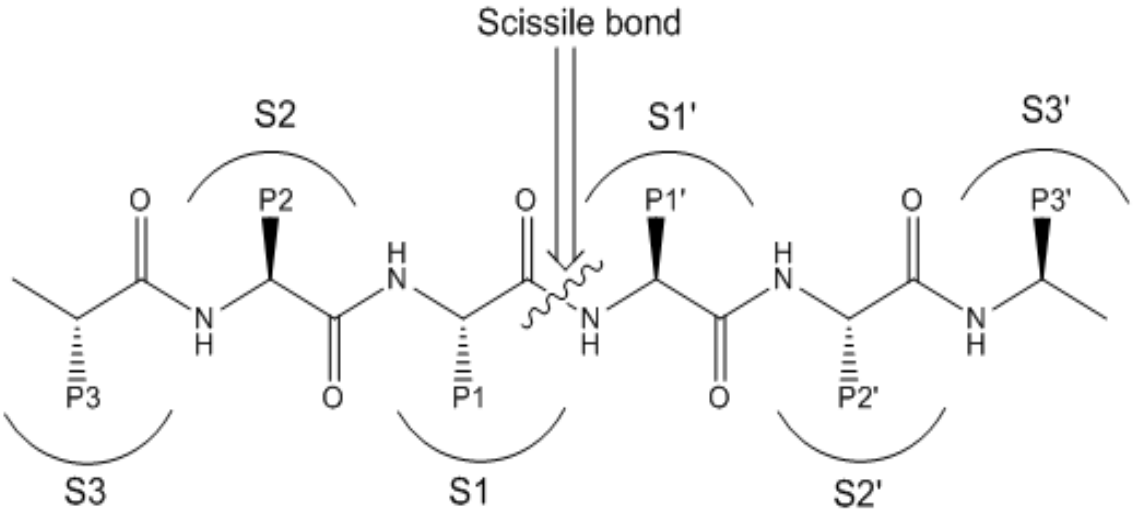


**Figure 1.9 Subsite Nomenclature [45].**

specificity residue [45]. The primary specificity site (S1) shows considerable variation between individual proteases even within the same class. These differences are frequently taken advantage of in the design of specific inhibitors for a target protease.

Peptide profiling of various substrates of DENV and WNV NS2B/NS3 pro revealed the preference for highly conserved dibasic amino acid residues on the N-terminal side and a short chain amino acid on the C-terminal side of their cleavage sites [4, 5, 16, 38, 46]. This unusual specificity is hardly shared by any mammalian proteases (except thrombin) and hence is a potential antiviral drug target to be exploited. DENV pro has a sequence preference for Lys-Arg-Arg, while WNV pro shows a preference for Lys-Lys-Arg at P3, P2, and P1 non-prime subsites respectively [16, 43, 44]. The interactions at the various sites is now well understood by the X-ray crystal structures of DENV-3 bound to the optimal tetrapeptide, Bz-Nle-Lys-Arg-Arg-H (Figure 1.10) [43], and WNV protease Bz-Nle-Lys-Arg-Arg-H complex (Figure 1.11 ) [41].

The S1 residues of the DENV protease involved in binding to the P1 side chain of the substrate are Asp129 of NS3, that forms a charge-charge interaction, and the backbone carbonyl of Phe130 of NS3, forming H bond [43, 44]. The different preference in WNV protease at the P2 residue is due to the shallow pocket formed between Asn84 residue of NS2B and Asn152 residue of NS3, whereas the equivalent residues to Asn84 of NS2B in DENV-3 and DENV-2 proteases are Thr83 and Ser83 respectively [16, 43, 44]. The P2 side chain does not interact with any of the residues of WNV protease [16, 43, 44]. The P2 and P3 residues of DENV-3 protease interact with backbone carbonyls of Gly82 and Met84 of NS2B respectively [43, 44]. The backbone carbonyl of Phe85 and Gln86 of NS2B in WNV protease forms a charge-reinforced hydrogen bond with the

P3 Lys [43, 44]. The P2 and P3 interactions stabilize the β-hairpin of NS2B in a closed conformation [43, 44].

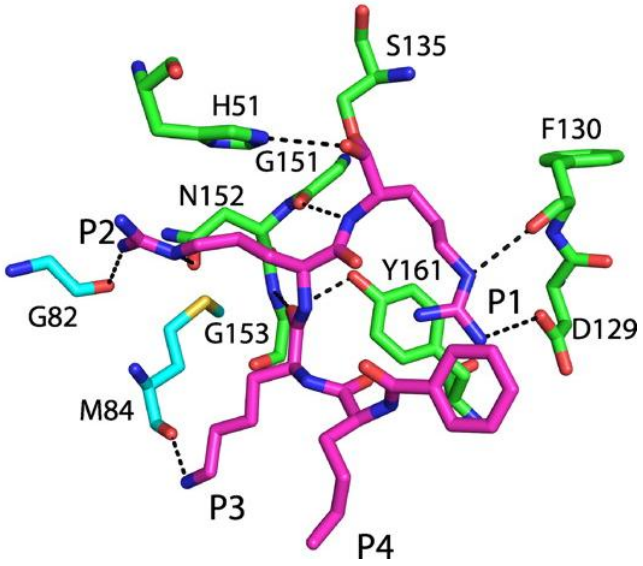


**Figure 1.10. Interactions of Bz-Nle-Lys-Arg-Arg-H with DENV-3 protease. Hydrogen bonds are shown by dashed lines [43].**

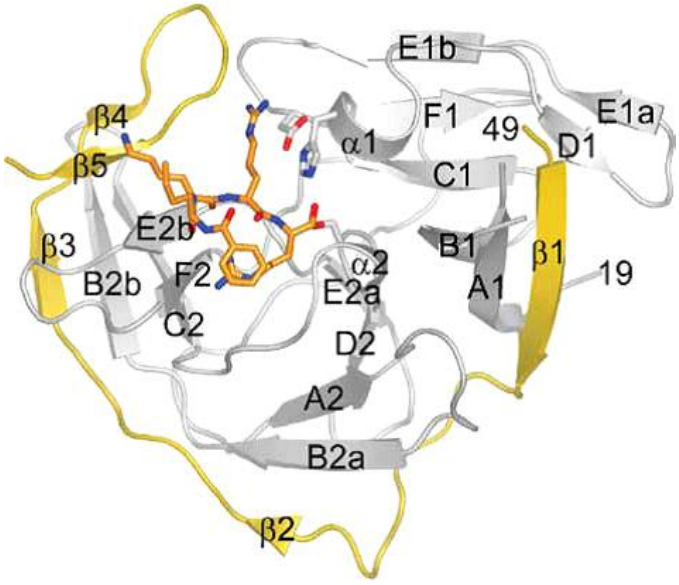


**Figure 1.11. WNV NS2B/NS3pro complexed with Bz-Nle-Lys-Arg-Arg-H (Orange) [41].**

The crystal structures of DENV-3 and WNV proteases bound to aprotinin (58-amino-acid polypeptide) shed more insights about the prime side of the substrate-binding site (Figures 1.12 & 1.13) [42, 43]. DENV protease shows preference for Ser at P1', acidic residue at P2', Ser at P3', and Gly at P4' [43, 44]. However, WNV protease shows a different sequence preference, Gly-Gly at P1'-P2' positions. [16, 42] The difference in the preferences at $S_1$', and $S_2$' pockets correlates with the different amino acid residues present in the helical turn formed between the $S_1$', and $S_2$' pockets in the two viral proteases [43, 44]. WNV protease has Pro and Thr, whereas DENV protease contains Lys and Pro residues at positions 131 and 132 of NS3 [16, 43, 44]. This is further corroborated by mutagenesis studies, where changing the WNV protease side chains to DENV protease sequence changed the P1', and P2' preferences more like that of DENV protease [16, 43, 44].

The other major difference is that, In WNV protease-aprotinin structure, the NS2B $\beta$-hairpin is predominantly bound to NS3, i.e., shows a closed conformation with one H-bond interaction with aprotinin which is also consistent with the NMR data, however the DENV-3 protease-aprotinin complex revealed that the $\beta$ hairpin of NS2B is largely disordered which indicates that interactions are not required for protease inhibition by aprotinin [43, 44]. This may also explain why aprotinin is 10-fold more potent against DENVpro than WNVpro [43, 44].

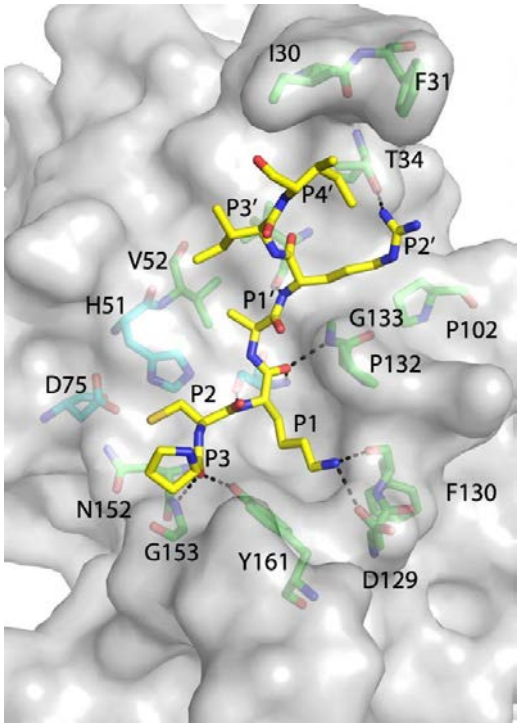


**Figure 1.12. Stereo diagram of the P3'-P4 residues of aprotinin (yellow sticks) showing interactions with DENV-3 protease [43].**

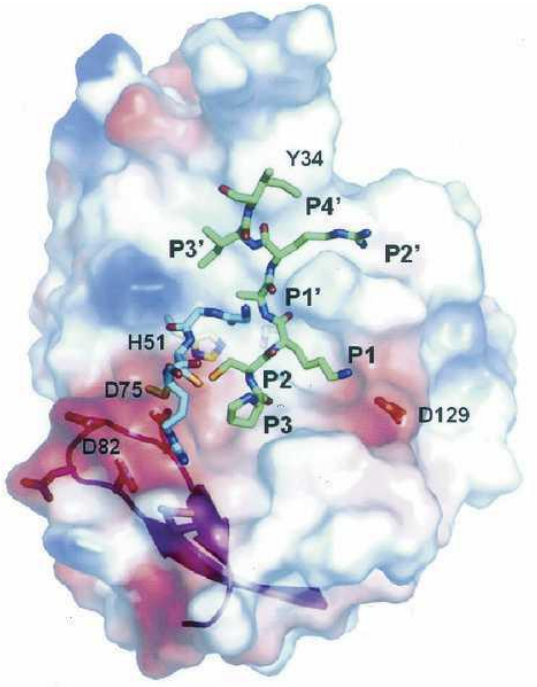


**Figure 1.13 Stereo diagram of WNV NS2B/NS3pro surface with selected aprotinin residues [42].**

### 1.9.4 Mechanism

NS2B/NS3pro is a chymotrypsin-like serine endopeptidase with a catalytic triad of His51, Asp75, and Ser135 [47, 48]. The catalytic mechanism (Figure 1.14) typically involves two processes, acylation and deacylation. Once NS2B/NS3pro binds the substrate to form the Michaelis complex, nucleophilic Ser135 attacks the scissile peptide carbonyl to form a tetrahedral intermediate (covalent catalysis) [47, 48]. The nucleophilic catalysis is augmented by the ideal positioning of Ser135 in space (proximity and orientation effects) and His51 further enhances the nucleophilicity by forming a hydrogen bond between Ser hydroxyl and imidazole (general base catalysis) in the ground state [47, 48]. The formation of imidazolium ion is assisted by the hydrogen bond to carboxylate ion of Asp75 (electrostatic catalysis) [47, 48]. The transient tetrahedral intermediate is stabilized by the hydrogen bonds with the oxyanion and NH groups of Gly133, Ser135 of the back bone of NS3, resulting in the oxyanion hole [47, 48]. In the DENV-3 protease-Bz-nKRR-H structure, a water molecule and a sulfate occupy the oxyanion hole (Figure 1.15) [43]. In the different ligand bound WNV protease structures the oxyanion hole is in either active or inactive conformation [16, 44]. The tetrahedral intermediate expels as an acyl-enzyme intermediate by the proton transfer from N3 of His51 $H^+$ (general acid catalysis) [47, 48]. The amine leaving group is finally released and replaced from the enzyme [47, 48]. The second half of the reaction, deacylation is essentially the reverse of the acylation process which involves the nucleophilic attack of acyl-enzyme by the water [47, 48]. This is assisted by general base catalysis of His51, resulting in second tetrahedral intermediate which collapses to the carboxylic product and regenerating the enzyme [47, 48].

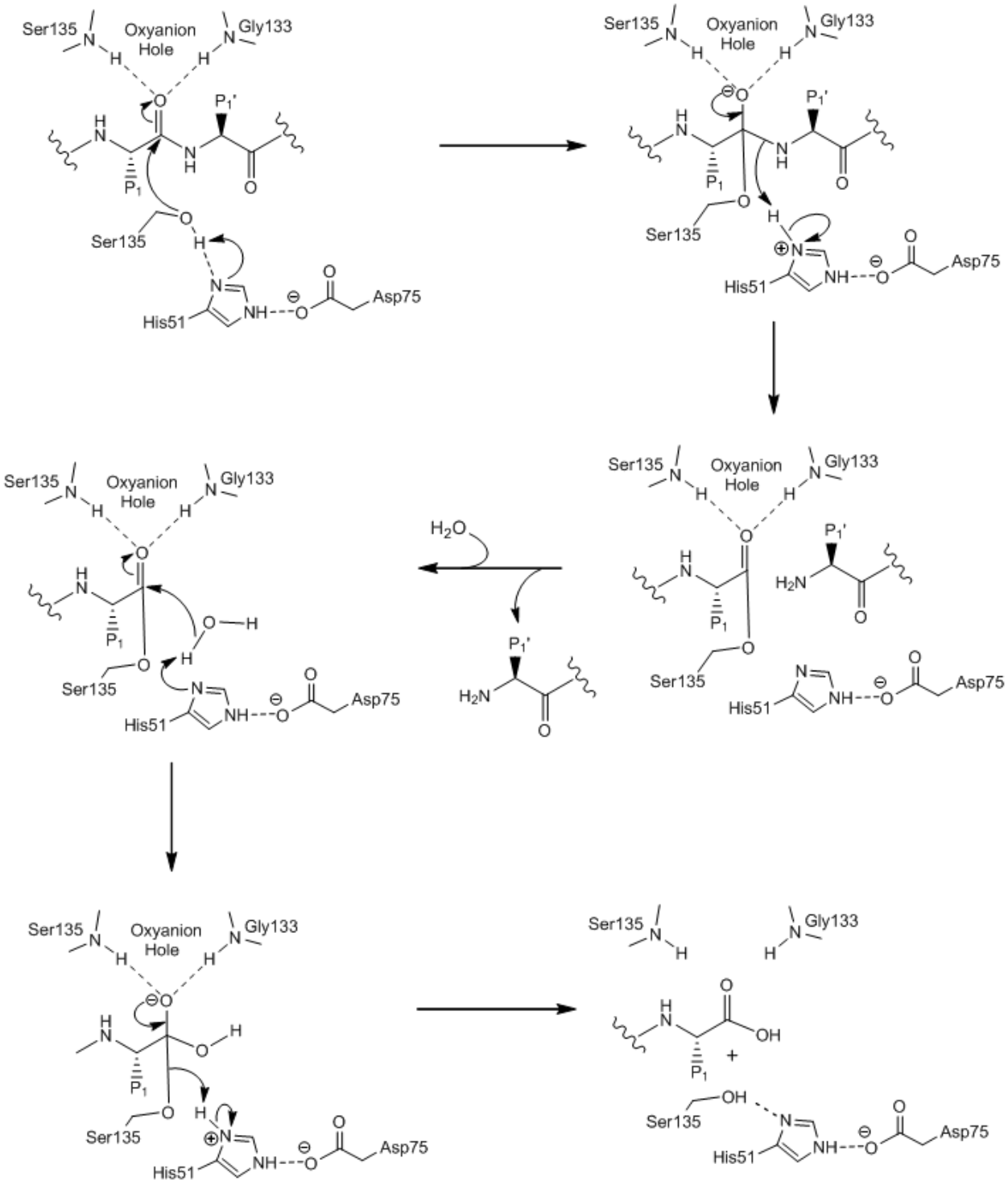


**Figure 1.14. Catalytic mechanism of serine protease [47, 48].**

Overall the catalytic mechanism is called “charge relay system”, this is because the negative charge on the carboxylate of Asp75 induces polarization on other catalytic residues through a web of H-bonds and ultimately leading to oxyanion [47].

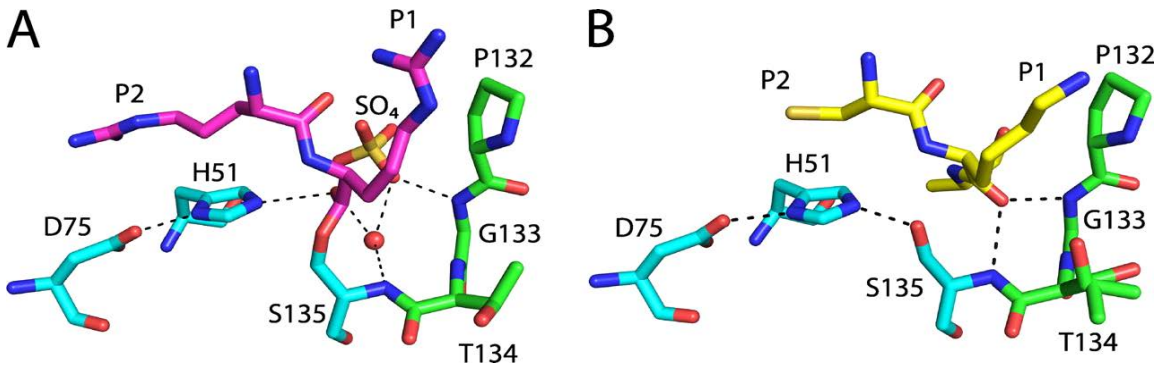


**Figure 1.15 Stereo view of DENV-3 protease structures showing catalytically competent geometry (A) Stick representation of oxyanion hole and catalytic triad (H51, D75, and S135) from the DENV-3 protease-Bz-Nle-Lys-Arg-Arg-H structure (B) Stick representation of oxyanion hole of the DENV-3 protease-aprotinin structure [43].**

### 1.9.5 Development of NS2B/NS3pro Inhibitors

There are many Dengue and West Nile viral proteins that have been targeted for drug discovery, including helicase [49, 50], methyl transferase [51, 52, 53], serine protease [54, 55, 56, 57, 58] and viral RNA [59, 60]. As NS2B/NS3pro plays vital roles in viral replication, and in post-translational proteolytic processing of the viral polyprotein, and maturation, the blockage of NS2B/NS3pro activity provides an effective means for designing DENV and WNV small-molecule therapeutics [43, 61, 62]. Small-molecule inhibitors of DENV2 and WNV proteases are of interest both as therapeutic agents and as chemical probes for investigating biological functions related to virus replication and reproduction [16, 63]. There are two possible strategies employed for inhibiting the NS2B/NS3pro, the first one involves blocking the interactions with its substrate by mimicking the substrate-binding cleft which has been the focus of attention to date, and the second strategy involves preventing the essential association between NS3pro and its cofactor NS2B [16]. Numerous approaches have been used to identify DENV/WNV NS2B/NS3pro inhibitors, including peptidomimetics, structure-based virtual screening, and high throughput sceening (HTS) [64].

#### 1.9.5.1 Substrate based Peptidomimetics

##### 1.9.5.1.1 Warhead peptidomimetics

These inhibitors mimic the natural catalytic substrate and typically are transition state inhibitors which basically have a recognition element (P1 residue) that dictates the binding and optimal spatial positioning of the inhibitor to the active site (substrate

recognition), and their C-terminal carboxyl group is chemically modified into reactive electrophilic 'warheads', which form reversible covalent bonds with the hydroxyl group of the active site serine, resulting in a highly stable enzyme-inhibitor adduct(Figure 1.16) [16, 65].

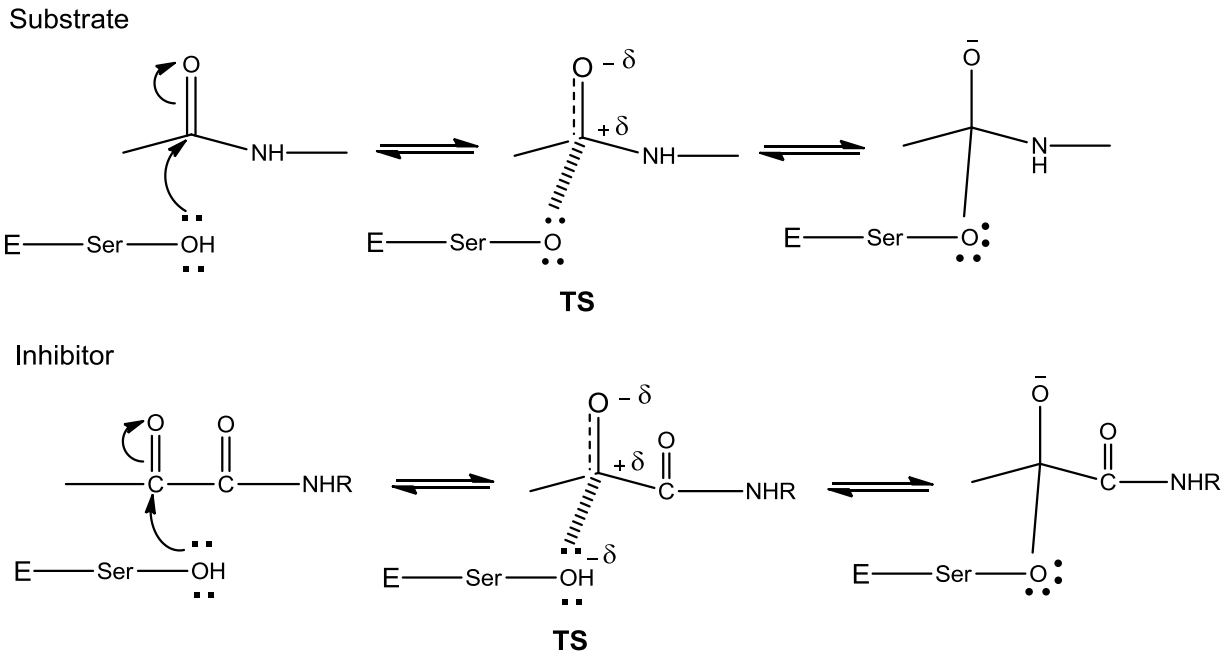


**Figure 1.16 Mechanism of transition state inhibitors**

The most commonly used warheads are aldehydes, α-ketoamides, α-ketoesters, and boronic acids [66, 67, 68, 69]. Examples of potent warhead peptidomimetics of DENV/WNV NS2B/NS3pro inhibitors are shown in the Figure 1.17

### 1.9.5.1.2 Non-covalent peptidomimetics

These peptidomimetics lack electrophilic warheads and do not react covalently with the catalytic serine of the active site but rather employ electrostatic and/or

a) Examples of transition state inhibitors

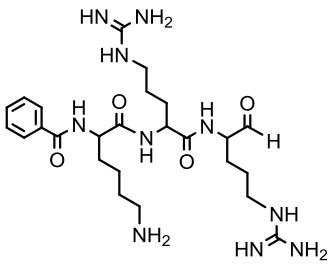

*i*

DENV $K_i$ = 1.5 μM

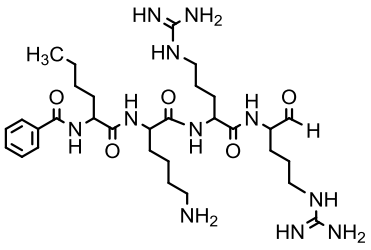

*ii*

DENV $K_i$ = 5.8 μM

WNV $K_i$ = 4.1μM

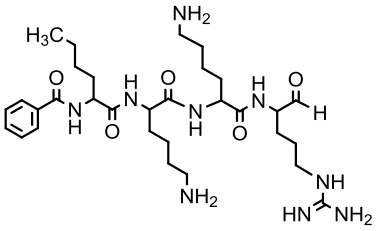

*iii*

DENV $K_i$ = 41 μM

WNV $K_i$ = 1.9 μM

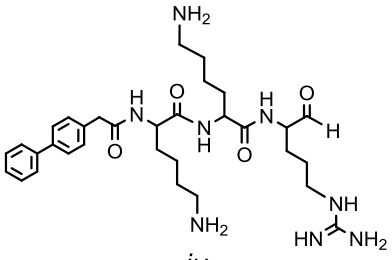

*iv*

WNV $K_i$ = 6 nm

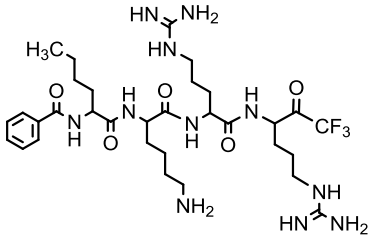

*v*

DENV $K_i$ = 0.85 μM

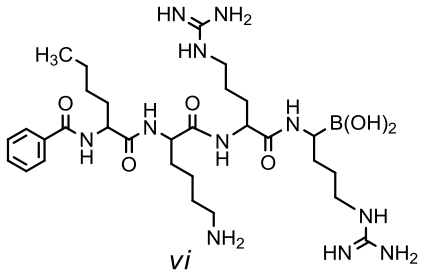

*vi*

DENV $K_i$ = 43 nM

b) Reversible competitive inhibitors

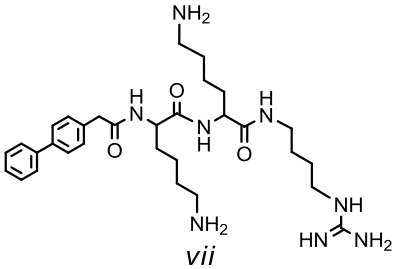

*vii*

WNV $K_i$ = 2.05 μM

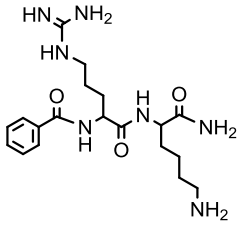

*viii*

DENV $K_i$ = 39.6 μM

WNV $K_i$ = 102 μM

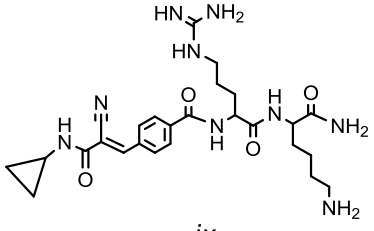

*ix*

DENV $K_i$ = 29 μM

WNV $K_i$ = 26 μM

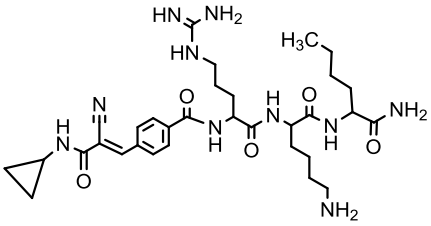

*x*

DENV $K_i$ = 4.9 μM

WNV $K_i$ = 92.5 μM

**Figure 1.17 Peptidomimetics [4, 16, 65, 70]**

hydrophobic interactions to bind at the active site, hence compete with the natural

substrate reversibly, examples of which are shown in the Figure 1.17 [65].

#### 1.9.5.1.3 Retro-peptide inhibitors

These inhibitors have been developed recently in which the N and C-termini are reversed. These inhibitors also lack electrophilic warhead but still inhibit the enzyme with low micromolar potency (Figure 1.17) [70].

#### 1.9.5.1.4 Drawbacks of peptidyl inhibitors

Even though peptidyl inhibitors display low micromolar potency *in vitro*, they are not drug-like candidates because these compounds have poor bioavailability due to the charged nature of side chains, and peptide degradation [16]. Moreover, the warhead peptidomimetics are less likely to be incorporated into drug candidates as the electrophilic warheads react indiscriminately with multiple receptors and organic molecules in the cell leading to less selectivity, cell toxicity, and off-target effects [16]. In addition, the warheads like aldehydes and $\alpha$–ketoamides are able to condense with P1 Arg side chains to form cyclic structures which have to be opened first before they interact with active serine nucleophile [16]. Due to the poor pharmacokinetic profile of these peptidyl inhibitors, these inhibitors lack potential to become antiviral drug candidates.

### 1.9.5.2 Non-covalent non-peptidyl inhibitors

These inhibitors do not react with active serine of the enzyme active site, and also do not mimic the catalytic substrate and yet competitively bind to the active of the

enzyme through various non-covalent forces. Several scaffolds have been explored including, phthalazine-based derivatives [71], arylcyanoacrylamides [72], benz[d]isothiazol-3(2H)-one derivatives [57], anthracene-based compounds [73], quinolone derivatives [56], and aminobenzamide derivatives [58]. These compounds along with others need further optimization in order to be more drug like candidates, as they all have limited potency or less physicochemical features.

#### 1.9.5.3 Challenges in the development of NS2B/NS3pro inhibitors

The main challenges associated with the development of NS2B/NS3pro inhibitors are as follows: First, there is no optimal NS2B/NS3pro *in vitro* assay that reflects the *in vivo* NS2/NS3 protease activity. The optimal NS2B/NS3pro activity requires a basic pH of 9.0 and around 20% glycerol. It seems that this high pH neutralizes the charge on Lys residues in NS2B/NS3pro and thereby enabling the conformational change of the enzyme, which is required for interaction with membrane/substrate [16, 64]. The basic pH in the assay causes protonation of compounds which result in false-positive or false-negative hits. Moreover, the robotic liquid-handling platforms employed in HTS do not tolerate the high content of glycerol since the higher viscosity leads to increased error rate while pipetting from small volumes into numerous well plates [64]. Second, the active site of DENV/WNV NS2B/NS3pro is relatively flat [41] and charged [64], thus making it difficult to design potent inhibitors.

## 1.10 Vaccine development

Even though there has been success for vaccination against other flaviviruses like YFV, JEV, and TBEV, progress towards vaccine development for DENV has been hampered for a multitude of reasons [13]. Firstly, the vaccine should not only provide long-lasting immunity against all the four DENV serotypes but also have to surpass the potential for Antibody-Dependent Enhancement (ADE) [13]. When a person is infected with one DENV serotype, the body produces cross-reactive, non-neutralizing antibodies. When the same individual is infected with a different serotype, these antibodies can recognize and bind to the second infecting virus, but will not neutralize it. The antibody-virus complex formed as a result will be taken up by Fc receptor-bearing cells such as macrophages and monocytes. This will lead to a cascade of events like, increased uptake of virus, increased replication and viral load, eventually leading to increased chances of complications [13, 20]. Therefore, developing monovalent vaccines will be hazardous as they produce antibodies more likely to tackle just one serotype, and the various tetravalent vaccines which are in the different stages of clinical trials must able to produce effective neutralizing antibodies against all four DENV serotypes [13, 20]. However, the development of a tetravalent vaccine is technically and economically demanding task [13, 20].

Secondly, the infection with heterotypic serotype activates the pre-sensitized cross-reactive T and B cells, which triggers the immune cascade and a cytokine storm that is not effective in clearing the newly infecting heterotypic serotype but rather leads to the capillary leakage [13, 20].

Thirdly, there is a lack of an animal model that recapitulates DENV infection in humans. This is a major stumbling block for vaccine development because the results of preclinical trials are not reliable in terms of safety and efficacy [13]. Typical clinical mammalian models like guinea pigs, mice, dogs, and goats, do not manifest the DENV syndrome as seen in DENV infected humans [13]. Many animal studies that have been conducted to date on nonhuman primates like *Macaca mulatta*, *Macaca fasicularis* develop viremia and immune response when inoculated through subcutaneous route, but not elicit the clinical disease [13].

### 1.10.1 Tetravalent vaccines

Despite these issues, a number of approaches have been investigated, such as: live attenuated vaccines, inactivated virus, dengue-dengue and dengue-yellow fever chimeric, subunit vaccines, and DNA vaccines [13, 20]. The various tetravalent vaccines which are in the different phases of clinical trials are listed in the Table 1.1 [20].

Currently, the most advanced tetravalent vaccine is in phase III clinical trials, and was developed by Sanofi Pasteur [20]. This vaccine is a chimeric dengue-yellow fever live vaccine that contains chimeric DENV 1-4 serotypes [20].

**Table 1.1 The various tetravalent vaccines in the clinical trials [20].**

| Developer | Vaccine | Clinical trial |
|---|---|---|
| Sanofi Pasteur | Chimeric live vaccine (yellow fever 17D back-bone) (Chimerivax) | Phase III |
| CDC-Inviragen | Chimeric live vaccine (dengue back-bone) (Chimerivax) | Phase I |
| NIH | Chimeric and specifically engineered live vaccine strains | Phase I |
| Walter Reed Army Institute of Research/GlaxoSmithKline | Conventional live attenuated vaccine | Phase II (on hold) |

## 1.11 **Types of Enzyme Inhibition**

Enzyme inhibition occurs when a molecule different from the substrate binds to the active site of the enzyme and decreases or prevents the enzyme's activity from taking place, and the molecule is termed as inhibitor. Enzyme inhibition can be reversible or irreversible.

### 1.11.1 Reversible Inhibition

Reversible inhibition occurs if the inhibitor (I) is bound to the active site of the enzyme (E) non-covalently, and prevents the substrate from binding to the active site [48, 74]. Reversible inhibitors establish a dynamic equilibrium system with the enzyme. This inhibition shows time-independent kinetics, since the degree of inhibition remains constant over a period of time. Reversible inhibition is mainly of three types, competitive inhibition, uncompetitive inhibition, and noncompetitive inhibition [74].

### 1.11.1.1 Competitive inhibition

In competitive inhibition, the inhibitor (I) binds reversibly to the active site of the free enzyme (E) and competes with the substrate (S) for the same binding site [48, 74]. Competitive inhibitors hence show structural similarity with substrates but differ from being unreactive. This provides a rational approach to structure based-drug design of inhibitors. The kinetic scheme and the kinetic behavior associated with competitive inhibition are shown in the Scheme 1.1 and Figure 1.18 [48, 74].

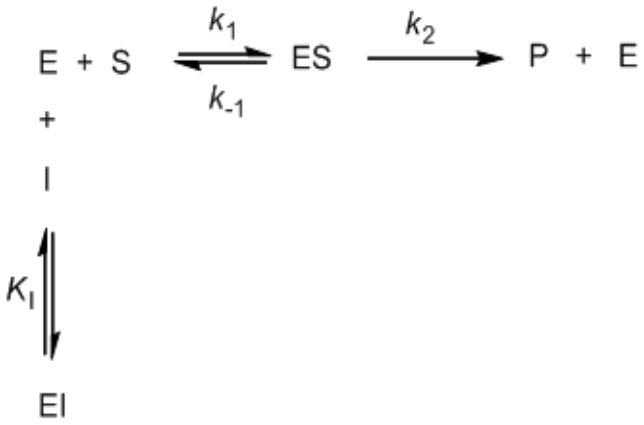


**Scheme 1.1 Kinetic scheme of competitive inhibition**

Assuming the steady state kinetics, the Michaelis-Menten equation (1.3) for the competitive inhibition can be derived [74]. The graphical representation of this equation in the absence and in the presence of various concentrations of an inhibitor gives a hyperbolic plot, which is diagnostic for competitive inhibition [74]. Recasting equation (1.3) yields the Lineweaver-Burk equation (1.4). A Lineweaver-Burk plot (Figure 1.19) of this equation is linear. The intercept ($1/V_{max}$) remains unchanged at various concentrations of I, which is the characteristic for competitive inhibition [74].

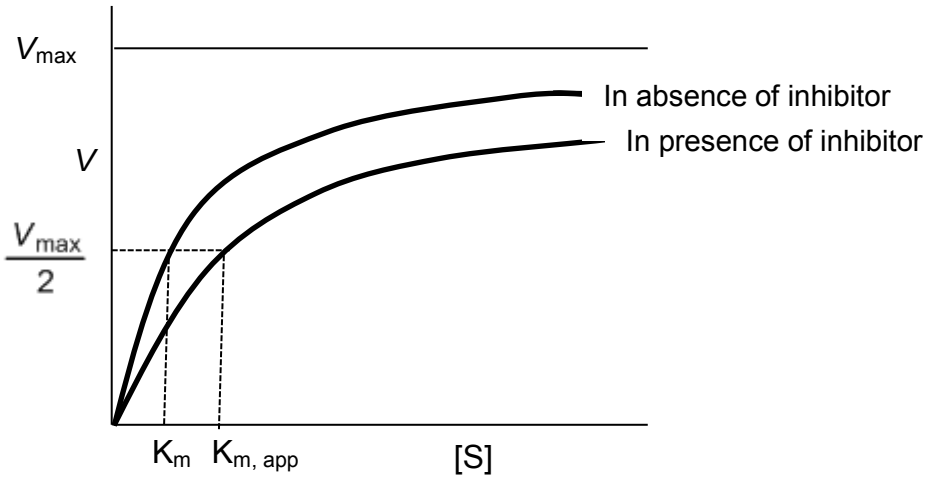


**Figure 1.18 Michaelis-Menten plot of competitive inhibition**

$$K_I = \frac{[E]\ [I]}{[EI]} \tag{1.1}$$

$$K_m = \frac{k_{-1} + k_2}{k_1} = \frac{[E]\ [S]}{[ES]} \tag{1.2}$$

$$V_o = \frac{V_{max}\,[S]}{K_m\left(1 + \frac{[I]}{K_I}\right) + [S]} \tag{1.3}$$

$$\frac{1}{V} = \frac{K_m}{V_{max}}\left(\frac{1}{[S]}\right)\left(1 + \frac{[I]}{K_I}\right) + \frac{1}{V_{max}} \tag{1.4}$$

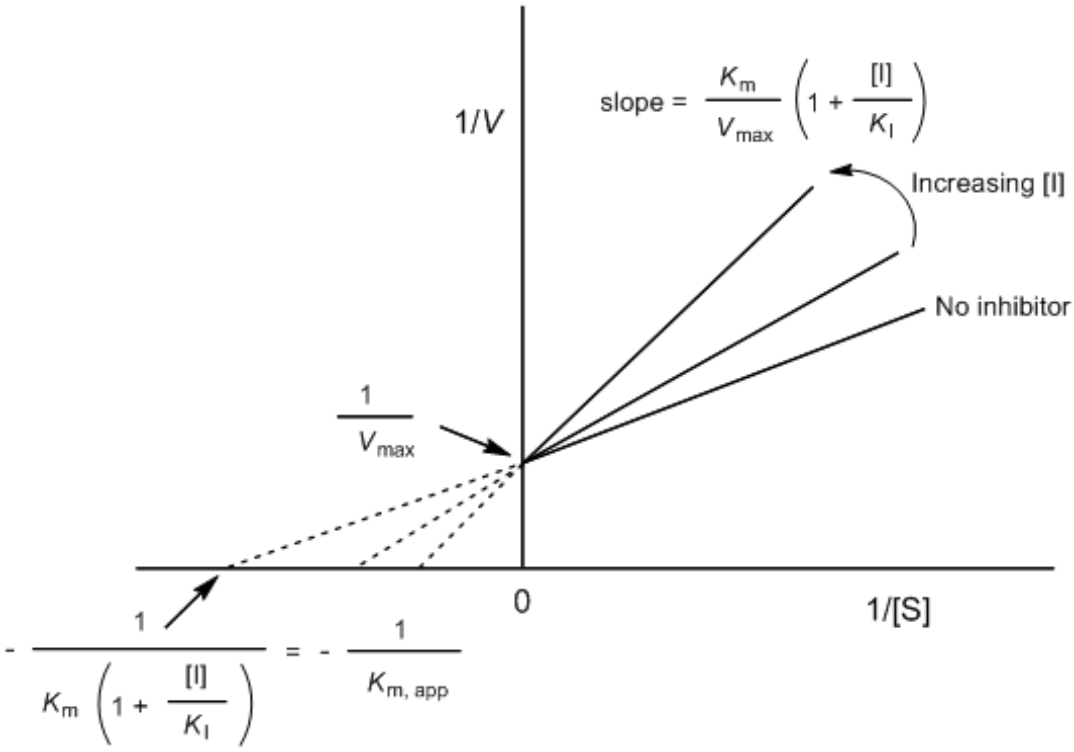


**Figure 1.19 Lineweaver-Burk plot of competitive inhibition**

### 1.11.1.2 Uncompetitive Inhibition

In uncompetitive inhibition, the inhibitor (I) binds only to the enzyme-substrate complex (ES) but not to the free enzyme, resulting in enzyme-substrate inhibitor complex (ESI) [48, 74]. This prevents the substrate reacting to form the normal product(s). This type of inhibition is more common in multisubstrate enzymes. The kinetic scheme for uncompetitive inhibition is

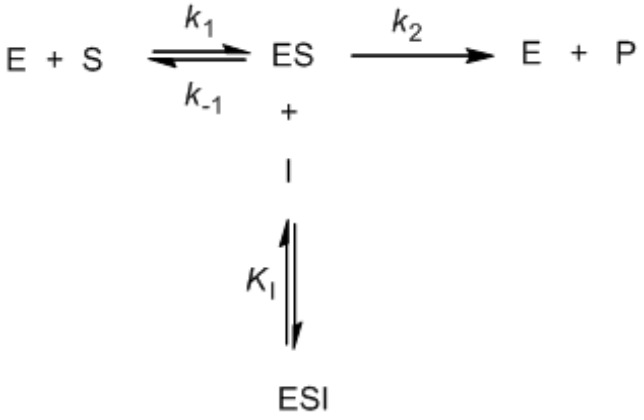


**Scheme 1.2 Kinetic scheme of uncompetitive inhibition**

shown in Scheme 1.2, and the Michaelis-Menten equation is given by:

$$V_o = \frac{\dfrac{V_{max}\,[S]}{\left(1 + \dfrac{[I]}{K_I}\right)}}{\dfrac{K_m}{\left(1 + \dfrac{[I]}{K_I}\right)} + [S]}$$

The transformation of the above equation to the Lineweaver-Burk equation is given by the equation:

$$\frac{1}{V} = \frac{K_m}{V_{max}}\left(\frac{1}{[S]}\right) + \frac{1}{V_{max}}\left(1 + \frac{[I]}{K_I}\right)$$

The Lineweaver-Burk plot (Figure 1.20) for uncompetitive inhibition is linear. The

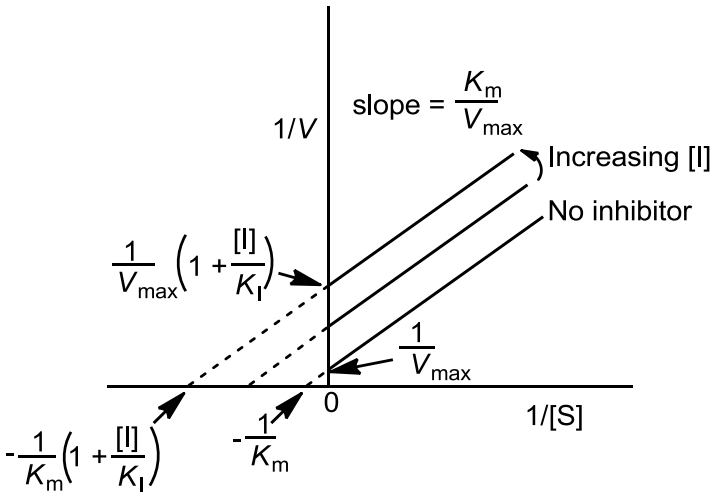


**Figure 1.20 Lineweaver-Burk plot for uncompetitive inhibition**

slope remains same but both intercepts change in the presence of an uncompetitive

inhibitor. The plot consists of a series of parallel lines, which is a characteristic for this kind of inhibition.

### 1.11.1.3 Noncompetitive Inhibition

Noncompetitive inhibition occurs when an Inhibitor binds to both the enzyme (E) and the enzyme-substrate complex (ES). This is shown in the Scheme 1.3.

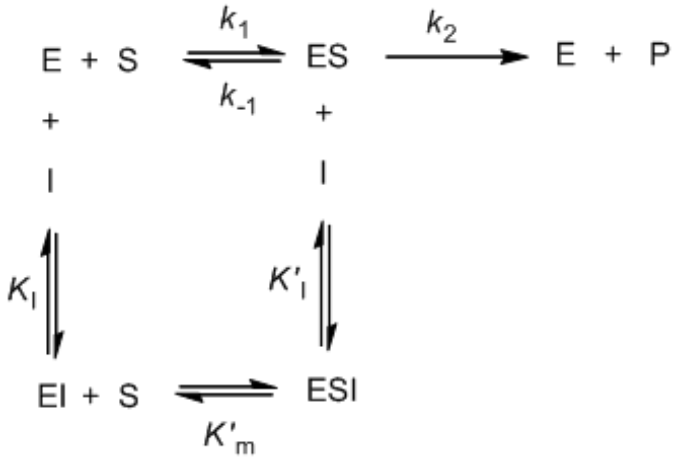


**Scheme 1.3 Kinetic scheme for noncompetitive inhibition**

Noncompetitive inhibition is observed in multiple-substrate systems, in which the inhibitor binds at a site different (not the active site) from the substrate. Assuming the

$$V_o = \frac{V_{max}[S] \Big/ \left(1 + \frac{[I]}{K_I}\right)}{K_m + [S]}$$

dissociation constants, $K_m$ and $K'_m$ are the same, the Michaelis-Menten equation takes the form of equation.

The Lineweaver-Burk equation for noncompetitive inhibition is:

$$\frac{1}{V} = \left[\frac{K_m}{V_{max}}\left(\frac{1}{[S]}\right) + \frac{1}{V_{max}}\right]\left(1 + \frac{[I]}{K_I}\right)$$

The Lineweaver-Burk plot for noncompetitive inhibition is shown in the Figure 1.21. As evident from the plot, the inhibitor does not affect the $K_m$ but changes the $V_{max}$.

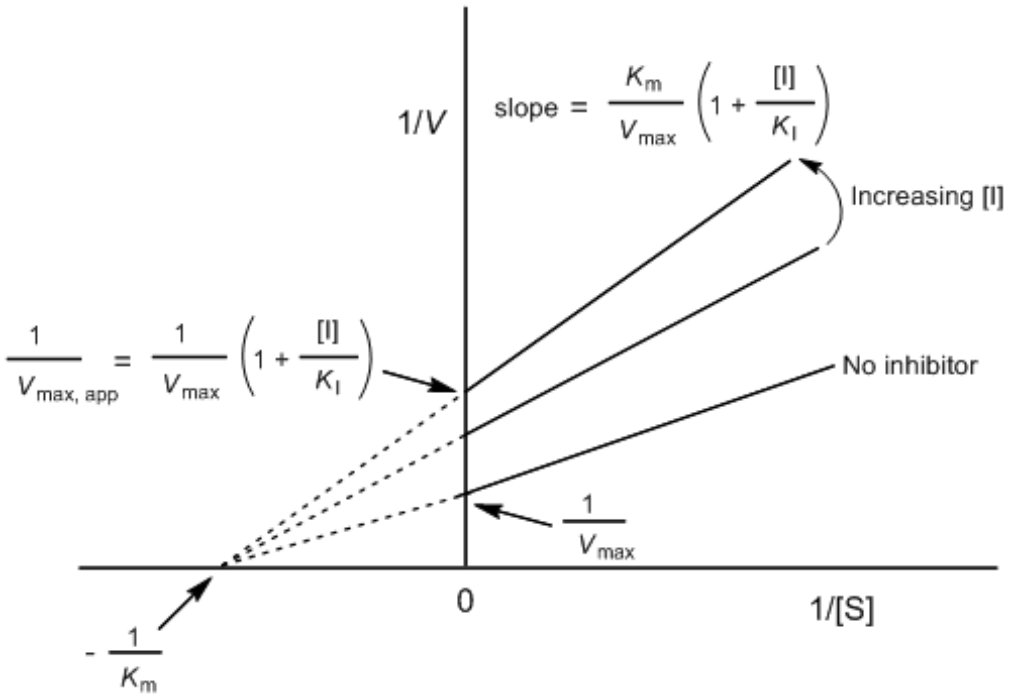


**Figure 1.21 Lineweaver-Burk plot of noncompetitive inhibition**

The table 1.2 shows the effect of various types of inhibition on the kinetic parameters, $V_{max}$, and $K_m$

**Table 1.2 Effects of inhibition on the kinetic parameters**

| Type of Inhibition | $V_{max}$ | $K_m$ |
|---|---|---|
| Competitive | unchange | change |
| Uncompetitive | change | change |
| Noncompetitive | change | unchange |

## 1.12 RESEARCH OBJECTIVES

DENV and WNV proteases are validated targets for the rational design of small molecule inhibitors. The main goals of the research described in this thesis were the following:

a) Design, synthesis, and *in vitro* biochemical evaluation of inhibitors of DENV and WNV NS2B/NS3 proteases based on the aminobenzamide scaffold;
b) Design, synthesis, and *in vitro* biochemical evaluation of 1,2-benzisothiazol-3(2H)-one and 1,3,4-oxadiazole hybrid inhibitors of NS2B/NS3 DENV and WNV proteases.

# Chapter 2

## Inhibitors of Dengue Virus and West Nile Virus Proteases Based on the Aminobenzamide Scaffold

### 2.1 Introduction

Dengue and West Nile viruses (WNV) are mosquito-borne members of flaviviruses that cause significant morbidity and mortality. There is no approved vaccine or antiviral drugs for human use to date. In this study, a series of functionalized *meta* and *para* aminobenzamide derivatives were synthesized and subsequently screened *in vitro* against Dengue virus and West Nile virus proteases. Four active compounds were identified which showed comparable activity toward the two proteases and shared in common a *meta* or *para*(phenoxy)phenyl group. The inhibition constants ($K_i$) for the most potent compound **7n** against Dengue and West Nile virus proteases were 8.77 and 5.55 μM, respectively. The kinetics data support a competitive mode of inhibition of both proteases by compound ***7n.*** This conclusion is further supported by molecular modeling. This study reveals a new chemical scaffold which is amenable to further optimization to yield potent inhibitors of the viral proteases via the combined utilization of iterative medicinal chemistry/structure-activity relationship studies and *in vitro* screening.

## 2.2 Chemistry

Compounds ***7a-t*** (Table 2.1) and ***8a-f*** (Table 2.2) were synthesized starting with methyl *p*-aminobenzoate or methyl *m*-aminobenzoate, respectively, as illustrated in Scheme 2.1. Thus, treatment with trichloromethyl chloroformate yielded the corresponding isocyanate which was reacted with propargylamine to form urea derivatives ***2a-b***. Click chemistry [75] with an array of structurally diverse azides yielded the corresponding functionalized urea derivatives which were further elaborated to form the final compounds.

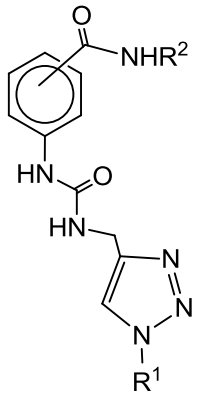

(I)

**Figure 2.1. General structure of aminobenzamide derivatives (I).**

## Table 2.1 Compounds 7a-t

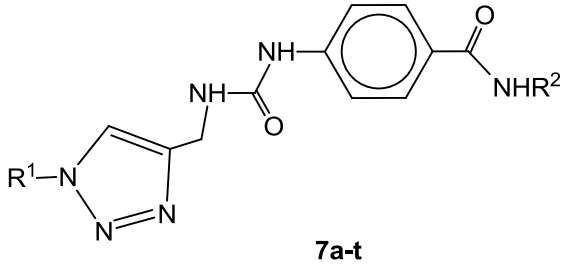

**7a-t**

| Compound | $R^1$ | $R^2$ | Compound | $R^1$ | $R^2$ |
|---|---|---|---|---|---|
| **7a** | phenylthiomethyl | 4-phenoxyphenyl | **7k** | benzyl | 2-furanylmethyl |
| **7b** | phenylthiomethyl | benzyl | **7l** | benzyl | 2-morpholinoethyl |
| **7c** | phenylthiomethyl | phenylethyl | **7m** | benzyl | 3-phenoxyphenyl |
| **7d** | phenylthiomethyl | phenyl | **7n** | 4-fluorobenzyl | 4-phenoxyphenyl |
| **7e** | phenylthiomethyl | 2-furanylmethyl | **7o** | 4-fluorobenzyl | benzyl |
| **7f** | phenylthiomethyl | 2-morpholinoethyl | **7p** | 4-fluorobenzyl | phenylethyl |
| **7g** | benzyl | 4-phenoxyphenyl | **7q** | 4-fluorobenzyl | phenyl |
| **7h** | benzyl | benzyl | **7r** | 4-fluorobenzyl | 2-furanylmethyl |
| **7i** | benzyl | phenylethyl | **7s** | 4-fluorobenzyl | 2-morpholinomethyl |
| **7j** | benzyl | phenyl | **7t** | 4-fluorobenzyl | 3-phenoxyphenyl |

## Table 2.2 Compounds 8a-f

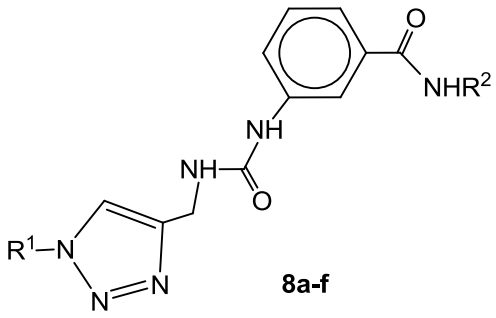


**8a-f**

| Compound | $R^1$ | $R^2$ |
|---|---|---|
| 8a | phenylthiomethyl | benzyl |
| 8b | phenylthiomethyl | phenylethyl |
| 8c | phenylthiomethyl | 3-phenoxyphenyl |
| 8d | benzyl | benzyl |
| 8e | benzyl | phenylethyl |
| 8f | benzyl | 3-phenoxyphenyl |

## Scheme 2.1

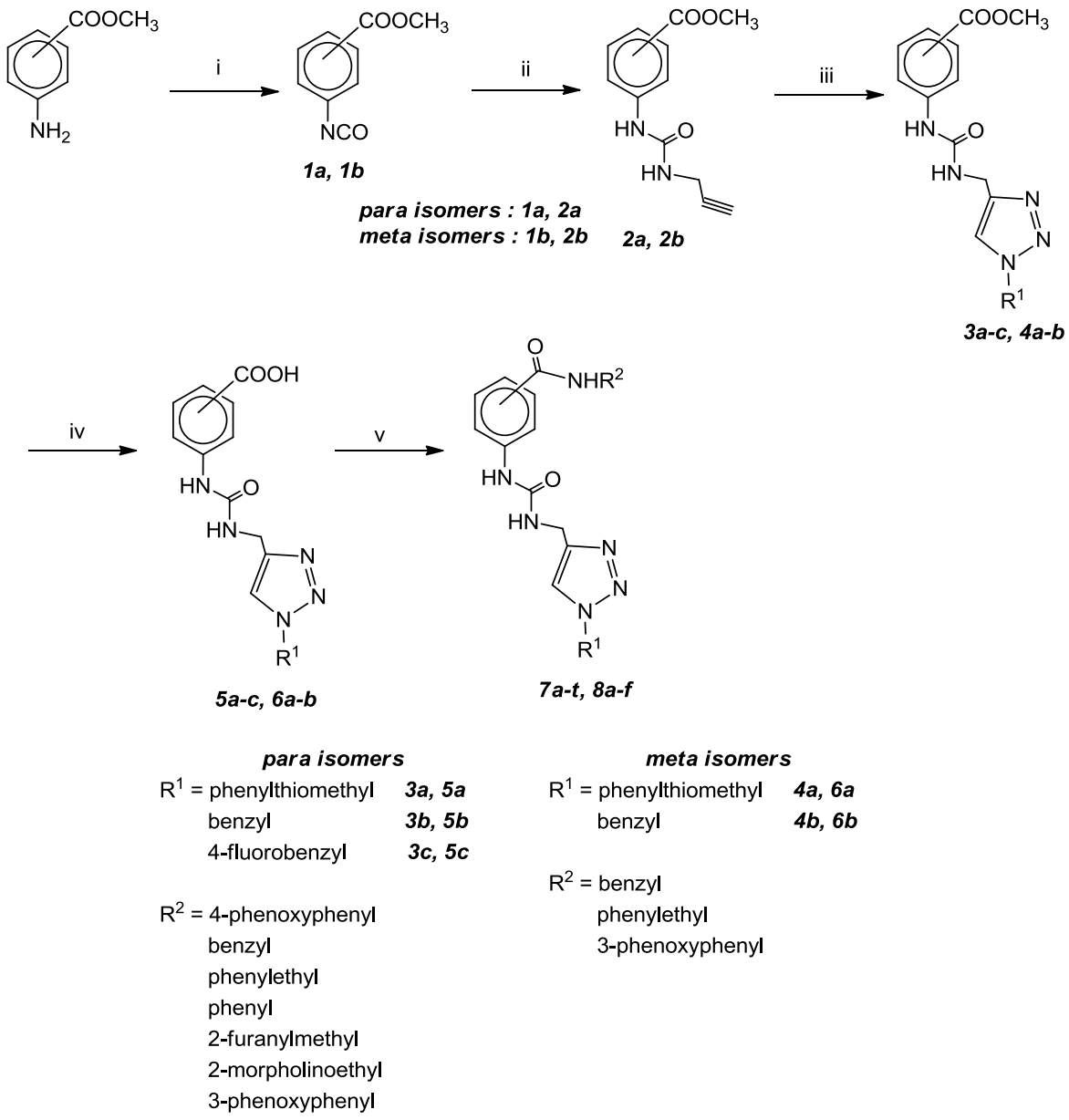


***para isomers : 1a, 2a***
***meta isomers : 1b, 2b***

***para isomers***

$R^1$ = phenylthiomethyl ***3a, 5a***
benzyl ***3b, 5b***
4-fluorobenzyl ***3c, 5c***

$R^2$ = 4-phenoxyphenyl
benzyl
phenylethyl
phenyl
2-furanylmethyl
2-morpholinoethyl
3-phenoxyphenyl

***meta isomers***

$R^1$ = phenylthiomethyl ***4a, 6a***
benzyl ***4b, 6b***

$R^2$ = benzyl
phenylethyl
3-phenoxyphenyl

**Scheme 2.1.** Reagents and conditions: i) Trichloromethyl chloroformate/THF, $\Delta$; ii) Propargyl amine/THF; iii) Arylalkyl azide, t-BuOH and $H_2O$ (1:1), $CuSO_4$ .$5H_2O$, sodium ascorbate; iv) aqLiOH/1,4-dioxane; v) CDI/THF, followed by amine

### 2.2.1 Experimental Section

#### 2.2.1.1 General.

The $^1$H spectra were recorded on a Varian XL-300 or XL-400 NMR spectrometer. Melting points were determined on a Mel-Temp apparatus and are uncorrected. High resolution mass spectra (HRMS) were performed at the University of Kansas Mass Spectrometry Lab. Reagents and solvents were purchased from various chemical suppliers (Aldrich, Acros Organics, TCI America, and Bachem). Silica gel (230-450 mesh) used for flash chromatography was purchased from Sorbent Technologies (Atlanta, GA). Thin layer chromatography was performed using Analtech silica gel plates. The TLC plates for the final compounds were eluted using two different solvent systems and were visualized using iodine and/or UV light. Each individual compound was identified as a single spot on TLC plate (purity was greater than 95% by $^1$H NMR). DENV2 NS2B/NS3 pro (or WNV NS2B/NS3 pro) substrate Bz-Nle-Lys-Arg-Arg-AMC was purchased from Bachem, Torrance, CA or custom synthesized by NeoBioScience, Cambridge, MA.

#### 2.2.1.2 Representative syntheses.

***Compound 1a:*** To methyl 4-aminobenzoate (30.23 g; 200 mmol) in anhydrous 1,4-dioxane (500 mL) was added trichloromethyl chloroformate (59.35 g; 300 mmol) dropwise and the reaction mixture was refluxed for 8 h. The solvent was removed on the rotary evaporator to yield ***1a*** as a yellow solid, which was purified by vacuum distillation to give a yellow solid (34 g, 96% yield). IR (neat) $\nu_{NCO}$ 2268 cm$^{-1}$. $^1$H NMR ($CDCl_3$): δ 3.88 (s, 3H), 7.14-7.18 (m, 2H), 7.96-8.02 (m, 2H).

***Compound 1b:*** Brown solid (94% yield). IR (neat) $\nu_{NCO}$ 2257 $cm^{-1}$. $^1H$ NMR ($CDCl_3$): δ 3.93 (s, 3H), 7.28-7.29 (m, 1H), 7.37-7.44 (m, 1H), 7.76-7.78 (1H), 7.85-7.89 (m, 1H).

***Compound 2a****:* To a solution of **1a** (15.06 g; 85 mmol) in anhydrous THF (150 mL) was added propargylamine (4.68 g; 85 mmol). The reaction mixture was stirred at room temperature overnight. The precipitate formed was collected by suction filtration to give ***2a*** as a white solid (18.5 g; 94% yield), mp 175-177 °C. $^1H$ NMR (DMSO-$d_6$): δ 3.13 (t, *J* = 2.45 Hz, 1H), 3.80 (s, 3H), 3.88 (dd, J = 5.70, 2.48 Hz, 2H), 6.71 (t, *J* = 5.69 Hz, 1H), 7.46-7.59 (m, 2H), 7.78-7.91 (m, 2H), 9.11 (s, 1H).

***Compound 2b:*** White solid (90% yield), mp 158-160 °C. $^1H$ NMR (DMSO-$d_6$): δ 3.11 (t, *J* = 2.46 Hz, 1H), 3.84 (s, 3H), 3.88 (dd, *J* = 5.72, 2.46 Hz, 2H), 6.61 (t, *J* = 5.73 Hz, 1H), 7.37 (t, *J* = 7.87 Hz, 1H), 7.49-7.52 (m, 1H), 7.58-7.62 (m, 1H), 8.12 (t, *J* = 1.80 Hz, 1H), 8.94 (s, 1H).

***Compound 3a:*** Compound ***2a*** (11.61 g; 50 mmol) and phenylthiomethyl azide (8.26 g; 50 mmol) were suspended in a 1:1 mixture of *t*-butanol and water (100 mL). Sodium ascorbate (1.00 g; 5 mmol) and $CuSO_4 \cdot 5H_2O$ (0.12 g; 0.5 mmol) were then added and the heterogeneous mixture was stirred vigorously at room temperature for 2 days. The progress of the reaction was monitored by TLC. The reaction mixture was diluted with water (200 mL) and cooled in an ice bath. The precipitate formed was collected by suction filtration to give ***3a*** as an off-white powder (19.47 g, 98% yield), mp 155-157 °C. $^1H$ NMR ($CDCl_3$): δ 3.88 (s, 3H), 4.48 (d, *J* = 5.84 Hz, 2H), 5.58 (s, 2H), 6.86 (t, *J* = 4.92 Hz, 1H), 7.21-7.34 (m, 5H), 7.39-7.42 (m, 2H), 7.66 (s, 1H), 7.91 (d, *J* = 8.73 Hz, 3H).

***Compound 3b:*** Light green solid (93% yield), mp 175-177 °C. $^1$H NMR (DMSO-$d_6$): δ 3.79 (s, 3H), 4.34 (d, *J* = 5.51 Hz, 2H), 5.57 (s, 2H), 6.79 (br s, 1H), 7.28-7.40 (m, 5H), 7.50-7.53 (m, 2H), 7.82-7.84 (m, 2H), 8.02 (s, 1H), 9.03 (s, 1H).

***Compound 3c:*** Light green solid (100% yield), mp 194-195 °C. $^1$H NMR (DMSO-$d_6$): δ 3.79 (s, 3H), 4.33 (d, *J* = 5.55 Hz, 2H), 5.56 (s, 2H), 6.78 (t, *J* = 5.61, Hz, 1H), 7.17-7.23 (m, 2H), 7.36-7.41 (m, 2H), 7.50-7.54 (m, 2H), 7.82-7.84 (m, 2H), 8.03 (s, 1H), 9.03 (s, 1H).

***Compound 4a:*** White solid (80% yield). $^1$H NMR (DMSO-$d_6$): δ 3.83 (s, 3H), 4.29 (d, *J* = 5.67 Hz, 2H), 5.92 (s, 2H), 6.69 (t, *J* = 5.67 Hz, 1H), 7.25-7.42 (m, 6H), 7.48-7.51 (m, 1H), 7.56-7.59 (m,1H), 7.91 (s, 1H), 8.13 (t, *J* = 1.92 Hz, 1H), 8.89 (s, 1H).

***Compound 4b:*** White solid (66% yield), mp 158-160 °C. $^1$H NMR (DMSO-$d_6$): δ 3.83 (s, 3H), 4.33 (d, *J* = 5.47 Hz, 2H), 5.57 (s, 2H), 6.66 (t, *J* = 5.37Hz, 1H), 7.29-7.40 (m, 6H), 7.48-7.50 (m, 1H), 7.56-7.59 (m, 1H), 8.02 (s, 1H), 8.13 (t, *J* = 1.76 Hz, 1H), 8.84 (s, 1H)

***Compound 5a:*** To a solution of ester ***3a*** (17 g; 42.5 mmol) in 1,4-dioxane (500 mL) was added a solution of LiOH ( 12.21 g; 510 mmol) in water (150 mL) and the reaction mixture was stirred at room temperature overnight. The reaction mixture was cooled in an ice bath and a 5% HCl solution was added dropwise until the pH was ~3. The precipitate formed was collected by suction filtration to give acid ***5a*** as a white solid (18.64 g, 97% yield), mp >230 °C. $^1$H NMR (DMSO-$d_6$): δ 4.30 (d, *J* = 5.61 Hz, 2H), 5.93 (s, 2H), 6.77 (t, *J* = 5.67 Hz, 1H), 7.23-7.42 (m, 5H), 7.48-7.51 (m, 2H), 7.80-7.83 (m, 2H), 7.92 (s, 1H), 9.01 (s, 1H), 12.49-12.72 (br s, 1H).

***Compound 5b:*** White solid (87% yield), mp >230 °C. $^1$H NMR (DMSO-$d_6$): δ 4.33 (s, 2H), 5.57 (s, 2H), 6.76-6.90 (br s, 1H), 7.28-7.40 (m, 5H), 7.47-7.51 (m, 2H), 7.78-7.82 (m, 2H), 8.02 (s, 1H), 9.10 (s, 1H).

***Compound 5c:*** White solid (99% yield), mp >230 °C. $^1$H NMR (DMSO-$d_6$): δ 4.33 (d, *J* = 5.61 Hz, 2H), 5.56 (s, 2H), 6.80 (t, *J* = 5.65 Hz, 1H), 7.16-7.24 (m, 2H), 7.35-7.42 (m, 2H), 7.46-7.50 (m, 2H), 7.78-7.82 (m, 2H), 8.03 (s, 1H), 9.03 (s, 1H), 12.25-12.84 (br s, 1H).

***Compound 6a:*** Off white solid (82% yield), mp 185-189 °C. $^1$H NMR (DMSO-$d_6$): δ 4.29 (d, *J* = 5.56 Hz, 2H), 5.92 (s, 2H), 6.74 (t, *J* = 5.72 Hz, 1H), 7.24-7.49 (m, 7H), 7.57-7.61 (m,1H), 7.91 (s, 1H), 8.06 (t, *J* = 1.78 Hz, 1H), 8.96 (s, 1H), 12.78-13.15 (br s, 1H).

***Compound 6b:*** Light green powder (88% yield), mp 192-194 °C. $^1$H NMR (DMSO-$d_6$): δ 4.33 (d, *J* = 5.60 Hz, 2H), 5.57 (s, 2H), 6.65 (t, *J* = 5.63 Hz, 1H), 7.25-7.39 (m, 6H), 7.45-7.49 (m, 1H), 7.55-7.60 (m, 1H), 8.02 (s, 1H), 8.04-8.06 (m,1H), 8.80 (s, 1H), 12.64-13.06 (br s, 1H).

***Compound 7a:*** To a solution of acid ***5a*** (0.5 g; 1.30 mmol) in anhydrous THF (20 mL) was added CDI (0.21 g; 1.304 mmol) and the mixture was refluxed for 20 min. 4-Phenoxyaniline (0.24 g; 1.30 mmol) was added and the mixture was stirred at room temperature for 2 h. The precipitate formed was collected by suction filtration to give ***7a*** as an off-white solid (0.23 g; 33% yield). $^1$H NMR (DMSO-$d_6$): δ 4.32 (d, *J* = 5.60 Hz, 2H), 5.93 (s, 2H), 6.81 (t, *J* = 5.67Hz, 1H), 6.96-7.14 (m, 5H), 7.23-7.43 (m, 8H), 7.50-7.57 (m, 2H), 7.74-7.81 (m, 2H), 7.93 (s, 2H), 9.01 (s, 1H), 10.09 (s, 1H). HRMS (ESI): Calculated for $C_{30}H_{26}N_6O_3SNa$ (M+Na) 573.1685; found 573.1689.

***Compound 7b:*** White solid (89% yield), mp 182-183 °C.$^1$H NMR (DMSO-$d_6$): δ 4.30 (d, *J* = 5.63 Hz, 2H), 4.45 (d, *J* = 5.99 Hz, 2H), 5.93 (s, 2H), 6.90 (t, *J* = 5.40 Hz 1H), 7.20-7.49 (m,12H), 7.79 (d, *J* = 8.83 Hz , 2H), 7.92 (s, 1H), 8.86 (d, *J* = 5.98 Hz, 1H), 9.04 (s, 1H). HRMS (ESI): Calculated for $C_{25}H_{24}N_6O_2SNa$ (M+Na) 495.1579; found 495.1596.

***Compound 7c:*** White solid (68% yield), mp 201-202 °C.$^1$H NMR (DMSO-$d_6$): δ 2.82 (t, *J* = 7.45 Hz, 2H), 3.41-3.49 (m, 2H), 4.30 (d, *J* = 5.59 Hz, 2H), 5.92 (s, 2H), 6.83 (t, 5.64 Hz, 1H), 7.19-7.35 (m, 8H), 7.38-7.46 (m, 4H), 7.70-7.73 (m, 2H), 7.91 (s, 1H), 8.36 (t, *J* = 5.64 Hz, 1H), 8.96 (s, 1H). HRMS (ESI): Calculated for $C_{26}H_{26}N_6O_2SNa$ (M+Na) 509.1736; found 509.1730.

***Compound 7d:*** Off white solid (88% yield), mp 190-191 °C.$^1$H NMR (DMSO-$d_6$): δ 4.29-4.35 (m, 2H), 5.94 (s, 2H), 6.76 (t, *J* = 5.71 Hz, 1H), 7.04-7.10 (m, 2H), 7.24-7.36 (m, 5H), 7.39-7.43 (m, 2H), 7.48-7.55 (m, 2H), 7.74-7.93 (m, 4H), 8.98 (s, 1H), 10.05 (s, 1H). HRMS (ESI): Calculated for $C_{24}H_{22}N_6O_2SNa$ (M+Na) 481.1423; found 481.1439.

***Compound 7e:*** Light brown solid (90% yield), mp 146-148 °C.$^1$H NMR (DMSO-$d_6$): δ 4.31 (d, *J* = 5.55 Hz, 2H), 4.44 (d, *J* = 5.62 Hz, 2H), 5.93 (s, 1H), 6.86 (t, *J* = 5.50 Hz, 1H), 7.04 (br s, 2H), 7.22-7.92 (m, 11H), 8.79 (t, *J* = 5.71Hz, 1H), 9.02 (s, 1H). HRMS (ESI): Calculated for $C_{23}H_{22}N_6O_3SNa$ (M+Na) 485.1372; found 485.1373

***Compound 7f:*** Off white solid (46% yield), mp 184-185 °C.$^1$H NMR (DMSO-$d_6$): δ 2.40-2.45 (m, 8H), 3.56 (t, *J* = 4.45 Hz, 4H), 4.30 (d, *J* = 5.57 Hz, 2H), 5.93 (s, 2H), 6.89 (t, *J* = 5.18 Hz, 1H), 7.24-7.47 (m, 7H), 7.71-7.73 (m, 2H), 7.92 (s, 1H), 8.21 (t, *J*

= 5.80 Hz, 1H), 9.02 (s, 1H). HRMS (ESI): Calculated for $C_{24}H_{30}N_3O_7S$ (M+H) 496.2131; found 496.2114.

***Compound 7g:*** Light pink solid (47% yield), mp > 230 °C. $^1$H NMR (DMSO-$d_6$): δ 4.35 (d, *J* = 5.56 Hz, 2H), 5.58 (s, 2H), 6.77 (t, *J* = 5.67 Hz, 1H), 6.96-7.05 (m, 4H), 7.08-7.14 (m, 1H), 7.31-7.41 (m, 7H), 7.53 (d, *J* = 8.78 Hz, 2H), 7.75-7.80 (m, 2H), 7.87 (d, *J* = 8.77 Hz, 2H), 8.03(s, 1H), 8.95 (s, 1H), 10.08 (s, 1H). $^{13}$C NMR (DMSO-$d_6$): δ 164.71, 157.27, 154.63, 151.71, 145.55, 143.43, 136.04, 135.17, 129.85, 128.62, 128.00, 127.85, 126.88, 122.84, 122.70, 122.57, 121.88, 119.18, 117.75, 116.53, 52.61, 34.74. HRMS (ESI): Calculated for $C_{30}H_{26}N_6O_3SNa$ (M+Na) 541.1964; found 541.1956.

**Compound *7h:*** White solid (54% yield)**,** mp 213-214 °C**.**$^1$H NMR (DMSO-$d_6$): δ 4.33 (d, *J* = 5.56 Hz, 2H), 4.45 (d, *J* = 5.96 Hz , 2H), 5.57 (s, 2H), 6.74 (t, *J* = 5.53 Hz, 1H), 7.30-7.40 (m, 10H), 7.44-7.48 (m, 2H), 7.76-7.82 (m, 2H), 8.02 (s, 1H), 8.78-8.94 (m, 2H). HRMS (ESI): Calculated for $C_{25}H_{24}N_6O_2SNa$ (M+Na) 463.1858; found 463.1844.

**Compound *7i:*** White solid (62% yield), mp 230 °C .$^1$H NMR (DMSO-$d_6$): δ 2.82 (t, *J* = 7.0 Hz, 2H), 3.41-3.48 (m, 2H), 4.33 (d, *J* = 5.57 Hz, 2H), 5.57 (s, 2H), 6.74 (t, *J* = 5.59 Hz, 1H), 7.16-7.40 (m, 10H), 7.42-7.47 (m, 2H), 7.70-7.73 (m, 2H), 8.02 (s, 1H), 8.38 (t, *J* = 5.65 Hz,1H), 8.87 (s, 1H). HRMS (ESI): Calculated for $C_{26}H_{26}N_6O_2SNa$ (M+Na) 477.2015; found 477.2036.

**Compound *7j:*** White solid (35% yield), mp > 230 °C. $^1$H NMR (DMSO-$d_6$): δ 4.35 (d, *J* = 5.56 Hz, 2H), 5.58 (s, 2H), 6.75 (t, *J* = 5.56 Hz, 1H), 7.07 (t, *J* = 7.37 Hz, 1H), 7.29-7.40 (m, 7H), 7.50-7.54 (m, 2H), 7.74-7.78 (m, 2H), 7.85-7.90 (m, 2H), 8.03 (s, 1H), 8.94 (s, 1H), 10.04 (s, 1H). HRMS (ESI): Calculated for $C_{24}H_{22}N_6O_2SNa$ (M+Na) 449.1702; found 449.1722.

**Compound *7k:*** White solid (35% yield), mp 207-208 °C. $^1$H NMR (DMSO-$d_6$): δ 4.33 (d, *J* = 5.56 Hz, 2H), 4.43 (d, J = 5.66 Hz, 2H), 5.57 (s, 2H), 6.24-6.25 (m, 1H), 6.38-6.39 (m, 1H), 6.76 (t, *J* = 5.59 Hz, 1H), 7.28-7.40 (m, 5H), 7.42-7.46 (m, 2H), 7.56-7.57 (m, 1H), 7.74-7.78 (m, 2H), 8.02 (s, 1H), 8.76(t, *J* = 5.80 Hz, 1H), 8.89 (s, 1H). HRMS (ESI): Calculated for $C_{23}H_{22}N_6O_3SNa$ (M+Na) 453.1651; found 453.1651.

***Compound 7l:*** White solid (45% yield), mp 204-206 °C. $^1$H NMR (DMSO-$d_6$): δ 2.36-2.45 (m, 6H), 3.33-3.37 (m, 2H), 3.56 (t, *J* = 4.59 Hz, 4H), 4.33 (d, *J* = 5.57 Hz, 2H), 5.57 (s, 2H), 6.77 (t, *J* = 5.63 Hz, 1H), 7.29-7.39 (m, 5H), 7.42-7.45 (m, 2 H), 7.70-7.73 (m, 2H), 8.02 (s, 1H), 8.21 (t, *J* = 5.67 Hz, 1H), 8.91(s, 1H). HRMS (ESI): Calculated for $C_{24}H_{30}N_7O_3$ (M+H) 464.2410; found 464.2422.

***Compound 7m:*** Light pink solid (25% yield), mp 199-200 °C. $^1$H NMR (DMSO-$d_6$): δ 4.34 ( d, *J* = 5.55 Hz, 2H), 5.57 (s, 2H), 6.72-6.77 (m, 2H), 7.02-7.07 (m, 2H), 7.12-7.18 (m, 1H), 7.30-7.44 (m, 8H), 7.49-7.58 (m, 4H), 7.82-7.85 (m, 2H), 8.02 (s, 1H), 8.94 (s, 1H), 10.10 (s, 1H). HRMS (ESI): Calculated for $C_{30}H_{26}N_6O_3Na$ (M+Na) 541.1964; found 541.1932.

***Compound 7n:*** White solid (49% yield), mp >230 °C. $^1$H NMR (DMSO-$d_6$): δ 4.32 (d, *J* = 5.59 Hz, 2H), 5.55 (s, 2H), 6.71 (t, *J* = 5.62 Hz, 1H), 6.93-7.04 (m, 4H), 7.05-7.12 (m, 1H), 7.14-7.24 (m, 2H), 7.32-7.42 (m, 4H), 7.47-7.52 (m, 2H), 7.72-7.80 (m, 2H), 7.82-7.90 (m, 2H), 8.02 (s, 1H), 8.91 (s, 1H), 10.06 (s, 1H). $^{13}$C NMR (DMSO-$d_6$): δ 164.72, 162.97, 160.54, 157.28, 154.64, 151.73, 145.62, 143.44, 135.18, 132.34, 130.24, 129.87, 128.54, 126.90, 122.86, 122.59, 121.85, 119.17, 117.77, 116.51, 115.58, 115.37, 51.80, 34.74. HRMS (ESI): Calculated for $C_{30}H_{25}FN_6O_3Na$ (M+Na) 559.1870; found 559.1859.

***Compound 7o:*** White solid (91% yield)***,*** mp 208-209 °C. $^1$H NMR (DMSO-$d_6$): δ 4.33 (d, *J* = 5.56 Hz, 2H), 4.45 (d, *J* = 5.94 Hz, 2H), 5.56 (s, 2H), 6.98 (t, *J* = 5.58 Hz, 1H), 7.15-7.26 (m, 3H), 7.28-7.33 (m, 4H), 7.34-7.43 (m, 2H), 7.46-7.49 (m, 2H), 7.77-7.80 (m, 2H), 8.03 (s, 1H), 8.85 (t, *J* = 5.95 Hz, 1H), 9.10 (s, 1H). HRMS (ESI): Calculated for $C_{25}H_{23}FN_6O_2Na$ (M+Na) 481.1761; found 481.1754.

***Compound 7p:*** White solid (90% yield), mp 207-209 °C. $^1$H NMR (DMSO-$d_6$): δ 2.82 (t, *J* = 7.46 Hz, 2H), 3.43 (m, 2H), 4.33 (d, *J* = 5.55 Hz, 2H), 5.56 (s, 2H), 7.05 (t, *J* = 5.56 Hz, 1H), 7.16-7.41 (m, 9H), 7.46 (d, *J* = 8.79 Hz, 2H), 7.71 (d, *J* = 8.75 Hz, 2H), 8.03 (s, 1H), 8.38 (t, *J* = 5.55 Hz, 1H), 9.17 (s, 1H). HRMS (ESI): Calculated for $C_{26}H_{25}FN_6O_2Na$ (M+Na) 495.1921; found 495.1921.

***Compound 7q:*** White solid (46% yield), mp >230 °C. $^1$H NMR (DMSO-$d_6$): δ 4.35 (d, *J* = 5.55 Hz, 2H), 5.57 (s, 2H), 6.86 (t, *J* = 5.62 Hz, 1H), 7.04-7.09 (m, 1H), 7.17-7.43 (m, 7H), 7.53 (d, *J* = 8.78 Hz, 1H), 7.75-7.79 (m, 2H), 7.88 (d, *J* = 8.75 Hz, 2H), 8.04 (s, 1H), 9.12 (s, 1H), s (10.06, 1H)***.*** HRMS (ESI): Calculated for $C_{24}H_{21}FN_6O_2Na$ (M+Na) 467.1608; found 467.1594.

***Compound 7r:*** White solid (99% yield)***,*** mp 189-191 °C. $^1$H NMR (DMSO-$d_6$): δ 4.33 (d, *J* = 5.60 Hz, 2H), 4.43 (d, *J* = 5.65 Hz, 2H), 5.56 (s, 2H), 6.24-6.25 (m, 1H), 6.37-6.39 (m, 1H), 6.79-6.86 (m, 1H), 7.02 (s, 1H) , 7.16-7.24 (m, 2H), 7.34-7.50 (m, 4H), 7.72-7.83 (m, 2H), 8.03 (s, 1H), 8.76 (t, *J* = 5.70Hz, 1H), 9.00 (s, 1H). HRMS (ESI): Calculated for $C_{23}H_{21}FN_6O_3Na$ (M+Na) 471.1557; found 471.1555.

***Compound 7s:*** (90% yield)***,*** mp 163-166 °C. $^1$H NMR (DMSO-$d_6$) δ 2.35-2.47 (m, 8H), 3.51- 3.63 (m, 4H), 4.32 (d, *J* = 5.56 Hz, 2H), 5.56 (s, 2H), 6.83 (t, *J* = 5.62 Hz, 1H), 7.01 (s, 1H), 7.16-7.24 (m, 2H), 7.36-7.47 (m, 4H), 7.69-7.73 (m, 2H), 8.02 (s, 1H), 8.21

(t, *J* = 5.64 Hz, 1H), 9.01 (s, 1H). HRMS (ESI): Calculated for $C_{24}H_{29}FN_7O_3$ (M+Na) 482.2316; found 482.2297.

***Compound 7t:*** Off white solid (16% yield), mp 211-212 °C. $^1$H NMR (DMSO-$d_6$): δ 4.34 (d, *J* = 5.50 Hz, 2H), 5.56 (s, 2H), 6.69-6.80 (m, 2H), 7.00-7.09 (m, 2H), 7.10-7.27 (m, 3H), 7.29-7.46 (m, 5H), 7.47-7.62 (m, 4H), 7.84 (d, *J* = 8.78 Hz, 2H), 8.03 (s, 1H), 8.95 (s, 1H), 10.10 (s, 1H). $^{13}$C NMR (DMSO-$d_6$): δ 164.96, 162.97, 160.54, 156.75, 156.43, 154.61, 145.61, 143.56, 140.89, 132.34, 130.24, 129.95, 128.66, 126.71, 123.39, 122.63, 118.68, 116.46, 115.58, 115.37, 114.89, 109.95, 51.79, 34.74. HRMS (ESI): Calculated for $C_{30}H_{25}FN_6O_3Na$ (M+Na) 559.1870; found 559.1862.

***Compound 8a:*** White solid (21% yield), mp 156-157 °C. $^1$H NMR (DMSO-$d_6$): δ 4.30 (d, *J* = 5.64 Hz, 2H), 4.45 (d, *J* = 5.99 Hz, 2H), 5.93 (s, 2H), 6.65 (t, *J* = 5.67 Hz, 1H), 7.22-7.44 (m, 12H), 7.56-7.61(m, 1H), 7.85 (t, *J* =1.79 Hz, 1H), 7.91 (s, 1H), 8.75 (s, 1H), 8.97 (t, *J* = 6.07 Hz, 1H). HRMS (ESI): Calculated for $C_{25}H_{24}N_6O_2SNa$ (M+Na) 495.1579; found 495.1567.

***Compound 8b:*** White solid (57% yield), mp 155-156 °C. $^1$H NMR (DMSO-$d_6$): δ 2.83 (t, *J* = 7.46 Hz, 2H), 3.45 (q, *J* = 6.30 Hz, 2H), 4.30 (s, 2H), 5.93 (s, 2H), 6.72 (br s, 1H), 7.19-7.42 (m, 12H), 7.55-7.59 (m, 1H), 7.79 (t, *J* = 1.80 Hz, 1H), 7.91 (s, 1H), 8.50 (t, *J* = 5.55 Hz, 1H), 8.83 (s, 1H). HRMS (ESI): Calculated for $C_{26}H_{26}N_6O_2SNa$ (M+Na) 509.1736; found 509.1757.

***Compound 8c:*** White solid (21% yield), mp 179-181 °C. $^1$H NMR (DMSO-$d_6$): δ 4.30 (d, *J* = 5.65 Hz, 2H), 5.93 (s, 2H), 6.72-6.82 (m, 2H), 7.02-7.08 (m, 2H), 7.12-7.20 (m, 1H), 7.22-7.47 (m, 10H), 7.50-7.65 (m, 3H), 7.87 (t, *J* = 1.76 Hz, 1H), 7.91 (s, 1H), 8.90 (s, 1H), 10.28 (s, 1H). $^{13}$C NMR (DMSO-$d_6$): δ 165.79, 156.79, 156.37, 154.89, 145.89,

140.70, 140.42, 135.42, 132.50, 130.25, 129.95, 129.84, 129.14, 128.54, 127.47, 123.43, 122.37, 120.63, 120.09, 118.71, 116.98, 114.87, 113.52, 109.93, 51.36, 34.69. HRMS (ESI): Calculated for $C_{30}H_{26}N_6O_3SNa$ (M+Na) 573.1685; found 573.1693.

***Compound 8d:*** White solid (80% yield), mp 162-164 °C. $^1$H NMR (DMSO-$d_6$): δ 4.33 (d, J = 5.58 Hz, 2H), 4.45 (d, *J* = 5.97 Hz, 2H), 5.57 (s, 2H), 6.67 (t, *J* = 5.61 Hz, 1H), 7.2-7.42 (m, 12H), 7.57-7.60 (m, 1H), 7.84 (t, *J* = 1.64 Hz, 1H), 8.01 (s, 1H), 8.75 (s, 1H), 8.96 (t, *J* = 5.96 Hz, 1H). HRMS (ESI): Calculated for $C_{25}H_{24}N_6O_2Na$ (M+Na) 509.1736; found 509.1757.

***Compound 8e:*** White solid (83% yield), mp 197-198 °C**.** $^1$H NMR (DMSO-$d_6$): δ 2.83 (t, *J* = 7.45 Hz, 2H), 3.41-3.49 (m, 2H), 4.33 (d, *J* = 5.56 Hz, 2H), 5.57 (s, 2H), 6.68 (t, *J* = 5.65 Hz, 1H), 7.17-7.40 (m, 12H), 7.55-7.58 (m, 1H), 7.78 (t, *J* = 1.65 Hz, 1H), 8.01 (s, 1H), 8.48 (t, *J* = 5.60 Hz, 1H), 8.74 (s, 1H). HRMS (ESI): Calculated for $C_{26}H_{26}N_6O_2Na$ (M+Na) 477.2015; found 477.2032.

***Compound 8f:*** White solid (64% yield), mp 201-202 °C**.** $^1$H NMR (DMSO-$d_6$): δ 4.33 (d, *J* = 5.53 Hz, 2H), 5.57 (s, 2H), 6.69-6.79 (m, 2H),7.02-7.08 (m, 2H), 7.13-7.19 (m, 1H), 7.29-7.46 (m, 10H), 7.51-7.64 (m, 3H), 7.86 (s, 1H), 8.01 (s, 1H), 8.83 (s, 1H), 10.28 (s, 1H). HRMS (ESI): Calculated for $C_{30}H_{26}N_6O_3Na$ (M+Na) 541.1945; found 541.1945.

## 2.3 Biochemistry

The expression and purification of DENV NS2B/NS3pro and WNV NS2B/NS3pro have been previously described [38, 55, 76]. Enzyme assays and inhibition studies were carried out as previously described [37, 54, 56] and the results are summarized in **Figures 2-4** and **Tables 3** and **4**.

### 2.3.1 In vitro DENV2 and WNV NS2B/NS3pro assays and inhibition studies.

The compounds were dissolved in dimethyl sulfoxide (DMSO) to make 50 mM stock solutions. The compounds were screened at 25 μM in 1% v/v DMSO in the final reaction mixture. Protease assays were performed in triplicates in Greiner Black 96 well plates. Each assay consisted of the reaction mixture of 100 μL containing 200 mM Tris·HCl buffer, pH 9.5, 30% glycerol, 25 nM DENV2 NS2B-NS3 pro (or 28 nM WNV NS2B/NS3pro) and the compound. The enzyme and the compound were pre-incubated at room temperature for 15 min prior to addition of the substrate (5 μM), Bz-Nle-Lys-Arg-Arg-AMC. The time course of the reaction at 37 °C was followed at every 90 sec intervals for up to 30 min in a monochrometer-based spectrofluorometer (Molecular Devices, Sunnyvale, CA) at excitation and emission wavelengths of 380 and 460 nm, respectively. The percent inhibition for each compound at 25 μM was first determined. For determining $IC_{50}$ values, twelve data points obtained from the range of 10 nM, 50 nM, 0.1, 0.5, 1, 2, 4, 6, 8, 10, 20, and 25 μM inhibitor concentrations of selected compounds were used. $IC_{50}$ values were calculated using the SigmaPlot 2001 v7.0 software [77].

### 2.3.2 Kinetics Analysis

To determine the $K_m$ and $V_{max}$ values of compound **7n**, four different concentrations of inhibitor (0, 1.0, 3.0 and 5.0 μM) were assayed at varying concentrations (0-50 μM) of substrate. The kinetics analysis methods have been previously described [78]. $K_i$ values were calculated from these data using a secondary plot of $K_{m,\ app}$ against the concentrations of selected compound **7n** using SigmaPlot 2001 v7.0 software [77].

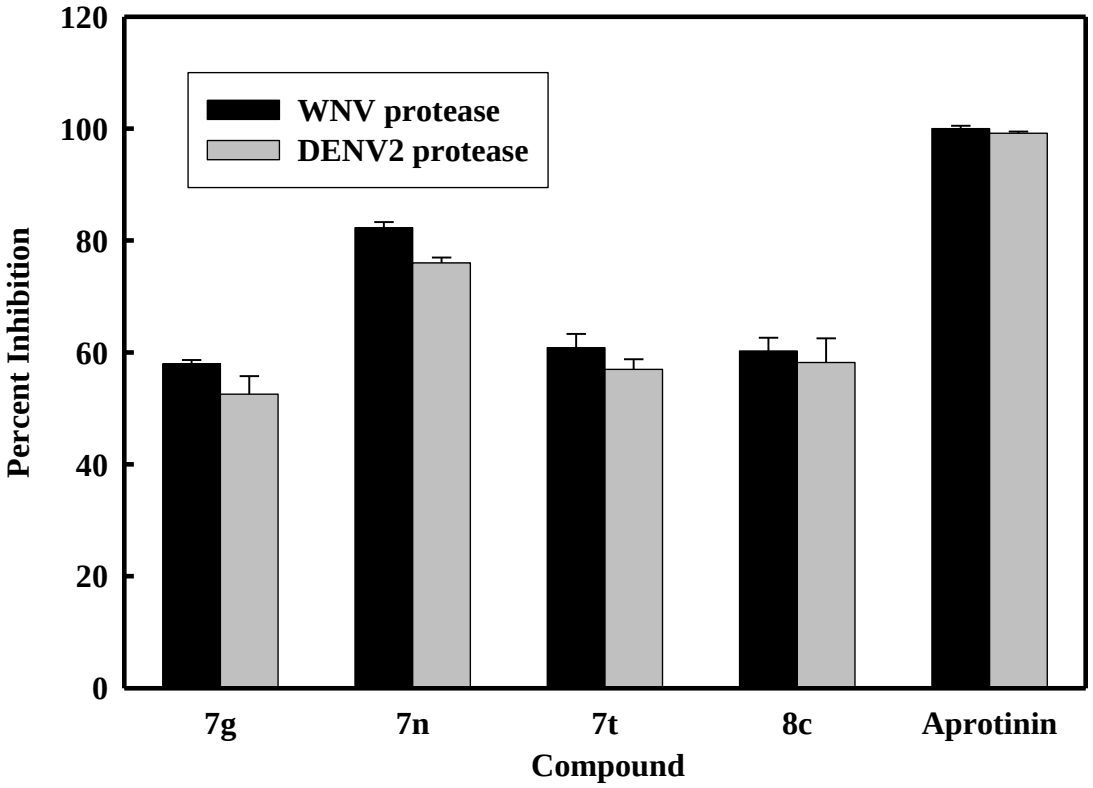


**Figure 2.2. Inhibition of DENV2 and WNV NS2B/NS3pro by selected compounds at 25 μM.** The concentrations of WNV and DENV2 NS2B/NS3pro protease were 28 nM and 25 nM, respectively. The buffer used contained 200 mM Tris·HCl, 6.0 mM NaCl, 30 % glycerol, and 0.1% CHAPS, pH 9.5. The percent values were calculated from the relative fluorescence units obtained in the presence and absence of tested compound. BPTI (Aprotinin) and DMSO were used as a positive and negative control, respectively. All assays were performed in triplicate and the average values are shown.

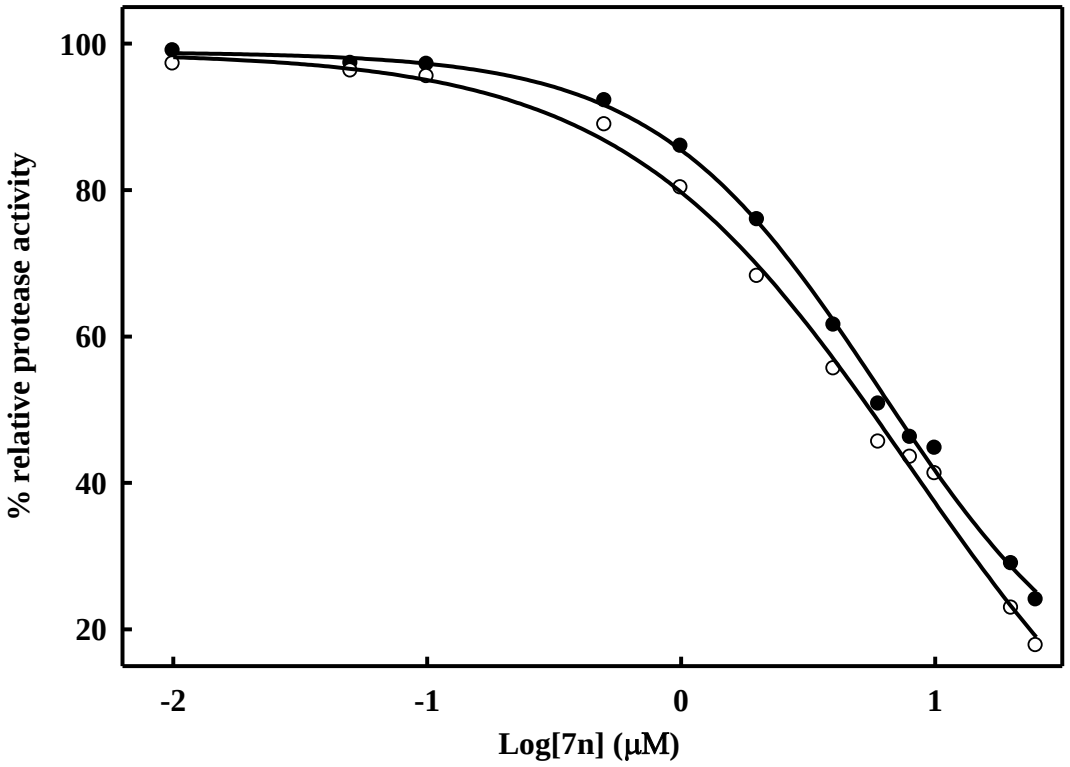


**Figure 2.3. Determination of $IC_{50}$ value of the inhibitor 7n against DENV-2 and WNV protease.** The inhibitor was incubated with DENV2 NS2B/NS3pro (25 nM) or WNV NS2B/NS3pro (28 nM) in buffer (200 mM Tris·HCl, 6 mM NaCl and 30% glycerol, pH 9.5) for 15 min. Bz-Nle-Lys-Arg-Arg-AMC (5.0 μM) was added to the mixture in a final volume of 100 μL. The fluorescence intensity was measured at 460 nm with excitation at 380 nm and converted to the percentage of protease activity in the absence and presence of inhibitors. The solid line is the theoretical fitting curve based on the Sigmoidal Equation.[41] The apparent $IC_{50}$ values for compound **7n** were 6.82 ± 0.09 and 5.51 ± 0.08 μM against DENV-2 (solid circle) and WNV (open circle), respectively.

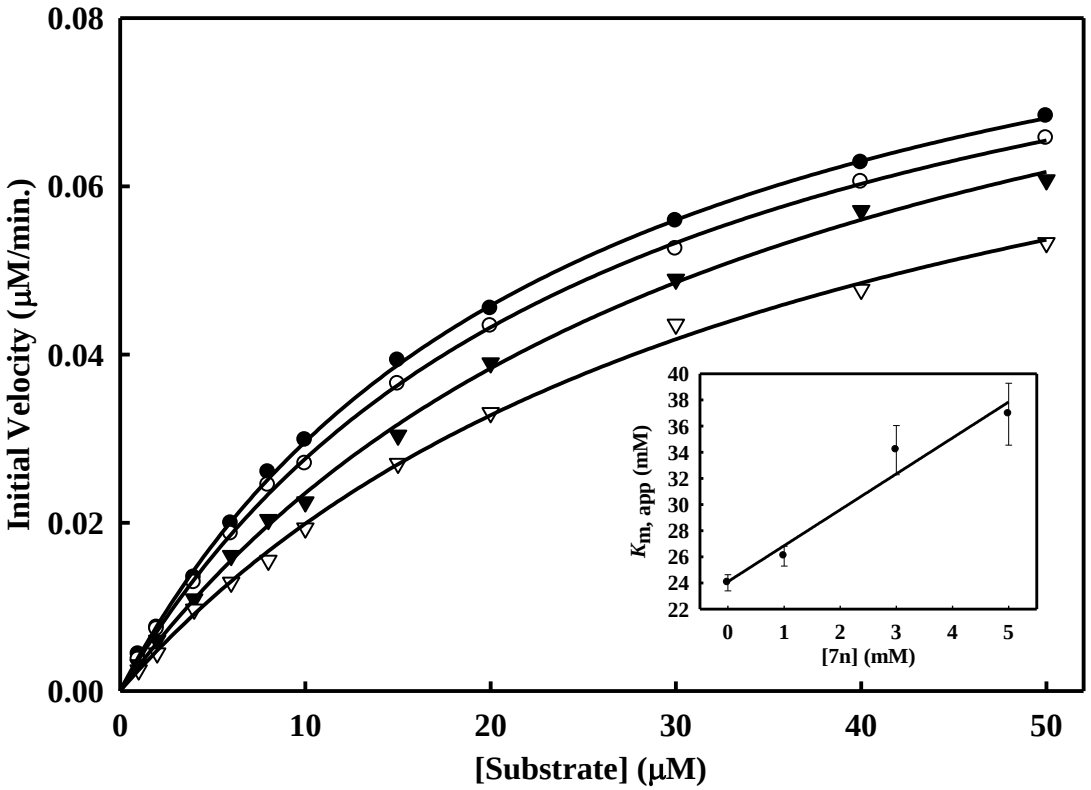


**Figure 2.4. Inhibition of WNV NS2B/NS3pro protease activity by compound 7n.** Initial reaction rates of the substrate (Bz-Nle-Lys-Arg-Arg-AMC) cleavage catalyzed by WNV NS2B/NS3pro protease (28 nM) in 200 mM Tris·HCl (pH 9.5), 6.0 mM NaCl, 30% glycerol and 0.1% CHAPS at 37 °C were determined by varying the substrate concentrations in the range of 0, 1, 2, 4, 6, 8, 10, 15, 20, 30, 40 and 50 μM at each concentration of inhibitor fixed at 0 (solid circle), 1.0 μM (open circle), 3.0 μM (solid triangle) and 5.0 μM (open triangle). The reactions were initiated by the addition of WNV NS2B/NS3pro protease and the fluorescence intensity at 460 nm was monitored with an excitation at 380 nm. Reactions were less than 5% completion in all cases to maintain valid steady-state measurements. The solid lines are fitted lines using the Michaelis-Menten equation. Inset: Secondary plot of $K_{m, app}$ against the concentration of compound **7n**. Kinetics studies were carried out as described utilizing substrate concentrations of 0-50 μM Bz-Nle-Lys-Arg-Arg-AMC. Each experiment was performed in duplicate and repeated three times. Data were analyzed using SigmaPlot 2001 v7.0 software [77] to determine values for apparent $K_m$ and $k_{cat}$.

**Table 2.3 Inhibition of DENV2 and WNV NS2B/NS3pro protease by compounds 7g, 7n, 7t and 8c.**

| Inhibitors | DENV2 | | *WNV* | |
|---|---|---|---|---|
| | % inhibition at 10 μM | % inhibition at 25 μM | % inhibition at 10 μM | % inhibition at 25 μM |
| ***7g*** | 39.41 ± 2.69 | 52.54 ± 3.21 | 46.51 ± 1.75 | 57.95 ± 0.71 |
| ***7n*** | 55.31 ± 1.39 | 76.01 ± 0.96 | 58.78 ± 1.62 | 82.26 ± 1.04 |
| ***7t*** | 41.06 ± 1.83 | 56.98 ± 1.81 | 44.45 ± 2.08 | 60.85 ± 2.46 |
| ***8c*** | 40.27 ± 1.11 | 58.21 ± 4.31 | 49.28 ± 1.87 | 60.27 ± 2.36 |
| [ WNV protease] = 28 nM; [DENV2 protease] = 25 nM | | | | |

**Table 2.4. Kinetics parameters for the *tetra*-peptide substrate and compound 7n against WNV NS2B/NS3pro at 37 ˚C**

| [7n] | $K_m$ | $k_{cat}$ | $k_{cat}/K_m$ |
|---|---|---|---|
| μM | *μM* | $s^{-1}$ | $M^{-1}\cdot s^{-1}$ |
| 0 | 24.01 ± 0.62 | 0.060 ± 0.0013 | 2499 ± 99 |
| 1 | 26.04 ± 0.75 | 0.059 ± 0.0014 | 2274 ± 100 |
| 3 | 34.16 ± 1.88 | 0.062 ± 0.0018 | 1811 ± 163 |
| 5 | 36.90 ± 2.36 | 0.055 ± 0.0020 | 1503 ± 162 |

## 2.4 Molecular Modeling

Molecular docking simulations were performed with the Surflex program [78]. The DENV NS3/NS2B receptor was modeled from the active form crystal structure of Noble et al. (PDB ID: 3U1I) [43] by extracting all ligands and waters, and protonating the receptor according to assumption of anionic aspartate and glutamate groups, and cationic arginines and lysines). The WNV NS2B/NS3pro receptor model was prepared in an analogous manner using the crystal structure of Erbel et al. (PDB ID 2FP7) [13]. In both cases, the co-crystallized ligand was used to define the Surflex protomol structure (which guides the original ligand binding site prediction), and 5 distinct randomized starting conformations and 100 final conformations were specified for the ligand. Ligands were constructed and refined according to default molecular mechanics constraints, force fields and optimization settings via the SYBYL 8.1 program (Tripos Associates, St. Louis, MO, 2009).

## 2.5 Results and Discussion

The world-wide health problem stemming from infection by Dengue virus and related flaviviruses, as well as the paucity of small-molecule therapeutics for combating flavivirus infection, have provided the impetus for the research described herein. The aminobenzamide scaffold was utilized in the synthesis of a series of structurally-diverse *meta* and *para*-substituted derivatives, represented by general structure (I), (Figure 2.1). The design of (I) rested on the following considerations: (a) the shallow active site of DENV NS2B/NS3pro presents a formidable challenge in terms of the design of potent inhibitors of the enzyme, necessitating the use of a suitably-embellished multifunctional

molecule capable of engaging in multiple favorable binding interactions with the enzyme in order to attain high potency, without compromising oral bioavailability and PK characteristics [79, 80, 81, 82, 83, 84, 85]. The problem is further compounded by the stringent substrate specificity requirements of the protease for positively charged substrates/inhibitors; (b) based on insights gained from examining the X-ray crystal structures of DENV2 NS2B/NS3pro with bound ligands [41, 43] and molecular modeling studies, it was hypothesized that the utilization of a planar platform capable of orienting appended non-peptidyl recognition elements in a precisely-defined vector relationship would lead to agents capable of interacting with multiple active site residues. Thus, the aminobenzamide platform was chosen for generating the desired compounds and for conducting exploratory studies. An added advantage is the flexibility afforded by the two points of diversity in the chosen scaffold, augmenting synthetic tractability; (c) a urea functionality was initially employed to lessen the conformational flexibility of the appended recognition elements. The latter included an electron-rich heterocycle having multiple hydrogen bond acceptor sites linked to an aryl alkyl group and, (d) it was furthermore envisaged that the initial attachment of an array of structurally-diverse aliphatic and aromatic amines to the carboxyl group of the aminobenzamide scaffold would provide additional binding sites.

The desired compounds were readily obtained as shown in Scheme 2.1. These were subsequently screened against DENV NS2B/NS3pro and WNV NS2B/NS3pro. Four of the compounds based on (I) were found to exhibit activity against both proteases and the results are summarized in Table 2.3 and Figure 2.2. It can be generally inferred from the SAR studies that the nature of both $R_1$ and $R_2$ influence

activity. Furthermore, activity is manifested when $R_1$ is a *meta* or *p*-(phenoxy)phenyl group. All other amides were inactive, suggesting that the *meta* or *p*-(phenoxy)phenyl group is accommodated in a hydrophobic cleft. It should be noted that some of the compounds were inactive despite the presence of a *meta* or *p*-(phenoxy)phenyl group (compounds ***7a*** and ***8f***).

The percent inhibition shown by compound ***7n*** against both DENV2 and WNV was found to be higher than any of the other selected compounds (Figure 2.2). The apparent $IC_{50}$ values of compound **7n** (Figure 2.3) were determined to be 6.82 $\pm$ 0.09 and 5.51 $\pm$ 0.08 μM against DENV2 and WNV protease, respectively. We also performed kinetics analyses to determine the $K_m$, $k_{cat}$ and $V_{max}$ values in the presence and absence of compound **7n** at four different concentrations (Figure 2.4 and Table 2.4). The apparent Michaelis-Menten constants ($K_{m,\ app}$) increased and $k_{cat}/K_m$ decreased proportionally with increasing concentration of compound **7n**. The results support a competitive mode of inhibition. Next, we employed molecular modeling to identify a plausible binding mode for ***7n***. Based on the molecular docking simulations, a high affinity bound conformer that is similar in both the DENV and WNV proteases was identified. Docking poses analysis yielded only one high potency conformer (i.e., one of the top five scoring poses) that conserved most of the key interactions in both DENV and WNV (Figures 2.5 and 2.6 respectively). Key features of this pose that are conserved across the two receptors include $\pi$-$\pi$ stacking interactions between the ligand fluorobenzyl group and the side chain of Tyr161, and hydrophobic interactions between the ligand phenoxyphenyl group and Val72. Visual inspection suggests that these interactions are not only conserved but are also likely to comprise most of the favorable

binding features in both cases. Furthermore confidence in this proposed pharmacophore is attained through comparison with predicted binding modes for inactive compounds ***7a*** and ***8f***. In the case of DENV NS2B/NS3pro in Figure 2.5, neither of the inactive compounds is predicted to exploit either of the two lipophiles listed above with the same effectiveness as ***7n***: compound ***8f*** has poor overlap with both lipophiles, and while compound ***7a*** is predicted to achieve some $\pi$-$\pi$ stacking with Tyr161, its furan group is not situated anywhere near any lipophiles. In the case of WNV NS2B/NS3pro (Figure 2.6), reasonable $\pi$-$\pi$ stacking is achieved with Tyr161 in all cases, but the furan group of ***7a*** is again poorly situated, while the phenoxyphenyl group of ***8f*** is not predicted to derive nearly as much a hydrophobic interaction as is achieved by the corresponding phenoxyphenyl group of **7n**, whose terminal phenyl group is predicted to wedge favorably between Val72 and the lipophilic portion of neighboring Lys73.

## 2.6 Conclusion

In summary, the studies described herein have demonstrated that the aminobenzamide scaffold can be employed in the synthesis of inhibitors of DENV and WNV NS2B/NS3pro.

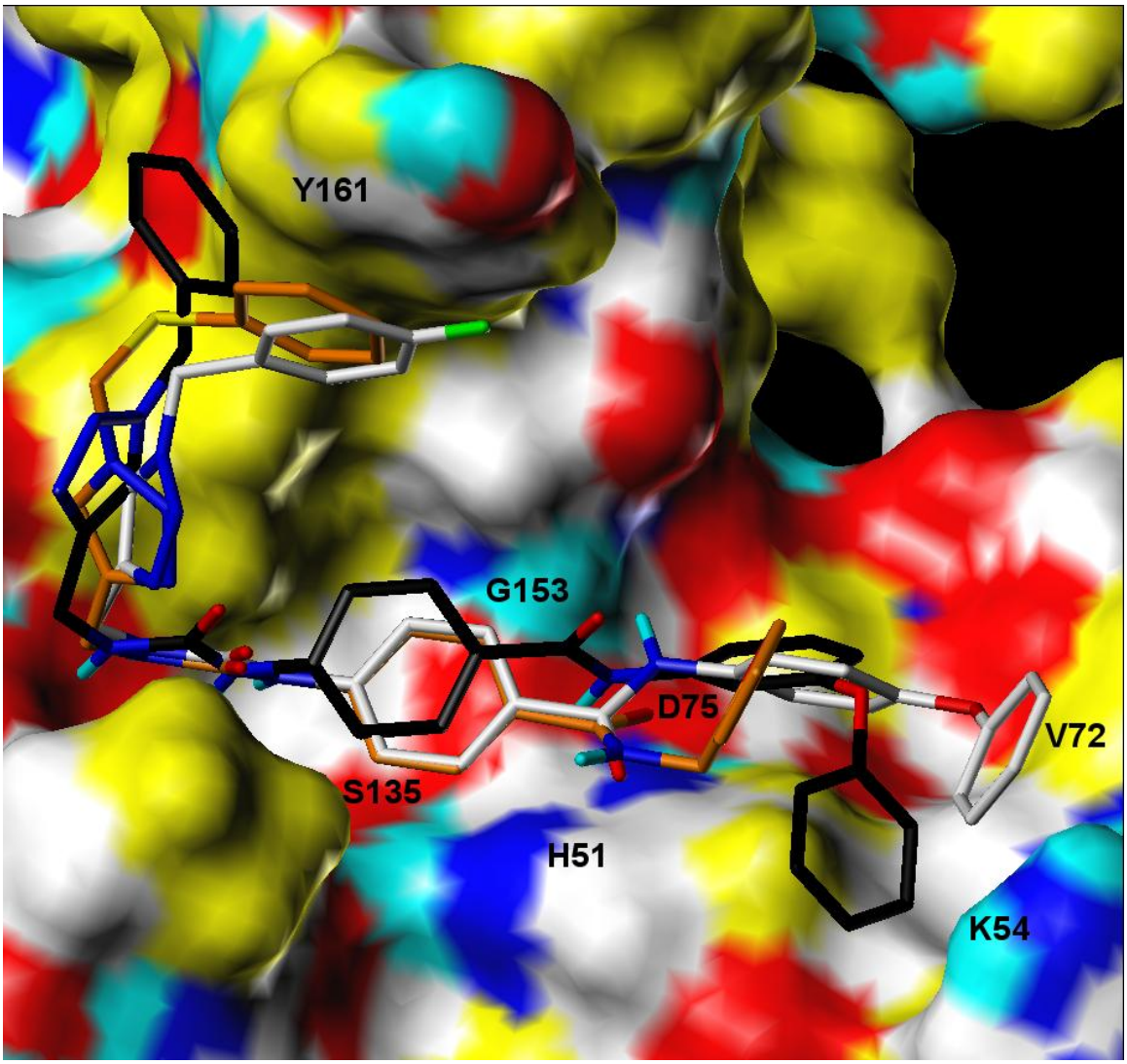


**Figure 2.5. Computationally predicted conformation of compounds 7a, 7n and 8f bound to the catalytic site of DENV2 NS2B/NS3 protease.** Ligands are rendered as CPK-colored sticks with the exception of carbon atoms (***7a***: orange, ***7n***: white, ***8f***: black), while the receptor surface is colored as follows: yellow = hydrophobic, white = polarized alkyl or aryl groups, cyan = polar hydrogens, blue = polar nitrogens and red = polar oxygens.

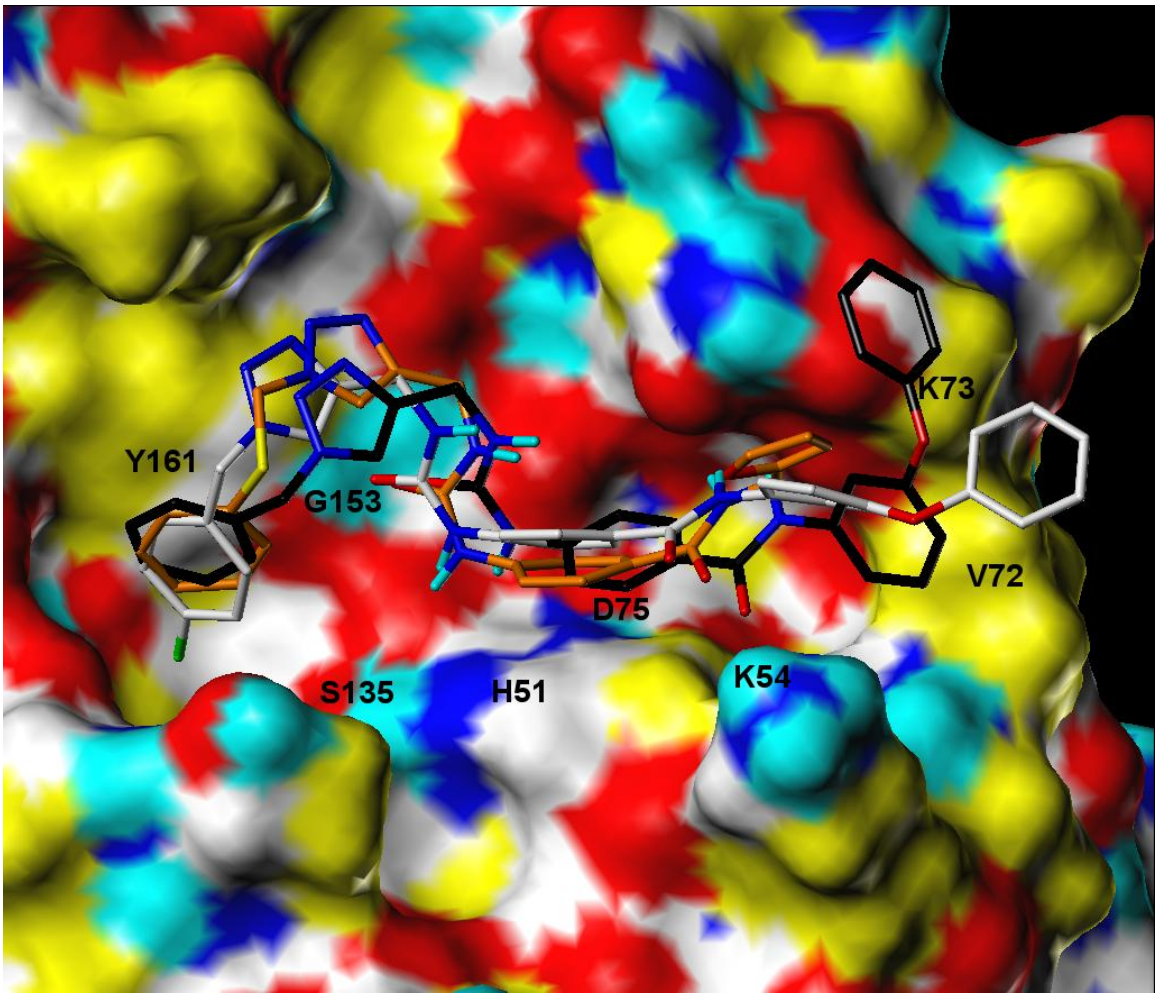


**Figure 2.6**. **Computationally predicted conformation of compound 7n bound to the catalytic site of WNV NS2B/NS3 protease**. Ligands are rendered as CPK-colored sticks with the exception of carbon atoms (***7a***: orange, ***7n***: white, ***8f***: black), while the receptor surface is colored as follows: yellow = hydrophobic, white = polarized alkyl or aryl groups, cyan = polar hydrogens, blue = polar nitrogens and red = polar oxygens.

# Chapter 3

## *Design, Synthesis and Characterization of Novel 1,2-Benzisothiazol-3(2H)-one and 1,3,4-Oxadiazole Hybrid Derivatives: Potent Inhibitors of Dengue and West Nile Virus NS2B/NS3 Proteases*

### 3.1 Introduction

1,2-Benzisothiazol-3(2H)-one derivatives play a significant role in various pharmaceutical applications [86, 87, 88]. As an important class of heterocyclic compounds, 1,2-benzisothiazol-3(2H)-ones show broad spectrum bioactivity [89, 90, 91, 92]. Among these, suitably-substituted 1,2-benzisothiazol-3(2H)-ones have been shown to exhibit potent antifungal [93] and antivirus activity [57]. Compounds containing a 1,3,4-oxadiazole template have also received significant attention in medicinal and pharmaceutical research as this structural motif has found use in a variety of applications [94], including as an essential component of the pharmacophore and as a bioisosteric replacement for carbonyl-containing compounds, such as esters, amides and others. Recently, sulfonamide-1,3,4-oxadiazole derivatives have been shown to exhibit noteworthy antibacterial and antifungal activity [95].

In this study, we describe the design, synthesis, and structure-activity relationship (SAR) studies of a series of novel 1,2-benzisothiazol-3(2H)-one and 1,3,4-oxadiazole hybrid derivatives, represented by general structure (I) (Figure 4.1) as potential inhibitors of DENV2 and WNV NS2B/NS3 proteases. Inhibition percentage and steady state kinetics against DENV2 and WNV NS2B/NS3 proteases were carried out. Ten out of twenty-four compounds showed greater than 50% inhibition against DENV2

and WNV proteases ([I] = 10 μM). The $IC_{50}$ values of compound **7n** against DENV2 and WNV NS2B/NS3 were found to be 3.75 ± 0.06 and 4.22 ± 0.07 μM, respectively. The kinetics data support a competitive mode of inhibition by compound **7n**. Molecular modeling studies were performed to delineate the putative binding mode of this series of compounds. This study reveals that the hybrid series arising from the linking of the two scaffolds provides a suitable platform for conducting a hit-to-lead optimization campaign via iterative structure-activity relationship studies, *in vitro* screening and X-ray crystallography.

### 3.2 Chemistry

In this study, twenty four 1,2-benzisothiazol-3(2H)-one - 1,3,4-oxadiazole hybrid derivatives were synthesized. The synthetic routes leading to compounds 7a-x (Table 3.1) are illustrated in the synthetic scheme 3.1. Compounds 7a-d were synthesized from compound ***2,*** which was in turn synthesized [93] by the sequential treatment of 1,2-benzisothiazolin-3[2H]-one with NaH and *t*-butyl bromoacetate in trifluoroethanol, followed by hydrolysis of the resulting ester with trifluoroacetic acid. Coupling of ***2*** with a series of hydrazides followed by *p*-toluenesulfonyl chloride-mediated cyclodehydration of the corresponding products yielded the desired compounds. Compounds 7e-l and 7w-x were prepared using 2,2'-dithiodibenzoic acid as the starting material via treatment with 1,1'-carbonyldiimidazole (CDI) and an appropriate amino acid methyl ester hydrochloride to afford the corresponding ester **3**. Intermediate **4** was obtained by reacting **3** with bromine, followed by the addition of triethylamine. The corresponding acids **5** were obtained following hydrolysis with LiOH in aqueous THF. Substituted

hydrazide derivatives **6** were obtained by reacting **5** with 1,1'-carbonyldiimidazole in THF and an array of substituted hydrazides. Finally, treatment of hydrazides **6** with *p*-toluenesulfonyl chloride in the presence of triethylamine in $CH_2Cl_2$ under ambient temperature gave cyclodehydration products **7.** Compounds 7m-v were conveniently prepared using a one-pot synthesis, as described in the literature [96]. The synthesized compounds are listed in Table 3.1.

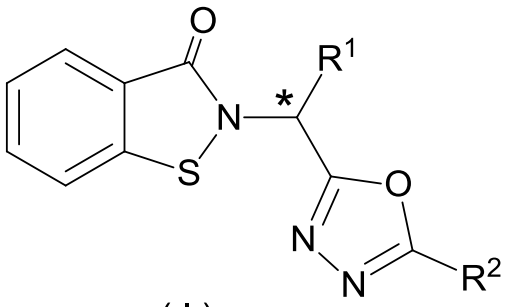


( I )

**Figure 3.1. General structure of Inhibitor (I).**

**Table 3.1 Compounds 7a-7x**

| Inhibitor | $R^1$ | $R^2$ | Inhibitor | $R^1$ | $R^2$ |
|---|---|---|---|---|---|
| **7a** | H | *m*-fluorophenyl | **7m** | benzyl | phenyl |
| **7b** | H | *m*-chlorophenyl | **7n** | benzyl | *p*-methoxyphenyl |
| **7c** | H | benzyl | **7o** | benzyl | *p*-ethoxyphenyl |
| **7d** | H | *p*-methoxybenzyl | **7p** | benzyl | *p*-pyridyl |
| **7e** | methyl | *p*-methoxybenzyl | **7q** | benzyl | *m*-pyridyl |
| **7f** | benzyl | benzyl | **7r** | benzyl | 2-furyl |
| **7g** | benzyl | *p*-methoxybenzyl | **7s** | benzyl | 2-thiophenyl |
| **7h** | benzyl | *m*-fluorophenyl | **7t** | benzyl | methyl |
| **7i** | benzyl | *m*-chlorophenyl | **7u** | benzyl | ethyl |
| **7j** | benzyl | *p*-fluorophenyl | **7v** | benzyl | propyl |
| **7k** | benzyl | *p*-chlorophenyl | **7w** | *m*-fluorobenzyl | *m*-chlorophenyl |
| **7l** | benzyl | *p*-cyanophenyl | **7x** | phenethyl | *m*-chlorophenyl |

## Scheme 3.1

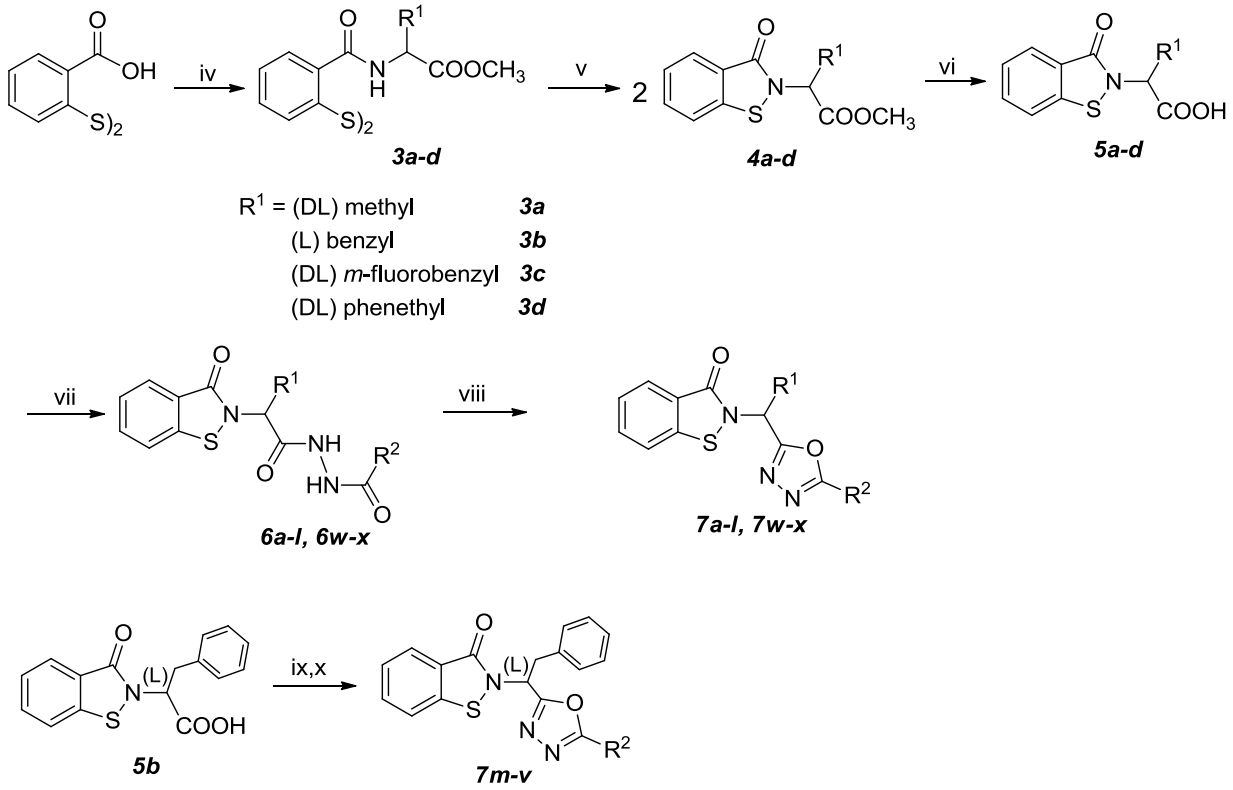


| | | | |
|---|---|---|---|
| $R^1$ = H, $R^2$ = *m*-fluorophenyl | ***6a/7a*** | $R^1$ = (L) benzyl, $R^2$ = phenyl | ***6m/7m*** |
| = *m*-chlorophenyl | ***6b/7b*** | = *p*-methoxyphenyl | ***6n/7n*** |
| = benzyl | ***6c/7c*** | = *p*-ethoxyphenyl | ***6o/7o*** |
| = *p*-methoxybenzyl | ***6d/7d*** | = *p*-pyridyl | ***6p/7p*** |
| $R^1$ = (DL) methyl, $R^2$ = *p*-methoxybenzyl | ***6e/7e*** | = *m*-pyridyl | ***6q/7q*** |
| $R^1$ = (L) benzyl, $R^2$ = benzyl | ***6f/7f*** | = 2-furyl | ***6r/7r*** |
| = *p*-methoxybenzyl | ***6g/7g*** | = 2-thiophenyl | ***6s/7s*** |
| = *m*-fluorophenyl | ***6h/7h*** | = methyl | ***6t/7t*** |
| = *m*-chlorophenyl | ***6i/7i*** | = ethyl | ***6u/7u*** |
| = *p*-fluorophenyl | ***6j/7j*** | = propyl | ***6v/7v*** |
| = *p*-chlorophenyl | ***6k/7k*** | $R^1$ = (DL) *m*-fluorobenzyl, $R^2$ = *m*-chlorophenyl | ***6w/7w*** |
| = *p*-cyanophenyl | ***6l/7l*** | $R^1$ = (DL) phenethyl, $R^2$ = *m*-chlorophenyl | ***6x/7x*** |

Reagents and conditions: i) $NaH/CH_3CN$; ii) $BrCH_2COOC(CH_3)_3$ /$CF_3CH_2OH$; iii) TFA; iv) CDI/THF, followed by amino acid and TEA; v) $Br_2/CH_2Cl_2$, TEA; vi) $LiOH/H_2O$, THF; vii) CDI/THF, $R^2CONHNH_2$; viii)*p*-TsCl/$CH_2Cl_2$, TEA; ix) $R^2CONHNH_2$, DIPEA, TBTU, dry $CH_3CN$; x) DIPEA, *p*-TsCl

### 3.2.1 Experimental Section

#### 3.2.1.1 Representative syntheses.

Compounds **1** and **2** were synthesized using a previously published procedure [93].

***t-Butyl (3-oxo-1,2-benzisothiazol-3(2H)-2-yl)-acetate (1):*** Yellowish oil (20.5 g; 77% yield) which was used in the next step without further purification. $^1$H NMR ($CDCl_3$): δ 1.51 (s, 9H), 4.57 (s, 2H), 7.20-8.29 (m, 4H).

***(3-Oxo-1,2-benzisothiazol-3(2H)-2-yl)-acetic acid (2):*** White solid (11.2 g; 69% yield), mp 229-230 °C. $^1$H NMR ($CDCl_3$): δ 4.57 (s, 2H), 7.40-8.12 (m, 4H).

***2,2'-Dithiodibenzoyl bis-alanine methyl ester (3a):*** Compound ***3a*** was prepared as described previously [93]. Briefly, a solution of 2,2'-dithiodibenzoic acid (1.53 g; 5 mmol) in 10 mL THF and 6 mL DMF was added dropwise a suspension of 1,1'-carbonyl diimidazole (1.70 g; 10 mmol) in 10 mL THF. The reaction mixture was stirred at room temperature for 20 min and refluxed for 20 min. The reaction mixture was allowed to cool to room temperature and (DL) alanine methyl ester hydrochloride (1.40 g; 10 mmol) and triethylamine (1.5 mL; 12 mmol) were added. The reaction mixture was stirred at room temperature overnight and concentrated. The residue was taken up in ethyl acetate (40 mL) and water (30 mL). The organic layer was washed with 5% HCl (3 × 30 mL), saturated $NaHCO_3$ (3 × 30 mL) and brine (30 mL). The organic layer was dried over anhydrous sodium sulfate, filtered, and concentrated, leaving behind ***3a*** as an yellow solid (1.8 g; 76% yield), mp 139-141°C. $^1$H NMR (DMSO-$d_6$): δ 1.44 (d, *J* = 7.3 Hz, 6H), 3.68 (s, 6H), 4.46-4.59 (m, 2H), 7.25-7.33 (m, 2H), 7.43-7.53 (m, 2H), 7.65-7.79 (m, 4H), 8.98 (d, *J* = 6.3 Hz, 2H).

***2,2'-Dithiodibenzoyl bis-phenylalanine methyl ester (3b):*** White solid (68% yield), mp 165-167 °C. $^1$H NMR ($CDCl_3$) δ 3.24 (dd, *J* = 13.9, 5.3 Hz, 2H), 3.36 (dd, *J* = 13.7, 5.8 Hz, 2H), 3.79 (s, 6H), 5.11 (dd, *J* = 10, 5.8 Hz, 2H), 6.58 (d, *J* = 7.6 Hz, 2H), 7.13-7.22 (m, 8H), 7.25-7.43 (m, 8H), 7.73-7.78 (m, 2H).

***2,2'-Dithiodibenzoyl bis-(m-fluoro)phenylalanine methyl ester (3c):*** Light brown solid (75% yield). mp 141-143 °C. $^1$H NMR ($CDCl_3$): δ. 3.25 (dd, *J* = 14.1, 5.1 Hz, 2H), 3.38 (dd, *J* = 15.8, 5.9 Hz, 2H), 3.80 (s, 6H), 5.14 (q, *J* = 5.4 Hz, 2H), 6.61 (d, *J* = 7.6 Hz, 2H), 6.82-7.00 (m, 6H), 7.17-7.28(m, 4H), 7.33-7.44 (m, 4H), 7.76 (d, *J* = 8.1 Hz, 2H).

***2,2'-Dithiodibenzoyl bis-benzylalanine methyl ester (3d):*** White solid (55% yield), mp 190-192 °C. $^1$H NMR (DMSO-$d_6$): δ 2.09 (q, *J* = 14.7 Hz, 4H), 2.62-2.82 (m, 4H), 3.65 (s, 6H), 4.38 (q, *J* = 7.3 Hz, 2H), 7.14-7.37 (m, 12H), 7.43-7.51 (m, 2H), 7.65-7.74 (m, 4H), 9.07 (d, *J* = 7.4 Hz, 2H).

***Methyl 2-(3-oxo-1,2-benzisothiazol-3(2H)-2-yl)-propanoic acetate (4a):*** Compound ***4a*** was prepared as described previously [93]. Briefly, a chilled solution of ***3a*** (1.8 g; 3.78 mmol) in 25 mL $CH_2Cl_2$ was added bromine (0.60 g; 3.78 mmol) and the reaction mixture was stirred for 30 min. Triethylamine (0.77 g; 7.5 mmol) was then added and the resulting mixture was stirred for 5 min. The reaction mixture was washed with water (2 × 15 mL) and the organic layer was dried over anhydrous sodium sulfate, dried and concentrated, leaving a pure compound ***4a*** as yellowish oil (1.8 g; 100% yield). $^1$H NMR ($CDCl_3$): δ 1.70 (d, *J* = 7.8 Hz, 3H), 3.77 (s, 3H), 5.50 (q, *J* = 8.2 Hz, 1H), 7.42 (t, *J* = 7.2 Hz, 1H), 7.56-7.66 (m, 2H), 8.09 (d, *J* = 8.8 Hz, 1H).

***Methyl 2-(3-oxo-1,2-benzisothiazol-3(2H)-2-yl)-3-phenylpropanoic acetate (4b):*** Yellow oil (14.92g; 70% yield). $^1$H NMR ($CDCl_3$): δ 3.24 (dd, *J* = 13.69, 9.83 Hz, 1H), 3.51 (dd, *J* = 14.52, 5.79 Hz, 1H), 3.74 (s, 3H), 5.68 (dd, *J* = 10.09, 5.80 Hz, 1H), 7.17-7.25 (m, 5H), 7.33-7.40 (m, 1H), 7.50-7.63 (2H), 7.95-7.99 (m, 1H).

***Methyl 2-(3-oxo-1,2-benzisothiazol-3(2H)-2-yl)-3-(3-fluorophenyl)propanoic acetate (4c):*** Reddish oil (2.3g; 92% yield). $^1$H NMR ($CDCl_3$): δ 3.23 (dd, *J* = 11.2, 8.9 Hz, 1H), 3.49 (dd, *J* = 11.2, 8.9 Hz, 1H), 3.76 (s, 3H), 5.62-5.69 (m, 1H), 6.82-7.00 (m, 3H), 7.10-8.00 (m, 5H).

***Methyl 2-(3-oxo-1,2-benzisothiazol-3(2H)-2-yl)-4-phenylbutanoic acetate (4d):*** Yellow oil (1.61g; 90% yield). $^1$H NMR ($CDCl_3$): δ 2.23-2.35 (m, 1H), 2.43-2.55 (m, 1H), 2.64 (t, *J* = 8.3 Hz, 2H), 3.75 (s, 3H), 5.40-5.46 (m, 1H), 7.16-7.68 (m, 5H), 8.03-8.08 (m, 1H).

***2-(3-Oxo-1,2-benzisothiazol-3(2H)-2-yl)-propanoic acid (5a):*** Compound ***5a*** was prepared as described previously [93]. Briefly, a solution of compound ***4a*** (2.37g; 10 mmol) was dissolved in 15 mL 1,4-dioxane and treated with 20 mL 1 M LiOH at 0 °C for 1 h. The solution was neutralized and the solvent was removed. The residue was adjusted to pH 1, forming a precipitate which was collected with vacuum filtration and washed with diethyl ether to give pure compound ***5a*** as a gray solid (1.73 g; 77% yield), mp 201-202 °C. $^1$H NMR (DMSO-$d_6$): δ 1.57 (d, *J* = 6.0 Hz, 3H), 5.14 (q, *J* = 6.5 Hz, 1H), 7.45 (t, *J* = 6.2 Hz, 1H), 7.70 (t, *J* = 6.0 Hz, 1H), 7.88 (d, *J* = 6.5 Hz, 1H), 7.97 (d, *J* = 6.5 Hz, 1H).

***2-(3-Oxo-1,2-benzisothiazol-3(2H)-2-yl)-3-phenylpropanoic acid (5b):*** White solid (2.43g; 44% yield), mp 180-182 °C. $^1$H NMR (DMSO-$d_6$): δ 3.23 (dd, *J* = 15.1, 11.0 Hz,

1H), 3.45 (dd, *J* = 15.1, 4.7 Hz, 1H), 5.42 (dd, *J* = 10.4, 4.7 Hz, 1H), 7.12-7.32 (m, 5H), 7.37-7.44 (m, 1H), 7.63-7.70 (m, 1H), 7.77-7.82 (m, 1H), 7.90-7.95 (m, 1H), 13.40 (br s, 1H).

***2-(3-Oxo-1,2-benzisothiazol-3(2H)-2-yl)-3-(3-fluorophenyl)propanoic acid (5c):*** Yellow oil (1.87g; 98% yield). $^1$H NMR ($CDCl_3$): δ 3.29-3.39 (m, 1H), 3.52-3.60 (m, 1H), 5.52-5.58 (m, 1H), 6.80-7.72 (m, 7H), 7.98-8.03 (m, 1H).

***2-(3-Oxo-1,2-benzisothiazol-3(2H)-2-yl)-4-phenylbutanoic acid (5d):*** Yellow solid (1.36g; 80% yield), mp 149-150 °C. $^1$H NMR (DMSO-$d_6$): δ 2.20-2.48 (m, 2H), 2.61 (t, *J* = 6.7 Hz, 2H), 5.05-5.11 (m, 1H), 7.18-7.36 (m, 5H), 7.46 (t, *J* = 6.7 Hz, 1H), 7.71 (t, *J* = 6.7 Hz, 1H), 7.90 (d, *J* = 8.3 Hz, 1H), 8.00 (d, *J* = 8.3 Hz, 1H).

***(3-Oxo-1,2-benzisothiazol-3(2H)-2-yl)-acetic acid, 2'-(3-fluorobenzoyl)hydrazide (6a)*****:** To a stirred solution of compound ***2*** (0.58 g; 2mmol) in dry DMF (6 mL) was added EDCI (0.46 g; 2.4 mmol), followed by ***m***-fluorobenzhydrazide (0.31 g; 2 mmol), and the reaction mixture was stirred at room temperature overnight. The solvent was removed and the residue was taken up in ethyl acetate (50 mL). The organic layer was washed with brine (15 mL), dried over anhydrous sodium sulfate, filtered, and concentrated. The crude product was purified using flash chromatography (silica gel/ethyl acetate/hexanes) to give pure compound ***6a***, as a white solid (0.27 g; 32% yield), mp 207-209 °C. $^1$H NMR (DMSO-$d_6$): δ 4.63 (s, 2H), 7.40-8.01 (m, 8H), 10.41 (s, 1H), 10.60 (s, 1H).

***(3-Oxo-1,2-benzisothiazol-3(2H)-2-yl)-acetic acid, 2'-(3-chlorobenzoyl)hydrazide (6b):*** Yellow solid (42% yield), mp 88-90 °C. $^1$H NMR (DMSO-$d_6$): δ 4.66 (s, 2H), 7.35-7.97 (m, 8H), 10.40 (s, 1H), 10.58 (s, 1H).

***(3-Oxo-1,2-benzisothiazol-3(2H)-2-yl)-acetic acid, 2-(2-phenylacetyl)hydrazide (6c):*** White solid (28% yield), mp 230-232 °C. $^1$H NMR (DMSO-$d_6$): δ 3.47 (s, 2H), 4.56 (s, 2H), 7.20-7.35 (m, 5H), 7.43 (t, *J* = 5.3 Hz, 1H), 7.69 (t, *J* = 5.3 Hz, 1H), 7.86 (d, *J* = 6.7 Hz, 1H), 7.98 (d, *J* = 6.7 Hz, 1H), 10.21 (s, 1H), 10.29 (s, 1H).

***(3-Oxo-1,2-benzisothiazol-(3(2H)-2-yl)-acetic acid, 2-[2-(4-methoxyphenyl)acetyl]hydrazide (6d):*** Gray solid (47% yield), mp 203-205 °C. $^1$H NMR (DMSO-$d_6$): δ 3.40 (s, 2H), 3.74 (s, 3H), 4.56 (s, 2H), 6.88 (d, *J* =8.0 Hz, 2H), 7.20 (d, *J* = 8.0 Hz, 2H), 7.45 (t, *J* = 7.3 Hz, 1H), 7.71 (t, *J* = 7.3 Hz, 1H), 7.89 (d, *J* = 8.0 Hz, 1H), 7.98 (d, *J* = 8.0 Hz, 1H), 10.18 (s, 1H), 10.28 (s, 1H).

***2-(3-Oxo-1,2-benzisothiazol-3(2H)-2-yl)-propanoic acid, 2-[2-(4-methoxyphenyl) acetyl]hydrazide (6e):*** White solid (21% yield), mp 135-137 °C. $^1$H NMR (DMSO-$d_6$): δ 1.46 (d, *J* = 4.7 Hz, 3H), 3.40 (s, 2H), 3.72 (s, 3H), 5.30-5.40 (m, 1H), 6.82 (d, *J* = 9.3 Hz, 2H), 7.19 (d, *J* = 9.3 Hz, 2H), 7.40 (t, *J* = 6.7 Hz, 1H), 7.65 (t, *J* = 6.7 Hz, 1H), 7.86 (d, *J* = 7.3 Hz, 1H), 7.95 (d, *J* = 7.3 Hz, 1H), 10.11 (s, 1H), 10.30 (s, 1H).

***2-(3-Oxo-1,2-benzisothiazol-3(2H)-2-yl)-3-phenylpropanoic acid, 2-(2-phenylacetyl)hydrazide (6f):*** Yellow oil (52% yield). $^1$H NMR (DMSO-$d_6$): δ 3.18-3.42 (m, 2H), 3.56 (s, 2H), 5.81-5.87 (m, 1H), 7.00-7.60 (m, 14H).

***2-(3-Oxo-1,2-benzisothiazol-3(2H)-2-yl)-3-phenylpropanoic acid, 2-[2-(4-methoxyphenyl)acetyl]hydrazide (6g):*** Yellow oil (53% yield). $^1$H NMR (DMSO-$d_6$): δ 3.16-3.45 (m, 2H), 3.51 (s, 2H), 3.75 (s, 3H), 5.76-5.81 (m, 1H), 6.78-7.82 (m, 13H).

***2-(3-Oxo-1,2-benzisothiazol-3(2H)-2-yl)-3-phenylpropanoic acid, 2-(3-fluorobenzoyl)hydrazide (6h):*** Brown oil (53% yield). $^1$H NMR (DMSO-$d_6$): δ 3.10-3.50 (m, 2H), 5.82-5.91 (m, 1H), 6.97-7.65 (m, 13H).

***2-(3-Oxo-1,2-benzisothiazol-3(2H)-2-yl)-3-phenylpropanoic acid, 2-(3-chlorobenzoyl)hydrazide (6i):*** Brown solid (50% yield), mp 96-97 °C. $^1$H NMR (DMSO-$d_6$): δ 3.20-3.60 (m, 2H), 5.64-5.75 (m, 1H), 7.20-7.98 (m, 13H).

***2-(3-Oxo-1,2-benzisothiazol-3(2H)-2-yl)-3-phenylpropanoic acid, 2-(4-fluorobenzoyl)hydrazide (6j):*** White solid (77% yield), mp 189-191 °C. $^1$H NMR ($CDCl_3$): δ 3.55 (dd, *J* = 41.8, 13.5 Hz, 2H), 5.85-5.90 (m, 1H), 7.00-7.47 (m, 10H), 7.71-7.83 (m, 2H), 8.05-8.13 (m, 1H), 9.08 (s, 1H), 9.50 (s, 1H).

***2-(3-Oxo-1,2-benzisothiazol-3(2H)-2-yl)-3-phenylpropanoic acid, 2-(4-chlorobenzoyl)hydrazide (6k):*** Yellow-green solid (92% yield), mp 110-112 °C. $^1$H NMR ($CDCl_3$): δ 3.29 (dd, *J* = 13.9, 9.1 Hz, 1H), 3.51 (dd, *J* = 14.3, 6.3 Hz, 1H), 5.82 (dd, *J* = 9.0, 6.6 Hz, 1H), 7.09-7.19 (m, 4H), 7.27-7.37 (m, 4H), 7.49-7.59 (m, 2H), 7.68-7.74 (m, 2H), 7.86-7.91 (m, 2H), 9.10 (s, 1H), 10.06 (s, 1H).

***2-(3-Oxo-1,2-benzisothiazol-3(2H)-2-yl)-3-phenylpropanoic acid, 2-(4-cyanobenzoyl)hydrazide (6l):*** White solid (42% yield), mp 168-170 °C. $^1$H NMR (DMSO-$d_6$): δ 3.55 (dd, *J* = 26.0, 14.3 Hz, 2H), 5.75 (dd, *J* = 9.6, 4.7 Hz, 1H), 7.20-7.45 (m, 6H), 7.49-7.55 (m, 1H), 7.63-7.69 (m, 1H), 7.87-8.03 (m, 4H), 8.73 (br s, 1H), 10.51 (br s, 1H), 10.75-10.87 (m, 1H)

***2-(3-Oxo-1,2-benzisothiazol-3(2H)-2-yl)-3-(3-fluorophenyl)propanoic acid, 2-(3-fluorobenzoyl)hydrazide (6w):*** White solid (63% yield), mp 93-95 °C. $^1$H NMR ($CDCl_3$): δ 3.15-3.40 (m, 2H), 5.39 (t, J = 7.1 Hz, 1H), 6.78-7.99 (m, 12H).

***2-(3-Oxo-1,2-benzisothiazol-3(2H)-2-yl)-4-phenylbutanoic acid, 2-(3-fluorobenzoyl)hydrazide (6x):*** White solid (47% yield), mp 105-106 °C. $^1$H NMR ($CDCl_3$): δ 2.45-2.72 (m, 4H), 5.11-5.17 (m, 1H), 7.00-8.02 (m, 13H).

***2-[(2-m-Fluorophenyl-1,3,4-oxadiazol-5-yl)methyl]-1,2-benzisothiazol-3(2H)-3-one (7a):*** To a stirred solution of compound ***6a*** (0.27 g; 0.63 mmol) in $CH_2Cl_2$ (10 mL) was added *p*-toluenesulfonyl chloride (0.12 g; 0.63 mmol) followed by triethylamine (0.20 mL; 1.5 mmol) and the resulting reaction mixture was stirred at room temperature overnight. $CH_2Cl_2$ (30 mL) was added and the solution was washed with water (30 mL), and brine (30 mL). The organic layer was dried over anhydrous sodium sulfate, filtered and concentrated. The crude product was purified by flash chromatography (silica gel/ ethyl acetate/hexanes) to give ***7a*** as a white solid (0.1g; 39% yield), mp 149-151 °C. $^1$H NMR ($CDCl_3$): δ 5.40 (s, 2H), 7.20-7.82 (m, 7H), 8.09-8.12 (m, 1H). $^{13}$C NMR ($CDCl_3$): δ 165.4, 164.0, 161.9, 161.5, 140.5, 132.7, 131.0, 127.2, 126.0, 125.2, 123.2, 122.9, 120.6, 119.3, 119.1, 114.3, 37.7. HRMS (ESI): Calcd for $C_{16}H_{10}FN_3O_2SNa$, m/z $[M+Na]^+$: 350.0375, found 350.0366.

***2-[(2-m-Chlorophenyl-1,3,4-oxadiazol-5-yl)methyl]-1,2-benzisothiazol-3(2H)-3-one (7b):*** White solid (57% yield), mp 136-137 °C. $^1$H NMR ($CDCl_3$): δ 5.40 (s, 2H), 7.40-7.68 (m, 5H), 7.90-8.12 (m, 3H). $^{13}$C NMR ($CDCl_3$): δ 165.4, 164.8, 161.9, 140.5, 135.3, 132.7, 132.2, 130.4, 129.1, 127.2, 127.2, 126.0, 125.2, 125.0, 123.3, 120.6, 37.7. HRMS (ESI): Calcd for $C_{16}H_{10}ClN_3O_2SNa$, m/z $[M+Na]^+$: 366.0080, found 366.0068.

***2-[(2-Benzyl-1,3,4-oxadiazol-5-yl)methyl]-1,2-benzisothiazol-3(2H)-3-one (7c):*** Yellow solid (0.10 g; 35% yield), mp 93-95 °C. $^1$H NMR ($CDCl_3$): δ 4.16 (s, 2H), 5.24 (s, 2H), 7.23-7.35 (m, 5H), 7.43 (t, *J* = 5.1 Hz, 1H), 7.53 (d, *J* = 5.5 Hz, 1H), 7.64 (t, *J* = 5.1 Hz, 1H), 8.05 (d, *J* = 5.5 Hz, 1H). $^{13}$C NMR ($CDCl_3$): δ 166.7, 165.4, 162.2, 140.5, 133.3, 132.6, 128.9, 128.8, 127.6, 127.1, 126.0, 123.3, 120.6, 37.7, 31.7. HRMS (ESI): Calcd for $C_{17}H_{13}N_3O_2SNa$, m/z $[M+Na]^+$: 346.0626, found 346.0635.

***2-[(2-p-Methoxybenzyl-1,3,4-oxadiazol-5-yl)methyl]-1,2-benzisothiazol-3(2H)-3-one (7d):*** Yellow solid (52% yield), mp 92-93 °C. $^{1}$H NMR ($CDCl_3$): δ 3.79 (s, 3H), 4.11 (s, 2H), 5.26 (s, 2H), 6.83 (d, J = 8.8 Hz, 2H), 7.20 (d, *J* = 8.8 Hz, 2H), 7.45 (d, *J* = 7.7 Hz, 1H), 7.53 (d, *J* = 8.9 Hz, 1H), 7.65 (t, *J* = 7.7 Hz, 1H), 8.08 (d, *J* = 8.9 Hz, 1H). $^{13}$C NMR ($CDCl_3$): δ 167.1, 165.4, 162.1, 159.0, 140.5, 132.6, 129.9, 127.1, 125.9, 125.2, 123.2, 120.6, 114.3, 55.3, 37.7, 30.9. HRMS (ESI): Calcd for $C_{18}H_{15}N_3O_3SNa$, m/z $[M+Na]^+$: 376.0732, found 376.0735.

***2-[(2-p-Methoxybenzyl-1,3,4-oxadiazol-5-yl)ethyl]-1,2-benzisothiazol-3(2H)-3-one (7e):*** White solid (48% yield), mp 139-141 °C. $^{1}$H NMR ($CDCl_3$): δ 1.86 (d, *J* = 7.7 Hz, 3H), 3.76 (s, 3H), 4.09 (dd, *J* = 19.6, 13.4 Hz, 2H), 6.20 (q, *J* = 7.2 Hz, 1H), 6.79 (d, *J* = 8.8 Hz, 2H), 7.16 (d, *J* = 8.8 Hz, 2H), 7.40 (t, *J* = 6.7 Hz, 1H), 7.52 (d, *J* = 8.3 Hz, 1H), 7.61 (t, *J* = 6.7 Hz, 1H), 8.03 (d, *J* = 8.3 Hz, 1H). $^{13}$C NMR ($CDCl_3$): δ 166.8, 165.4, 165.1, 158.9, 140.4, 132.4, 129.8, 127.0, 125.8, 125.3, 124.0, 120.6, 114.2, 55.2, 44.6, 30.8, 17.9. HRMS (ESI): Calcd for $C_{19}H_{17}N_3O_3SNa$, m/z $[M+Na]^+$: 390.0888, found 390.0869.

***2-[2-Phenyl-1-(2-benzyl-1,3,4-oxadiazol-5-yl)ethyl]-1,2-benzisothiazol-3(2H)-3-one (7f):*** Colorless oil (56% yield). $^{1}$H NMR ($CDCl_3$): δ 3.47 (dd, *J* = 13.9, 8.6 Hz, 1H), 3.67 (dd, *J* = 13.9, 8.6 Hz, 1H), 4.12 (d, *J* = 12.2 Hz, 2H), 6.38 (dd, *J* = 8.9, 6.9 Hz, 1H), 7.12-7.62 (m, 13H), 7.96 (d, *J* = 9.1 Hz, 1H). $^{13}$C NMR ($CDCl_3$): δ 166.3, 165.3, 164.6, 140.4, 134.8, 133.3, 132.4, 129.1, 129.0, 128.8, 128.7, 127.5, 127.3, 127.0, 125.7, 123.6, 120.5, 49.8, 38.2, 31.7. HRMS (ESI): Calcd for $C_{24}H_{19}N_3O_2SNa$, m/z $[M+Na]^+$: 436.1096, found 436.1077.

***2-[2-Phenyl-1-(2-p-mehoxybenzyl-1,3,4-oxadiazol-5-yl)ethyl]-1,2-benzisothiazol-3(2H)-3-one (7g):*** Colorless oil (64% yield). $^{1}$H NMR ($CDCl_3$): δ 3.48 (dd, *J* = 13.6, 9.9 Hz, 1H), 3.68 (dd, *J* = 13.6, 9.9 Hz, 1H), 3.77 (s, 3H), 4.06 (d, *J* = 3.1 Hz, 2H), 6.37 (dd, *J* = 9.1, 7.0 Hz, 1H), 6.77-7.62 (m, 12H), 7.92-7.98 (m, 1H). $^{13}$C NMR ($CDCl_3$): δ 152.3, 150.8, 150.1, 126.0, 120.5, 117.9, 117.6, 115.4, 114.7, 114.2, 112.9, 112.6, 111.3, 110.9, 109.3, 106.1, 99.9, 40.9, 35.5, 23.8, 16.4. HRMS (ESI): Calcd for $C_{25}H_{21}N_3O_3SNa$, m/z $[M+Na]^+$: 466.1201, found 466.1178.

***2-[2-Phenyl-1-(2-m-fluorophenyl-1,3,4-oxadiazol-5-yl)ethyl]-1,2-benzisothiazol-3(2H)-one (7h):*** Colorless oil (33% yield). $^{1}$H NMR ($CDCl_3$): δ 3.54 (dd, *J* = 12.9, 9.2 Hz, 1H), 3.78 (dd, *J* = 12.9, 9.2 Hz, 1H), 6.52 (dd, *J* = 8.8, 7.0 Hz, 1H), 7.19-8.03 (m, 13H). $^{13}$C NMR ($CDCl_3$): δ 165.3, 164.4, 164.2, 161.1, 134.9, 132.5, 131.0, 129.2, 128.8, 127.4, 127.1, 125.8, 122.9, 120.6, 119.3, 119.0, 114.3, 114.0, 49.9, 38.2. HRMS (ESI): Calcd for $C_{23}H_{17}N_3O_2SF$, m/z $[M + Na]^+$: 440.0845, found 440.0840.

***2-[2-Phenyl-1-(2-m-chlorophenyl-1,3,4-oxadiazol-5-yl)ethyl]-1,2-benzisothiazol-3(2H)-one (7i):*** Colorless oil (26% yield). $^{1}$H NMR ($CDCl_3$): δ 3.55 (dd, *J* = 13.1, 8.2 Hz, 1H), 3.81 (dd, *J* = 13.1, 8.2 Hz, 1H), 6.53 (dd, *J* = 8.8, 7.0 Hz, 1H), 7.20-7.63 (m, 11H), 7.97-8.02 (m, 2H). $^{13}$C NMR ($CDCl_3$): δ 165.6, 165.4, 164.2, 164.0, 135.1, 132.4, 132.0, 129.4, 129.2, 129.0, 128.7, 127.4, 127.2, 125.8, 125.1, 123.8, 123.4, 120.6, 50.0, 38.3. HRMS (ESI): Calcd for $C_{23}H_{17}N_3O_2SCl$, m/z $[M + Na]^+$: 456.0550, found 456.0559.

***2-[2-Phenyl-1-(2-p-fluorophenyl-1,3,4-oxadiazol-5-yl)ethyl]-1,2-benzisothiazol-3(2H)-one (7j):*** Light yellow solid (23% yield), mp 161-163 °C. $^{1}$H NMR ($CDCl_3$): δ 3.56 (dd, *J* = 14.3, 8.9 Hz, 1H), 3.8 (dd, *J* = 14.2, 7.0 Hz, 1H), 6.51 (dd, *J* = 8.7, 7.0 Hz, 1H),

7.12-7.44 (m, 9H), 7.51-7.66 (m, 2H), 7.96-8.04 (m, 2H). $^{13}C$ NMR ($CDCl_3$): δ 166.2, 165.2, 164.8, 140.4, 134.9, 132.4, 129.5, 129.2, 128.7, 127.4, 127.1, 125.8, 123.7, 120.6, 119.6, 116.5, 116.3, 49.8, 38.2. HRMS (ESI): Calcd for $C_{23}H_{16}FN_3O_2SNa$, m/z $[M+Na]^+$: 440.0845; found 440.0824.

***2-[2-Phenyl-1-(2-p-chlorophenyl-1,3,4-oxadiazol-5-yl)ethyl]-1,2-benzisothiazol-3(2H)-one (7k):*** White solid (24% yield), mp 164-166 °C. $^1H$ NMR ($CDCl_3$): δ 3.55 (dd, *J* = 12.8, 8.8 Hz, 1H), 3.80 (dd, *J* = 14.7, 7.0 Hz, 1H), 6.51 (dd, *J* = 8.7, 7.0 Hz, 1H), 7.18-7.35 (m, 5H), 7.37-7.48 (m, 3H), 7.52-7.57 (m, 1H), 7.59-7.66 (m, 1H), 7.89-7.96 (m, 2H), 7.99-8.04 (m, 1H). $^{13}C$ NMR ($CDCl_3$): δ 165.2, 164.8, 164.1, 140.4, 138.4, 134.9, 132.5, 129.4, 129.2, 128.7, 128.4, 127.4, 127.1, 125.8, 123.6, 121.7, 120.6, 49.8, 38.2. HRMS (ESI): Calcd for $C_{23}H_{16}ClN_3O_2SNa$, m/z $[M+Na]^+$: 456.0549; found 456.0554.

***2-[2-Phenyl-1-(2-p-cyanophenyl-1,3,4-oxadiazol-5-yl)ethyl]-1,2-benzisothiazol-3(2H)-one (7l):*** White solid (20% yield), mp 182-184 °C. $^1H$ NMR ($CDCl_3$): δ 3.57 (dd, *J* = 14.4, 8.7 Hz, 1H), 3.81 (dd, *J* = 14.3, 7.1 Hz, 1H), 6.52 (dd, *J* = 8.7, 7.1 Hz, 1H), 7.18-7.35 (m, 5H), 7.38-7.44 (m, 1H), 7.53-7.57 (m, 1H), 7.60-7.66 (m, 1H), 7.74-7.80 (m, 2H), 7.98-8.04 (m, 1H), 8.08-8.14 (m, 2H). $^{13}C$ NMR ($CDCl_3$): δ 165.3, 164.8, 164.1, 140.3, 134.7, 132.8, 132.6, 130.2, 129.4, 129.1, 128.8, 127.6, 127.1, 125.9, 123.5, 120.6, 117.8, 115.5, 49.8, 38.2. HRMS (ESI): Calcd for $C_{24}H_{16}N_4O_2SNa$, m/z $[M+Na]^+$: 447.0892; found 447.0883.

***2-[2-Phenyl-1-(2-phenyl-1,3,4-oxadiazol-5-yl)ethyl]-1,2-benzisothiazol-3(2H)-one (7m):*** To a stirred solution of compound ***5b*** (1.20 g; 4mmol) in dry $CH_3CN$ (40 mL) was added phenyl hydrazide (0.55 g; 4 mmol) followed by diisopropylethylamine (1.55 g; 12 mmol), and then TBTU (1.42 g; 4.4 mmol). The resulting reaction mixture was stirred at

room temperature for 24 h. TLC of the reaction mixture showed formation of the intermediate. Diisopropylethyl amine (1.03 g; 8 mmol) and *p*-toluenesulfonyl chloride (2.29 g; 12 mmol) were added and the reaction mixture was stirred at room temperature overnight. Removal of the solvent left a crude residue which was adsorbed on silica gel and purified using flash chromatography (silica gel/ethyl acetate/ hexanes) to give compound ***7m*** as an yellow oil (0.37g; 23% yield). $^{1}$H NMR ($CDCl_3$): δ 3.55 (dd, *J* = 14.3, 8.7 Hz, 1H), 3.81 (dd, *J* = 14.8, 6.9 Hz, 1H), 6.53 (dd, *J* = 8.8, 6.9 Hz, 1H), 7.18-7.29 (m, 3H), 7.31-7.35 (m, 2H), 7.38-7.42 (m, 1H), 7.44-7.55 (m, 4H), 7.59-7.65 (m, 1H), 7.97-8.04 (m, 3H). $^{13}$C NMR ($CDCl_3$): δ 165.6, 165.2, 163.9, 140.4, 135.0, 132.4, 132.0, 129.2, 129.0, 128.7, 127.4, 127.1, 127.0, 125.7, 123.7, 123.3, 120.6, 49.9, 38.2. HRMS (ESI): Calcd for $C_{23}H_{17}N_3O_2SNa$, m/z $[M+Na]^+$: 422.0939; found 422.0923.

***2-[2-Phenyl-1-(2-p-methoxyphenyl-1,3,4-oxadiazol-5-yl)ethyl]-1,2-benzisothiazol-3(2H)-one (7n):*** White solid (20% yield), mp 187-189 °C. $^{1}$H NMR ($CDCl_3$): δ 3.54 (dd, *J* = 13.3, 8.7 Hz, 1H), 3.79 (dd, *J* = 14.3, 7.0 Hz, 1H), 3.85 (s, 3H), 6.49 (dd, *J* = 8.9, 7.0 Hz, 1H), 6.93-6.98 (m, 2H), 7.17-7.35 (m, 5H), 7.37-7.43 (1H), 7.51-7.55 (m, 1H), 7.59-7.64 (m, 1H), 7.90-7.95 (m, 2H), 7.99-8.03 (m, 1H). $^{13}$C NMR ($CDCl_3$): δ 165.6, 165.2, 163.4, 162.5, 140.4, 135.1, 132.4, 129.2, 128.9, 128.7, 127.3, 127.0, 125.7, 123.7, 120.6, 115.7, 114.4, 55.5, 49.8, 38.2. HRMS (ESI): Calcd for $C_{24}H_{19}N_3O_3SNa$, m/z $[M+Na]^+$: 452.1045, found 452.1042.

***2-[2-Phenyl-1-(2-p-ethoxyphenyl-1,3,4-oxadiazol-5-yl)ethyl]-1,2-benzisothiazol-3(2H)-one (7o):*** White solid (28% yield), mp 98-100 °C. $^{1}$H NMR ($CDCl_3$): δ 1.43 (t, *J* = 7.0 Hz, 3H), 3.54 (dd, *J* = 14.0, 8.9 Hz, 1H), 3.79 (dd, *J* = 14.7, 6.9 Hz, 1H), 4.07 (q, *J* = 7.0, 2H), 6.49 (dd, *J* = 8.5, 6.9 Hz, 1H), 6.91-6.96 (m, 2H), 7.17-7.28 (m, 3H), 7.30-7.35

(m, 2H), 7.37-7.42 (m, 1H), 7.51-7.55 (m, 1H), 7.59-7.64 (m, 1H), 7.89-7.93 (m, 2H), 7.99-8.03 (m, 1H). $^{13}$C NMR ($CDCl_3$): δ 165.6, 165.2, 163.3, 162.0, 140.4, 135.1, 132.4, 129.2, 128.9, 128.7, 127.3, 127.0, 125.7, 123.7, 120.6, 115.5, 114.8, 63.7, 49.8, 38.2, 14.6. HRMS (ESI): Calcd for $C_{25}H_{21}N_3O_3SNa$, m/z $[M+Na]^+$: 466.1201; found 466.1196.

***2-[2-Phenyl-1-(2-p-pyridyl-1,3,4-oxadiazol-5-yl)ethyl]-1,2-benzisothiazol-3-one (7p):*** White solid (20% yield), mp 176-177 °C. $^1$H NMR ($CDCl_3$): δ 3.57 (dd, *J* = 14.2, 8.7, 1H), 3.81 (dd, *J* = 14.3, 6.9 Hz, 1H), 6.53 (dd, *J* = 8.6, 7.1 Hz, 1H),7.19-7.35 (m, 5H), 7.39-7.44 (m, 1H), 7.53-7.57 (m, 1H), 7.61-7.66 (m, 1H), 7.82-7.87 (m, 2H), 8.00-8.05 (m, 1H), 8.75-8.82 (m, 2H). $^{13}$C NMR ($CDCl_3$): δ 165.3, 165.0, 163.8, 150.9, 140.3, 134.7, 132.6, 130.4, 129.2, 128.8, 127.5, 127.1, 125.9, 123.5, 120.6, 120.5, 49.9, 38.2. HRMS (ESI): Calcd for $C_{22}H_{16}N_4O_2SNa$, m/z $[M+Na]^+$: 423.0892; found 423.0880.

***2-[2-Phenyl-1-(2-m-pyridyl-1,3,4-oxadiazol-5-yl)ethyl]-1,2-benzisothiazol-3(2H)-one (7q):*** White solid (19% yield), mp 148-149 °C. $^1$H NMR ($CDCl_3$): δ 3.57 (dd, *J* = 14.1, 8.7 Hz, 1H), 3.81 (dd, *J* = 13.8, 7.1 Hz, 1H), 6.53 (dd, *J* = 8.9, 7.1 Hz, 1H), 7.18-7.35 (m, 5H), 7.38-7.45 (m, 2H), 7.53-7.56 (m, 1H), 7.61-7.66 (m, 1H), 8.00-8.04 (m, 1H), 8.25-8.30 (m, 1H), 8.73-8.78 (m, 1H), 9.19-9.23 (m, 1H). $^{13}$C NMR ($CDCl_3$): δ 165.3, 164.5, 163.5, 152.7, 148.0, 140.4, 134.8, 134.4, 132.5, 129.2, 128.8, 127.5, 127.1, 125.8, 123.8, 123.6, 120.6, 49.9, 38.3 HRMS (ESI): Calcd for $C_{22}H_{16}N_4O_2SNa$, m/z $[M+Na]^+$: 423.0892; found 423.0884.

***2-[2-Phenyl-1-(2-(2-furyl)-1,3,4-oxadiazol-5-yl)ethyl]-1,2-benzisothiazol-3(2H)-one (7r):*** White solid (32% yield), mp 142-144 °C. $^1$H NMR (DMSO-$d_6$): δ 3.56 (dd, *J* = 14.0, 10.8 Hz, 1H), 3.73 (dd, *J* = 14.3, 5.1 Hz, 1H), 6.42 (dd, *J* = 10.6, 5.1 Hz, 1H), 6.77-6.80 (m, 1H), 7.14-7.27 (m, 3H), 7.28-7.33 (m, 2H), 7.36-7.45 (m, 2H), 7.65-7.72 (m, 1H),

7.80-7.84 (m, 1H), 7.94-7.99 (m, 1H), 8.04-8.07 (m, 1H). $^{13}$C NMR ($CDCl_3$): δ 165.4, 163.4, 158.6, 146.2, 140.5, 139.0, 135.1, 132.6, 129.4, 128.9, 127.6, 127.3, 126.0, 123.8, 120.8, 115.1, 112.4, 49.9, 38.4. HRMS (ESI): Calcd for $C_{21}H_{15}N_3O_3SNa$, m/z $[M+Na]^+$:412.0732; found 412.0746.

***2-[2-Phenyl-1-(2-(2-thiophenyl)-1,3,4-oxadiazol-5-yl)ethyl]-1,2-benzisothiazol-3(2H)-one (7s):*** White solid (25% yield), mp 128-130 °C. $^1$H NMR ($CDCl_3$): δ 3.51 (dd, *J* = 14.6, 8.8 Hz, 1H), 3.76 (dd, *J* = 14.2, 7.0 Hz, 1H), 6.46 (dd, *J* = 9.3, 7.0 Hz, 1H), 7.08-7.12 (m, 1H), 7.15-7.32 (m, 5H), 7.35-7.40 (m, 1H), 7.49-7.54 (m, 2H), 7.57-7.63 (m, 1H), 7.65-7.69 (m, 1H), 7.96-8.00 (m, 1H). $^{13}$C NMR ($CDCl_3$): δ 165.2, 163.3, 161.8, 140.4, 134.9, 132.4, 130.7, 130.5, 129.2, 128.7, 128.2, 127.4, 127.0, 125.8, 124.5, 123.7, 120.6, 49.8, 38.3. HRMS (ESI): Calcd for $C_{21}H_{15}N_3O_2S_2Na$, m/z $[M+Na]^+$: 428.0503; found 428.0496.

***2-[2-Phenyl-1-(2-methyl-1,3,4-oxadiazol-5-yl)ethyl]-1,2-benzisothiazol-3(2H)-one (7t):*** White solid (25% yield), mp 98-99 °C. $^1$H NMR ($CDCl_3$): δ 2.48 (s, 3H), 3.49 (dd, *J* = 14.1, 9.1 Hz, 1H), 3.75 (dd, *J* = 14.3, 6.6 Hz, 1H), 6.39 (dd, *J* = 9.1, 6.6 Hz, 1H), 7.17-7.31 (m, 5H), 7.37-7.42 (m, 1H), 7.52-7.55 (m, 1H), 7.59-7.64 (m, 1H), 7.98-8.01 (m, 1H). $^{13}$C NMR ($CDCl_3$): δ 165.2, 164.8, 164.3, 140.3, 135.0, 132.4, 129.1, 128.7, 127.3, 127.0, 125.7, 123.7, 120.6, 49.6, 37.9, 11.0. HRMS (ESI): Calcd for $C_{18}H_{15}N_3O_2SNa$, m/z $[M+Na]^+$:360.0783; found 360.0779.

***2-[2-Phenyl-1-(2-ethyl-1,3,4-oxadiazol-5-yl)ethyl]-1,2-benzisothiazol-3(2H)-one (7u):*** White solid (21% yield), mp 78-80 °C. $^1$H NMR ($CDCl_3$): δ 1.32 (t, *J* = 7.6 Hz, 3H), 2.84 (q, *J* = 7.6 Hz, 2H), 3.49 (dd, *J* = 14.1, 9.0 Hz, 1H), 3.73 (dd, *J* = 14.2, 6.8 Hz, 1H), 6.39 (dd, *J* = 8.9, 6.9 Hz, 1H), 7.16-7.32 (m, 5H), 7.36-7.43 (m, 1H), 7.50-7.66 (m, 2H),

7.97-8.02 (m, 1H). $^{13}$C NMR ($CDCl_3$): δ 168.9, 165.2, 164.1, 140.4, 135.0, 132.4, 129.2, 128.7, 127.3, 127.0, 125.7, 123.7, 120.6, 49.7, 38.1, 19.1, 10.6. HRMS (ESI): Calcd for $C_{19}H_{17}N_3O_2SNa$, m/z $[M+Na]^+$: 374.0939; found 374.0932.

***2-[2-Phenyl-1-(2-propyl-1,3,4-oxadiazol-5-yl)ethyl]-1,2-benzisothiazol-3(2H)-one (7v):*** Light yellow solid (25% yield), mp 83-84 °C. $^1$H NMR ($CDCl_3$): δ 0.95 (t, *J* = 7.4 Hz, 3H), 1.69-1.80 (m, 2H), 2.74-2.81 (m, 2H), 3.49 (dd, *J* = 14.1, 9.0 Hz, 1H), 3.73 (dd, *J* = 14.4, 6.8 Hz, 1H), 6.40 (dd, *J* = 8.7, 6.8 Hz, 1H), 7.17-7.30 (m, 5H), 7.37-7.42 (m, 1H), 7.52-7.56 (m, 1H), 7.59-7.64 (m, 1H), 7.97-8.02 (m, 1H). $^{13}$C NMR ($CDCl_3$): δ 168.0, 165.2, 164.1, 140.4, 135.0, 132.4, 129.1, 128.7, 127.3, 127.0, 125.7, 123.7, 120.6, 49.7, 38.2, 27.1, 19.9, 13.5. HRMS (ESI): Calcd for $C_{20}H_{19}N_3O_2SNa$, m/z $[M+Na]^+$:388.1096; found 388.1111.

***2-[2-m-Fluorophenyl-1-(2-m-chlorophenyl-1,3,4-oxadiazol-5-yl)ethyl]-1,2-benzisothiazol-3(2H)-one (7w):*** Yellow oil (29% yield). $^1$H NMR ($CDCl_3$): δ 3.56 (dd, J = 12.4, 9.1 Hz, 1H), 3.80 (dd, J = 12.4, 9.1 Hz, 1H), 6.51 (dd, *J* = 8.9, 6.8 Hz, 1H), 6.85-8.05 (m, 12H). $^{13}$C NMR ($CDCl_3$): δ 165.3, 164.6, 164.4, 164.0, 140.3, 137.3, 135.2, 132.2, 130.8, 130.4, 130.0, 127.1, 125.9, 125.2, 124.8, 123.5, 120.7, 116.4, 116.1, 114.6, 114.4, 49.6, 37.8. HRMS (ESI): Calcd for $C_{23}H_{16}N_3O_2SClF$, m/z $[M+H]^+$: 452.0636, found 452.0637.

***2-[3-Phenyl-1-(2-m-chlorophenyl-1,3,4-oxadiazol-5-yl)propyl]-1,2-benzisothiazol-3(2H)-one (7x):*** Yellow oil (31% yield). $^1$H NMR ($CDCl_3$): δ 2.60-2.82 (m, 4H), 6.21-6.27 (m, 1H), 7.18-8.11 (m, 13H). $^{13}$C NMR ($CDCl_3$): δ 165.7, 164.7, 164.6, 140.7, 139.7, 135.3, 132.8, 132.3, 130.6, 128.8, 128.7, 127.3, 127.2, 126.7, 126.1, 125.4, 125.1,

123.9, 120.9, 48.4, 34.1, 32.0. HRMS (ESI): Calcd for $C_{24}H_{19}N_3O_2SCl$, m/z $[M+H]^+$: 448.0887, found 448.0875.

### 3.3 X-Ray crystal analysis.

Compound ***7p*** crystallizes as colorless needles. The crystal was affixed to a nylon cryoloop using oil (Paratone-n, Exxon) and mounted in the cold stream of a Bruker Kappa-Apex-II area-detector diffractometer. The temperature of the crystal was maintained at 150 K using a Cryostream 700EX Cooler (Oxford Cryosystems). Data were measured with a redundancy using a CCD detector at a distance of 50 mm from the crystal with a combination of phi and omega scans. A scan width of 0.5 degrees and scan time of 10 seconds was employed using graphite monochromated Molybdenum Kα radiation (λ= 0.71073 Å) that was collimated to a 0.6 mm diameter. Data collection, reduction, structure solution, and refinement were performed using the Bruker Apex2 suite (v2.0-2) [97]. All available reflections to $2\theta_{max}$ = 52° were harvested (35207 reflections, 3812 unique) and corrected for Lorentz and polarization factors with Bruker SAINT (v6.45) [98]. Reflections were then corrected for absorption (numerical correction, μ=0.222 $mm^{-1}$), interframe scaling, and other systematic errors with SADABS 2004/1 [99]. The structure was solved (direct methods) and refined (full-matrix least-squares against $F^2$) with the Bruker SHELXTL package (v6.14-1) [100]. All non-hydrogen atoms were refined using anisotropic thermal parameters. All hydrogen atoms were included at idealized positions; hydrogen atoms were not refined. Absolute stereochemistry was assigned based on the synthetic protocol and confirmed by a Flack

parameter of 0.02. Pertinent crystal, data collection, and refinement parameters are given in Table 2.2.

**Table 3.2 X-ray data collection and processing parameters for compound 7p.**

| | |
|---|---|
| Molecular formula | $C_{22}H_{16}N_4O_2S$ |
| Formula weight | 400.45 |
| Diffractometer | Bruker Kappa Apex II |
| Radiation/λ (Å) | Mo Kα/0.71073 |
| Temperature (K) | 150 |
| Color/habit | colorless/ |
| Crystal size ($mm^3$) | 0.288 x 0.302 x 0.318 |
| Crystal system | Orthorhombic |
| Space group | $P2_12_12_1$ |
| *a* (Å) | 10.397(3) |
| *b* (Å) | 11.313(3) |
| *c* (Å) | 16.606(5) |
| V ($Å^3$) | 1953.1(10) |
| Z-value | 4 |
| $D_{calc}$ (g $cm^{-3}$) | 1.362 |
| Octants collected | ±*h*, ±*k*, ±*l* |
| Max. *h*, *k*, *l* | 12, 13, 20 |
| Θ range (°) | 3.60 to 25.99 |
| Absorption coefficient ($mm^{-1}$) | 0.192 |
| F(000) | 832 |
| Reflections/unique ($R_{int}$) | 35207/3812 (0.0405) |
| Observed (>2σ)/parameters | 3812 /262 |
| $R_{obs}/R_{all}$ | 0.0266/0.0307 |
| Goodness-of-fit | 1.030 |
| Absolute structure parameter | 0.02(5) |
| Largest diff. peak and hole ($e.Å^{-3}$) | 0.159-0.178 |

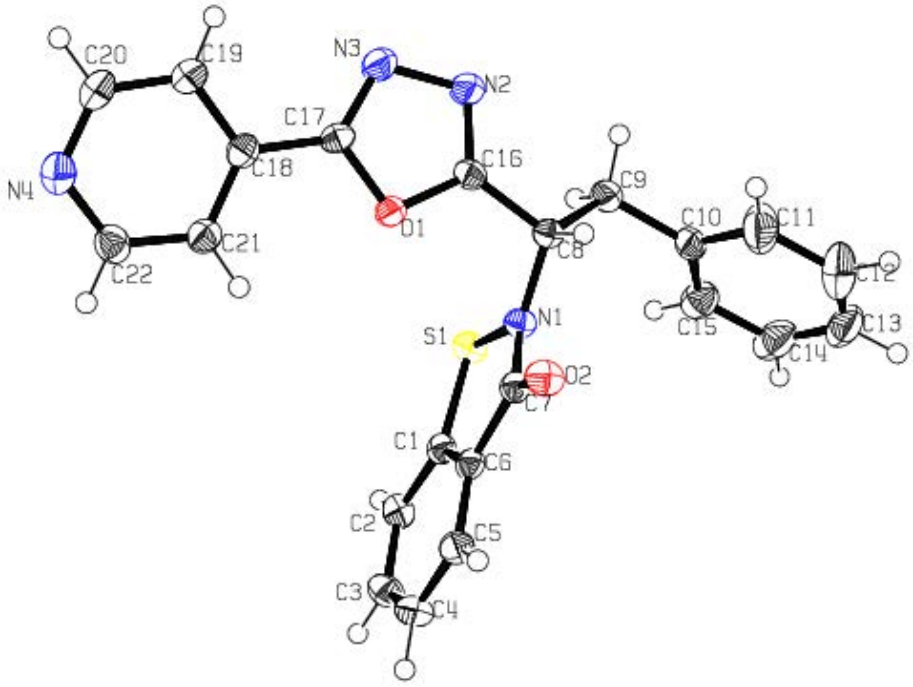


**Figure 3.2. ORTEP drawing of compound 7p showing the 30% thermal ellipsoids.** Hydrogen atoms have been omitted for clarity.

## 3.4 Biochemistry

### 3.4.1 In vitro DENV2 and WNV NS2B/NS3pro assays and inhibition studies.

Selected compounds **7a**-**7x** were analyzed by *in vitro* protease assays performed in opaque 96-well plates. Standard reaction mixtures (100 µL) containing 200 mM Tris·HCl (pH 9.5), 6 mM NaCl, 30 % glycerol, 25 nM DENV2 NS2B/NS3 protease, and 10 µM or 25 µM inhibitor (dissolved in DMSO) in each assay were incubated 15 min at 37 °C. Reactions were started by the addition of 5.0 µM tetra-peptide substrate Bz-Nle-Lys-Arg-Arg-AMC. Conditions were the same for WNV protease except 28 nM WNV NS2B/NS3pro was used in the assay.

Release of free AMC was measured using a spectrofluorometer (Molecular Devices) at excitation and emission wavelengths of 380 and 460 nm, respectively. Control fluorescence values obtained in the absence of inhibitor were taken as 100%, and those in the presence of inhibitors were calculated as the percentage of inhibition of the control using Microsoft Excel and plotted using SigmaPlot 2001 v7.1 (Systat Software Inc.). The background of AMC in the absence of protease was subtracted before the data analysis. All assays were performed in triplicate. Compounds with more than 50% percent inhibition at 25 µM were chosen to determine the $IC_{50}$ values. Twelve data points obtained from the range of 10 nM, 50 nM, 0.1, 0.5, 1, 2, 4, 6, 8, 10, 20, and 25 µM inhibitor concentrations of selected compounds were used. $IC_{50}$ values were calculated using the SigmaPlot 2001 v7.1 software.

**Table 3.3. Inhibition of DENV2 and WNV NS2B/NS3pro by compounds 7a-7x at 10 and 25 μM.**

| Inhibitor | DENV2 | | WNV | |
|---|---|---|---|---|
| | % inhibition at 10 μM | % inhibition at 25 μM | % inhibition at 10 μM | % inhibition at 25 μM |
| **7a** | 3.24 ± 0.93 | 9.11 ± 1.76 | 7.68 ± 0.98 | 10.07 ± 0.87 |
| **7b** | 5.21 ± 2.17 | 16.74 ± 1.97 | 6.15 ± 1.11 | 9.15 ± 0.79 |
| **7c** | 3.56 ± 1.09 | 16.43 ± 1.84 | 8.27 ± 1.37 | 14.73 ± 1.04 |
| **7d** | 5.27 ± 1.46 | 7.90 ± 1.94 | 5.96 ± 1.07 | 8.68 ± 0.95 |
| **7e** | 8.08 ± 1.56 | 17.82 ± 1.99 | 4.17 ± 0.63 | 9.79 ± 1.02 |
| **7f** | 22.38 ± 0.87 | 31.23 ± 1.23 | 20.54 ± 0.91 | 30.12 ± 1.02 |
| **7g** | 28.49 ± 1.82 | 38.64 ± 1.69 | 24.23 ± 0.61 | 34.86 ± 0.45 |
| **7h** | 39.03 ± 1.06 | 50.87 ± 1.55 | 30.36 ± 0.84 | 38.91 ± 0.61 |
| **7i** | 34.27 ± 2.07 | 42.12 ± 1.89 | 29.01 ± 0.75 | 43.11 ± 0.71 |
| **7j** | 60.34 ± 1.12 | 75.74 ± 1.95 | 51.12 ± 1.47 | 59.09 ± 1.35 |
| **7k** | 53.25 ± 1.64 | 70.52 ± 2.37 | 53.46 ± 1.27 | 63.24 ± 1.24 |
| **7l** | 63.86 ± 1.71 | 72.94 ± 1.24 | 63.57 ± 1.59 | 70.87 ± 1.32 |
| **7m** | 56.73 ± 0.95 | 69.24 ± 1.42 | 51.71 ± 1.16 | 64.09 ± 0.91 |
| **7n** | 65.49 ± 1.18 | 80.01 ± 1.73 | 68.58 ± 1.38 | 73.42 ± 1.22 |
| **7o** | 40.65 ± 1.79 | 61.27 ± 1.71 | 56.09 ± 1.18 | 71.84 ± 2.67 |
| **7p** | 62.43 ± 1.82 | 70.87 ± 1.27 | 63.13 ± 1.49 | 72.68 ± 0.88 |
| **7q** | 58.06 ± 1.55 | 69.97 ± 1.02 | 55.83 ± 1.32 | 62.52 ± 0.98 |
| **7r** | 52.28 ± 1.74 | 64.74 ± 1.51 | 44.32 ± 1.53 | 57.67 ± 1.02 |
| **7s** | 52.34 ± 2.23 | 69.81 ± 1.64 | 43.68 ± 1.36 | 59.66 ± 1.46 |
| **7t** | 19.98 ± 1.45 | 31.59 ± 1.37 | 22.32 ± 0.82 | 40.39 ± 2.19 |
| **7u** | 22.54 ± 1.55 | 34.22 ± 2.43 | 25.07 ± 1.75 | 44.26 ± 1.69 |
| **7v** | 25.58 ± 1.07 | 36.68 ± 1.91 | 34.94 ± 1.83 | 46.19 ± 2.25 |
| **7w** | 15.97 ± 1.72 | 31.61 ± 2.06 | 27.44 ± 0.59 | 35.65 ± 0.22 |
| **7x** | 26.06 ± 1.15 | 35.01 ± 2.21 | 23.86 ± 0.84 | 33.85 ± 0.54 |

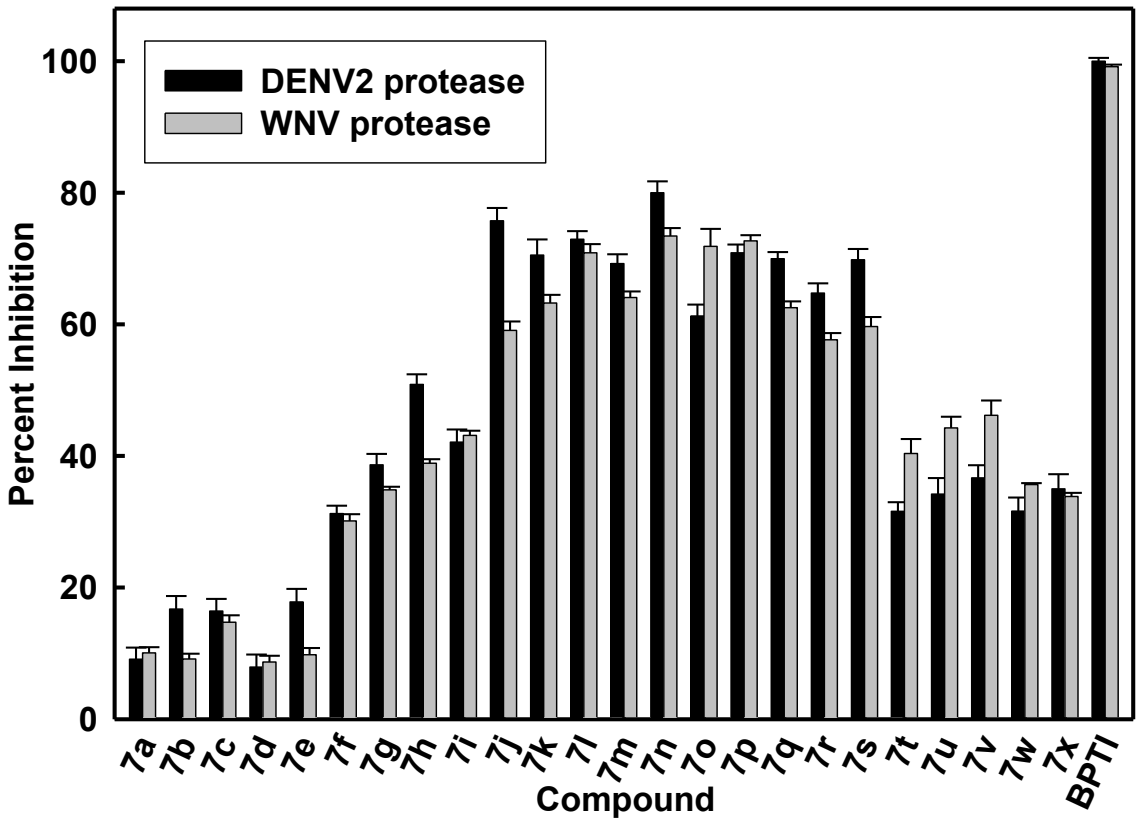


**Figure 3.3. Inhibition of DENV2 and WNV NS2B/NS3pro by selected compounds at 25 μM.** The concentrations of DENV2 and WNV proteases were 25 nM and 28 nM, respectively. Substrate concentration was 5.0 μM. The buffer used contained 200 mM Tris·HCl, 6.0 mM NaCl, 30 % glycerol, and 0.1% CHAPS, pH 9.5 and the reactions were run at 37°C. The percent values were calculated from the relative fluorescence units obtained in the presence and absence of tested compound. BPTI (Aprotinin) and DMSO were used as a positive and negative control, respectively. All assays were performed in triplicate and the average values are shown.

### 3.4.2 Steady-state kinetics analysis

The tetra-peptide Bz-Nle-Lys-Arg-Arg-AMC was used as the substrate for analyzing the solution kinetics of protease inhibition. Reaction progress was monitored by release of free AMC every 1.5 min for at least 10 min in 200 mM Tris·HCl (pH 9.5), 6 mM NaCl, 30 % glycerol containing 0.1% CHAPS at 37 ˚C unless otherwise specified. The tetra-peptide with an AMC tag was incubated with and without the inhibitor in the above buffer in the presence of varying concentrations of substrate. The reactions were initiated by the addition of NS2B/NS3 protease. The protease activity was monitored by the initial rates of the increase of fluorescence intensity at 460 nm with an excitation wavelength of 380 nm. All reactions were carried out to less than 5% completion. The results were analyzed using Sigma-plot 2001 v7.1 and the Michaelis-Menten equation to obtain the apparent Michaelis-Menten constants and maximal velocities. All assays were performed two times in duplicate. For each tested compound, four different concentrations of inhibitor (0, 1.0, 3.0 and 5.0 μM) were used at varying concentrations (0-50 μM) of substrate. The mechanism of inhibition was determined to be competitive by observing the deviation of the apparent $K_m$ while a relative constant $k_{cat}$ was maintained [101]. The kinetics analysis methods have been previously described [102]. $K_i$ values were calculated from these data using a secondary plot of $K_{m,\ app}$ against the concentrations of selected compound **7n** using SigmaPlot 2001 v7.0 software. The results are summarized in Figures 3.4 and 3.5, and Table 3.4.

**Table 3.4 Kinetic parameters for the tetra-peptide substrate and compound 7n against DENV2 NS2B/NS3pro at 37 ˚C.**

| ***7n*** (μM) | $K_{m,\,app}$ (μM) | $k_{cat}$ ($s^{-1}$) | $k_{cat}/K_m$ ($M^{-1}\cdot s^{-1}$) |
|---|---|---|---|
| 0 | 11.69 ± 0.41 | 0.064 ± 0.0008 | 5751 ± 275 |
| 1 | 17.59 ± 0.54 | 0.065 ± 0.0009 | 3879 ± 169 |
| 3 | 20.98 ± 1.05 | 0.0623 ± 0.0014 | 3176 ± 225 |
| 5 | 31.47 ± 3.25 | 0.062 ± 0.0034 | 2327 ± 349 |

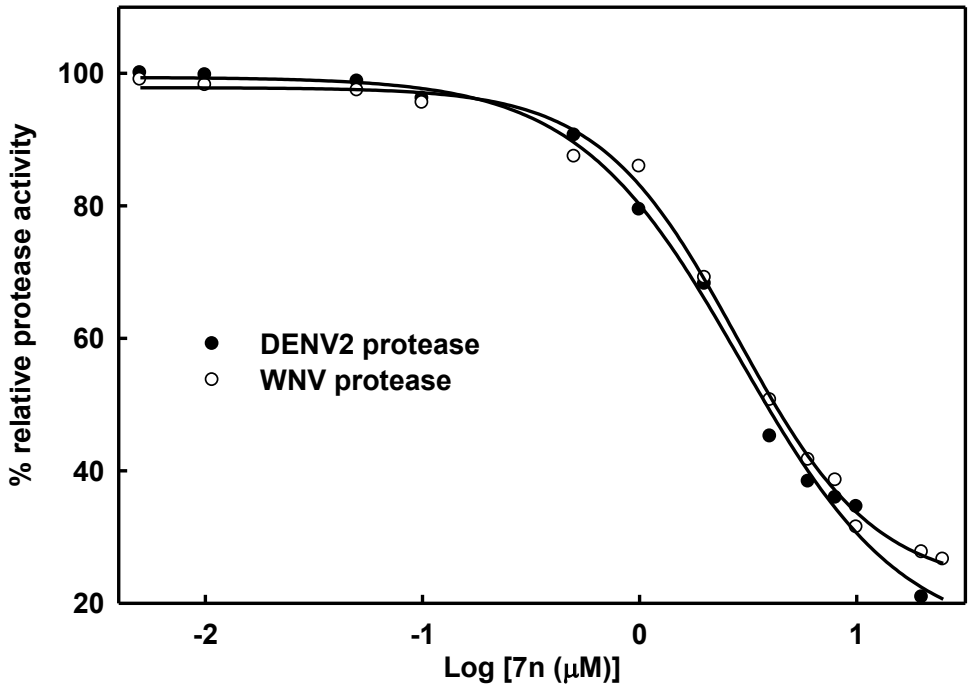


**Figure 3.4. Determination of $IC_{50}$ values of inhibitor 7n against DENV2 and WNV proteases.** Inhibitor ***7n*** was incubated with DENV2 NS2B/NS3pro (25 nM) or WNV NS2B/NS3pro (28 nM) in buffer (200 mM Tris·HCl, 6 mM NaCl and 30% glycerol, pH 9.5) for 15 min at 37°C. Bz-Nle-Lys-Arg-Arg-AMC (5.0 μM) was added to the mixture in a final volume of 100 μL. The fluorescence intensity was measured at 460 nm with excitation at 380 nm and converted to the percentage of protease activity in the absence and presence of inhibitors. The solid line is the theoretical fitting curve based on the Sigmoidal Equation. The apparent $IC_{50}$ values for compounds **7n** were 3.75 ± 0.06 and 4.22 ± 0.07 μM against DENV2 (solid circle) and WNV (open circle), respectively.

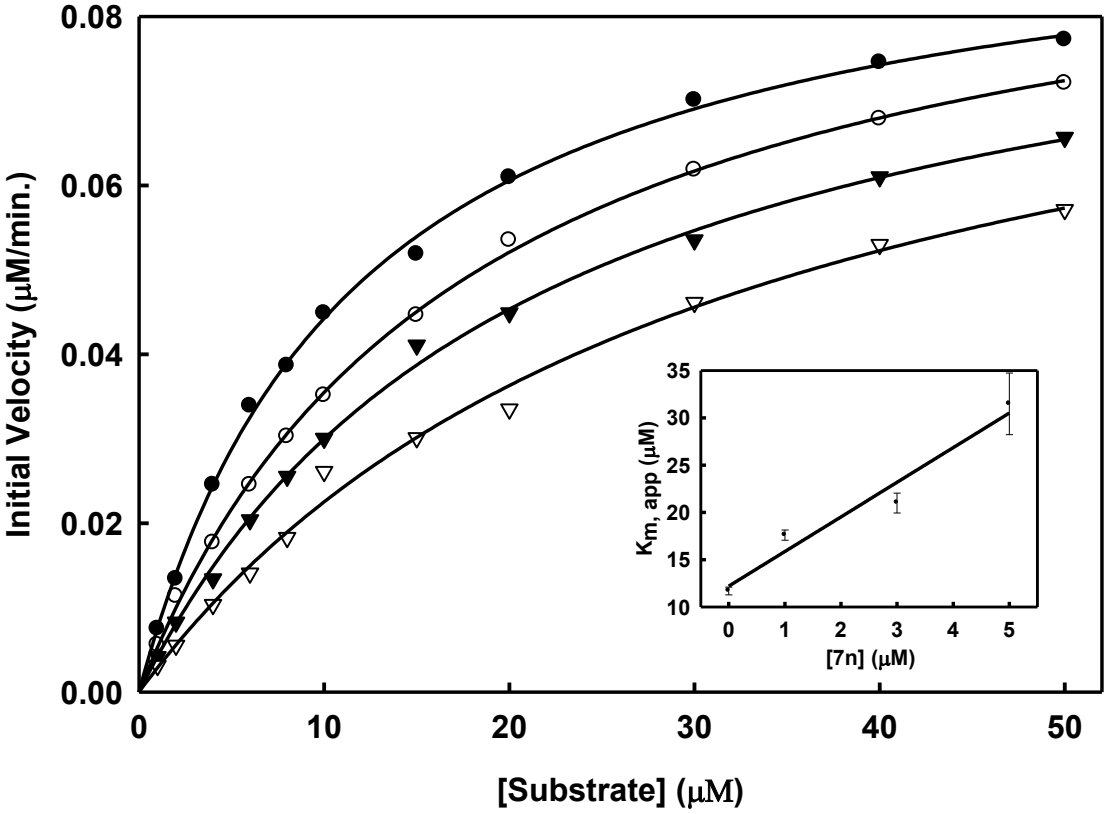


**Figure 3.5. Inhibition of DENV2 NS2B/NS3 protease activity by compound 7n.** Initial reaction rates of the substrate (Bz-Nle-Lys-Arg-Arg-AMC) cleavage catalyzed by DENV2 NS2B/NS3 protease (25 nM) in 200 mM Tris·HCl (pH 9.5), 6.0 mM NaCl, 30% glycerol and 0.1% CHAPS at 37 °C were determined by varying the substrate concentrations in the range of 0, 1, 2, 4, 6, 8, 10, 15, 20, 30, 40 and 50 μM at each concentration of inhibitor fixed at 0 (solid circle), 1.0 μM (open circle), 3.0 μM (solid triangle) and 5.0 μM (open triangle). The reactions were initiated by the addition of DENV2 NS2B/NS3 protease and the fluorescence intensity at 460 nm was monitored with an excitation at 380 nm. Reactions were less than 5% complete in all cases to maintain valid steady-state measurements. The solid lines are fitted lines using the Michaelis-Menten equation. Inset: Secondary plot of $K_{m,app}$ against the concentration of selected compound **7n**. Kinetics studies were carried out as described utilizing substrate concentrations of 0-50 μM Bz-Nle-Lys-Arg-Arg-AMC. Each experiment was performed in duplicate and repeated three times. Data were analyzed using SigmaPlot 2001 v7.0 software to determine values for apparent $K_m$ and $k_{cat}$.

## 3.5 Molecular Modeling

Molecular docking simulations were performed with the Vina program [103]. To describe the DENV2 NS2B/NS3 enzyme, modeling was performed on both the active form (PDB: 3U1I) [43] and on the structure with a co-crystallized substrate-based inhibitor (PDB: 2FOM) [41]. WNV NS2B/NS3pro was modeled via a structure (PDB: 2FP7) [41] analogous to the latter DENV model and via a more recent structure (PDB: 3E90) in complex with the Naph-KKR-H inhibitor [104]. In each case, the receptor model was prepared by extracting all ligands and waters, and protonating the receptor according to assumption of anionic aspartate and glutamate groups, and cationic arginines and lysines. The co-crystallized ligand from each crystal structure was used to define center of the grid space into which the ligand was docked. In each case, a cubic grid was defined with a buffer that extended 8.0 Å beyond the extent of the cocrystallized ligand. Ligand docking was then pursued by requesting a level-10 search, so as to achieve a reasonably comprehensive conformational sampling. All other Vina parameters were left at default values.

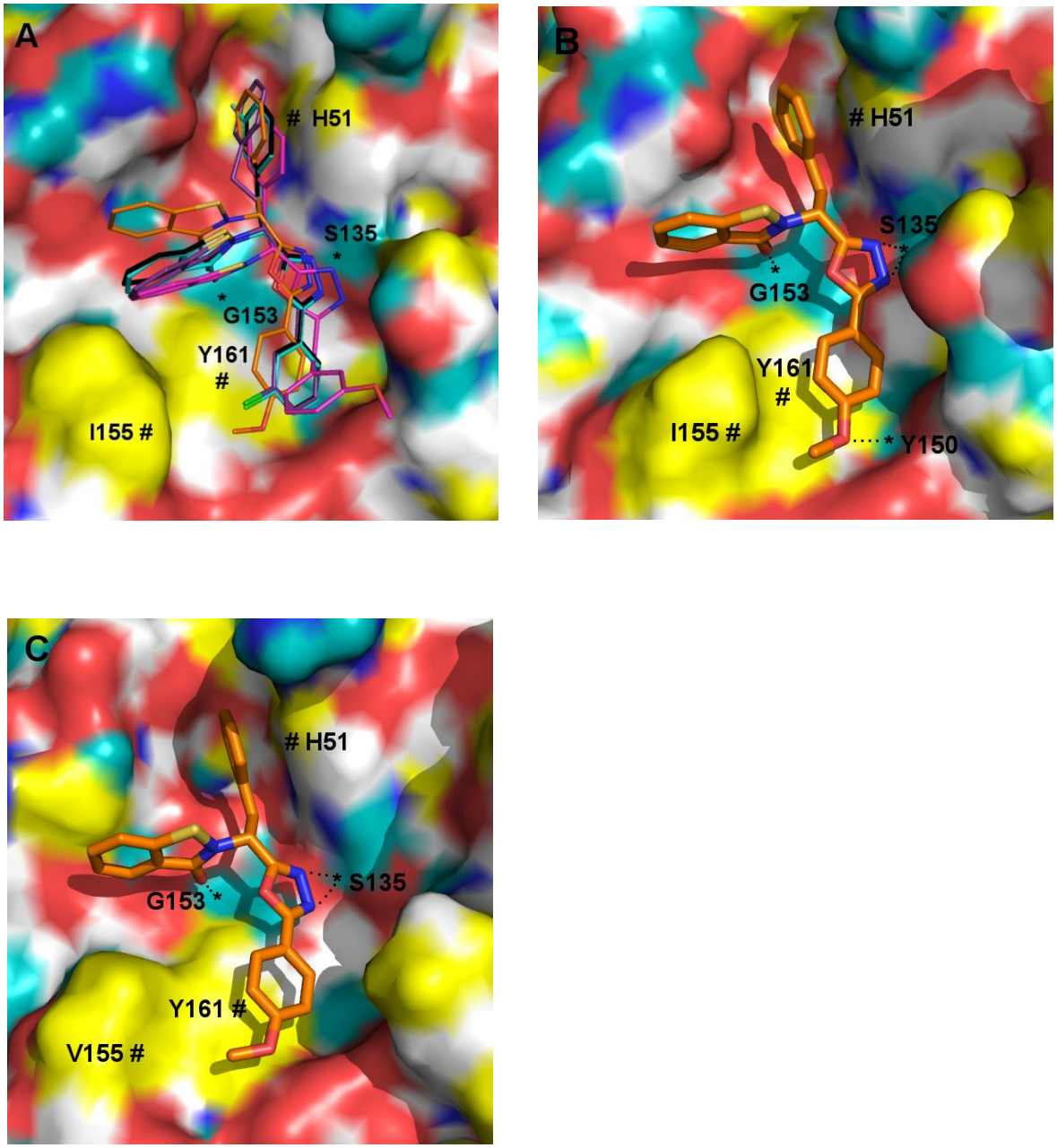


**Figure 3.6**. **Putative binding mode of selected compounds interacting with DENV2 (A and B) and WNV (C) proteases, as predicted by molecular modeling.** All compounds have CPK-colored heteroatoms, and are distinguished according to the color of their carbon atoms as follows: black = ***7i***, cyan = ***7w***, purple = ***7x***, magenta = ***7g*** and orange = ***7n***. The protease receptor surfaces are colored as follows: yellow = lipophilic, white = weakly polar, cyan = polar H, blue = polar N and red = polar O. Apparent H-bonding features of the receptor are marked with "*" and hydrophobic interactions with "#"

## 3.6 Results and Discussion

The armamentarium of antiviral therapeutics for the treatment of Dengue and West Nile virus infections is currently very limited; consequently, small-molecule anti-Dengue and anti-West Nile therapeutics are urgently needed. A series of structurally-diverse 1,2-benzisothiazol-3(2H)-one - 1,3,4-oxadiazole hybrid derivatives represented by general structure (I) (Figure 3.1) were synthesized and their activity against DENV2 and WNV NS2B/NS3 proteases investigated. The design of this series of inhibitors was based on the following considerations: (a) it was envisaged that an entity comprised of two heterocyclic scaffolds would provide multiple loci for hydrogen bond donor and/or acceptor interactions between the protease and inhibitors, leading to enhanced pharmacological activity. This approach was anticipated to be advantageous in the case of DENV2 NS2B/NS3pro because of its rather shallow active site; (b) molecular modeling using the known X-ray crystal structures of DENV2 NS2B/NS3pro [41, 43, 105] suggested that derivatives of (I) can be accommodated at the protease active site and, (c) linking the two heterocyclic scaffolds could potentially result in the creation of a novel entity that displays superior drug-like characteristics. Thus, the 1,2-benzisothiazoli-2(3H)-one-1,3,4-oxadiazole hybrid platform was chosen for generating a focused library of compounds and for conducting exploratory studies.

The desired compounds were readily obtained as shown in the synthetic scheme and the structure and stereochemistry of a representative member was established using X-ray crystallography (Figure 3.2). The compounds were subsequently screened against DENV2 NS2B/NS3pro and WNV NS2B/NS3pro. It is evident from Figure 3.3 and Table 3.3 that several derivatives of (I) are active against both proteases, with nine

out of twenty-four compounds exhibiting more than 50% inhibitory activity ([Inhibitor] = 10 μM). It can be generally inferred from the SAR studies that the nature of both $R^1$ and $R^2$ influences activity. Furthermore, $R^1$ exerts a more dominant effect on activity than $R^2$. Variation of $R^1$ while keeping $R^2$ constant reveals that inhibitory activity follows the order for $R^1$ benzyl > H, corresponding to **7i**, and **7b**, respectively. This hierarchy is further confirmed when $R^2$ is substituted with a *p*-methoxybenzyl group: benzyl is better than H (**7g** > **7d**). Similarly, when $R^2$ is a benzyl group, compound **7f** ($R^1$ = benzyl) is a better inhibitor than **7c** ($R^1$ = H). The inhibition studies indicate that highest inhibitory activity is manifested where $R^1$ is a benzyl group, while lowest inhibition is observed where $R^1$ is hydrogen. A direct comparison between ***7w*** and ***7x*** versus ***7i*** cannot be made because the former compounds were screened as racemic mixtures while the latter compound was screened as the pure (L) enantiomer.

One of the most potent compounds (compound **7n),** was chosen for further kinetics studies. The percent inhibition of compound **7n** ($R^1$ = benzyl and $R^2$ = *p*-methoxyphenyl) against both DENV2 and WNV proteases is higher than the rest of the compounds (Figure 3.3). The apparent $IC_{50}$ values of compound **7n** (Figure 3.4) against DENV2 and WNV proteases were determined to be 3.75 $\pm$ 0.06 and 4.22 $\pm$ 0.07 μM, respectively. We performed kinetics analysis to determine the $K_m$, $k_{cat}$ and $V_{max}$ values in the presence and absence of compound **7n** at four different concentrations (Figure 3.5 and Table 3.4). The apparent Michaelis-Menten constants ($K_{m,\ app}$) increased and $k_{cat}/K_m$ decreased proportionally with increasing concentration of compound **7n**. These results are supportive of a competitive mode of inhibition. The inhibition constant ($K_i$) of ***7n*** against DENV2 NS2B/NS3pro was determined to be 3.61 μM. Next, we employed

molecular modeling to identify a plausible binding mode for a series of compounds, including ***7n*** and analogs thereof, with the goal of identifying the binding domains of 1,2-benzisothiazol-3[2H]-one and 1,3,4-oxadiazole moieties as a basis for pharmacophore perception. In the case of DENV2 NS2B/NS3pro, we compared the distribution of docked conformers for compounds 7b, 7i, 7g, 7n, 7w and 7x within models produced from the 3U1I [43] and 2FOM [41] crystal structures to determine whether a consistent ligand binding mode was evident for either case. For the 3U1I receptor model, all compounds except 7b exhibited at least one predicted binding mode within the five top-scoring poses that satisfied both of the following two pharmacophore features: H-bond acceptance of the Gly 153 backbone amide proton by the 1,2-benzisothiazol-3(2H)-one O, and H-bond acceptance of the Ser 135 side chain hydroxyl proton by one or two nitrogens on the 1,3,4-oxadiazole ring. A similar binding mode was predicted for these compounds in docking to WNV NS2B/NS3pro with additional conservation of ligand hydrophobic interactions with His 51 and Tyr 161, however, no consistent binding mode was resolved within the manifold of top five poses of these ligands for the DENV2 NS2B/NS3pro model based on the 2FOM [41] crystal structure. For consistency of interpretation, we have thus chosen to focus on the docking poses generated for the 3U1I (DENV) [43], 3E90 (WNV) [104] and 2FP7 (WNV) [105] structure models.

In a preliminary sense, the docking results corroborate some general activity trends observed in the tested compounds. Variation of $R^1$ with constant $R^2$ (Figure 3.6A) suggests that the significant penalty incurred by absence of a hydrophobic $R^1$ group (compound ***7b***) likely arises from lost hydrophobic interactions which our model suggests as arising for DENV2 NS2B/NS3pro from contact with His 51, resulting in a

failure to dock to the receptor in a pose analogous to those of other more potent inhibitors. A benzyl $R^1$ group as per compound ***7i***, appears to fit well in this hydrophobic pocket, whereas the larger fluorobenzyl (***7w***) and phenethyl (***7x***) groups, while not sterically forbidden, may incur a marginal receptor desolvation penalty by protruding into a more polar region of the cavity. Variation of $R^2$ (Figure 3.6B) suggests that, relative to benzyl analogs, the substituted phenyl groups in our library achieve a marginally better steric fit within the cavity around Tyr 161 and Val/Ile 155 for DENV2/WNV, respectively, which could explain a binding preference for the latter compounds. The *p*-methoxy group located on the phenyl group of 7n seems to possess an excellent steric fit for this cavity, which may help to explain the strong potency of this compound. Furthermore, the 7n pose solved for the 3U1I [43] crystal structure (Figure 3.6B) suggests the possibility that the methoxy group may serve as a H-acceptor for the receptor hydroxy proton on Tyr 150, although this is not corroborated by the other crystal structures.

## 3.7 Conclusion

In summary, we have synthesized a focused library of 1,2-benzisothiazol-3(2H)-one – 1,3,4-oxadiazole hybrid derivatives and have investigated their inhibitory activity against DENV2 NS2B/NS3pro and WNV NS2B/NS3pro. Several members of this series of compounds were found to inhibit the two enzymes, and a low micromolar inhibitor capable of inhibiting both enzymes has been identified. Importantly, biochemical studies indicate that the compounds act as competitive inhibitors. Furthermore, the interaction of the compounds with the two enzymes was probed using molecular graphics and modeling and a mode of binding that is congruent with the

results of SAR studies is proposed. The findings reported herein have laid the groundwork for conducting hit-to-lead optimization studies [82, 106, 107] encompassing iterative medicinal chemistry, *in vitro* screening, and X-ray crystallography.

# REFERENCES

# REFERENCES


[1] Lindenbach, B. D.; Thiel, H-J.; Rice, C. M. in Fields Virology (Knipe, D. M. and Howley, P. M., eds), Volume 1, pp 1101-1152, Lippincott, Williams, and Wilkins, 5th ed., Philadelphia (2007).

[2] World Health Organization. Dengue: Guidelines for diagnosis, treatment, prevention and control. Available at: http://whqlibdoc.who.int/ publications/ 2009/9789241547871_eng.pdf. Accessed November 15, 2012.

[3] Guzman, M.G.; Halstead, S.B.; Artsob, H.; Buchy, P.; Farrar, J.; Gubler, D.J.; Hunsperger. E.; Kroeger, A.; Margolis, H.S.; Martinez, E.; Nathan, M.B.; Pelegrino, JL., Simmons, C.; Yoksan, S.; Peeling, R.W.; Dengue: a continuing global threat. *Nature Reviews Microbiology* **2010,** *8* (12), S7-S16.

[4] Tomlinson, S.M.; Malmstrom, R.D.; Watowich, S.J.; New Approaches to Structure-Based Discovery of Dengue Protease Inhibitors. *Infectious Disorders-Drug Targets* **2009,** *9* (3), 327-343.

[5] Melino, S.; Paci, M.; Progress for dengue virus diseases. Towards the NS2B-NS3pro inhibition for a therapeutic-based approach. *FEBS Journal* **2007**, *274* (12), 2986-3002.

[6] Cregar-Hernandez, L.; Jiao, G.; Johnson, A.T.; Lehrer, A.T.; Wong, T.A.S.; Margosiak, S.A.; Small molecule pan-dengue and West Nile virus NS3 protease inhibitors. *Antiviral Chemistry & Chemotherapy* **2011,** *21* (4), 209-218.

[7] Whitehorn, J.; Farrar, J.; Dengue. *British Medical Bulletin* **2010,** *95* (1), 161-173.

[8] Rossi, S.L.; Ross, T.M.; Evans, J.D.; West Nile Virus. *Clinics in Laboratory Medicine* **2010,** *30* (1), 47-65.

[9] Gubler, D.J.; The continuing spread of West Nile virus in the western hemisphere. *Clinical Infectious Diseases* **2007,** *45* (8), 1039-1046.

[10] West Nile Virus: Statistics. Available at: http://www.cdc.gov/ncidod/dvbid/westnile /surv&control_archive.htm. Accessed November 15, 2012.

[11] West Nile Virus Human Infections Reported to ArboNET, by State, United States, 2012. Available at: http://www.cdc.gov/ncidod/dvbid/westnile/surv&control Case Count12_detailed.htm. Accessed November 15, 2012.

[12] Geographic distribution of Dengue. Available at: http://www.healthmap.org/ dengue/index.php. Accessed November 15, 2012.

[13] Rajapakse, S.; Rodrigo, C.; Rajapakse, A.; Treatment of dengue fever. *Infection and Drug Resistance* **2012,** *5*, 103-112.

[14] The rising incidence of dengue. Available at: http://www.who.int/csr/disease/dengue/impact/en/. Accessed November 15, 2012.

[15] Dow, G.; Mora, E.; The maximum potential market for dengue drugs V 1.0. *Antiviral Research* **2012,** *96* (2), 203-212.

[16] Chappell, K. J.; Stoermer, M. J.; Fairlie, D. P.; Young, P. R.; West Nile Virus NS2B/NS3 protease as an antiviral target. *Current Medicinal Chemistry* **2008,** *15* (27), 2771-2784.

[17] Petersen, L.R.; Marfin, A.A.; West Nile Virus: A Primer for the Clinician. *Annals of Internal Medicine* **2002,** *137* (3), 173-179.

[18] Gubler, D.J.; Dengue and Dengue Hemorrhagic Fever. *Clinical Microbiology Reviews* **1998,** *11* (3), 480-496.

[19] Ligon, B.L.; Dengue fever and dengue hemorrhagic fever: A review of the history, transmission, treatment, and prevention. *Seminars in Pediatric Infectious Diseases* **2005,** *16* (1), 60-65.

[20] Heinz, F.X.; Stiasny. K.; Flavivirus and flavivirus vaccines. *Vaccine* **2012,** *30* (29), 4301-4306.

[21] Ray, D.; Shi, P.; Recent Adavances in Flavivirus Antiviral Drug Discovery and Vaccine Development. *Recent Patents on Anti-Infective Drug Discovery* **2006,** *1* (1), 45-55.

[22] Dengue Virion. Available at: http://www.sciencecentric.com/images/ news/dengue_virus_1440_1440.jpg. Accessed November 15, 2012.

[23] Stevens, A.J.; Gahan, M.E.; Mahalingam, S.; Keller, P.A.; The Medicinal Chemistry of Dengue Fever. *Journal of Medicinal Chemistry* **2009**, *52* (24), 7911-7926.

[24] Sampath, A.; Padmanabhan, R.; Molecular targets for flavivirus drug discovery. *Antiviral Research* **2009**, *81* (1), 6-15.

[25] Mukhopadhyay, S.; Kuhn, R.J.; Rossmann, M.G.; A structural perspective of the flavivirus life cycle. *Nature Reviews Microbiology* **2005**, *3* (1), 13-22.

[26] Lescar, J.; Luo, D.; Xu, T.; Sampath, A.; Lim, S. P.; Canard, B.; Vasudevan, S. G.; Towards the design of antiviral inhibitors against flaviviruses: The case for the

multifunctional NS3 protein from Dengue virus as a target. *Antiviral Research* **2008**, *80* (2), 94-101.

[27] Botting, C.; Kuhn R.J.; Novel approaches to flavivirus drug discovery. *Expert Opinion on Drug Discovery* **2012,** *7* (5), 417–428.

[28] Tong, L.; Viral proteases. *Chemical Reviews* **2002,** *102* (12), 4609-4626.

[29] Anderson, J.; Schiffer, C.; Lee, S.; Swanstrom, R.; Viral protease inhibitors. *Handbook of Experimental Pharmacology* **2009,** *189*, 85-110.

[30] Lendeckel, U.; Hooper, N.M., Viral proteases and antiviral protease inhibitor therapy. *Proteases in biology and disease* **2009,** *8*, 1st Ed.

[31] Menendez-Arias, L.; Molecular basis of human immunodeficiency virus drug resistance: an update. *Antiviral Research* **2010,** *85* (1), 210-231.

[32] Soriano, V.; Madejon, A.; Vispo, E.; Labarga, P.; Garcia-Samaniego, J.; Martin-Carbonero, L.; Sheldon, J.; Bottecchia, M.; Tuma, P.; Barrerio, P.; Emerging drugs for hepatitis C. *Expert Opinion on Emerging Drugs* **2008,** *13* (1), 1-19.

[33] Mani, N.; Rao, B.G.; Kieffer, T.L.; Kwong, A.D.; Recent Progress in the Development of HCV Protease Inhibitors. *Antiviral Drug Strategies* **2011,** *de Clerq, E., Ed,* 307–328.

[34] Li, H.; Clum, S.; You, S.; Ebner, K.E.; Padmanabhan, R.; The Serine Protease and RNA-Stimulated Nucleoside Triphosphatase and RNA Helicase Functional Domains of Dengue Virus Type 2 NS3 Converge within a Region of 20 Amino Acids. *Journal of Virology* **1999,** 73 (4), 3108-3116.

[35] Wang, C..C.; Huang, Z.S.; Chiang, P.L.; Chen, C.T.; Wu, H.N.; Analysis of the nucleoside triphosphatase, RNA triphosphatase, and unwinding activities of the helicase domain of dengue virus NS3 protein. *FEBS Letters* **2009,** *583* (4), 691-696.

[36] Bartelma, G.; Padmanabhan, R.; Expression, Purification, and Characterization of the RNA 5′-Triphosphatase Activity of Dengue Virus Type 2 Nonstructural Protein 3. *Virology* **2002,** *299* (1), 122-132.

[37] Li, J.; L, S.P.; Beer, D.; Patel, V.; Wen, D.; Tumanut, C.; Tully, D.C.; Williams, J.A.; Jiricek, J.; Priestle, J.P.; Harris, J.L.; Vasudevan, S.G.; Functional Profiling of Recombinant NS3 Proteases from All Four Serotypes of Dengue Virus Using Tetrapeptide and Octapeptide Substrate Libraries. *Journal of Biological Chemistry* **2005,** *280* (31), 28766-28774.

[38] Yusof, R.; Clum, S.; Wetzel, M.; Murthy, H. M.; Padmanabhan, R.; Purified NS2B/NS3 serine protease of dengue virus type 2 exhibits cofactor NS2B

dependence for cleavage of substrates with dibasic amino acids in vitro. *Journal of Biological Chemistry* **2000**, *275* (14), 9963-9969.

[39] Niyomrattanakit, P.; Winoyanuwattikun, P.; Chanprapaph, S.; Angsuthanasombat, C.; Panyim, S.; Katzenmeier, G.; Identification of residues in the dengue virus type 2 NS2B cofactor that are critical for NS3 protease activation. *Journal of Virology* **2004**, *78* (24), 13708-13716.

[40] Wichapong, K.; Pianwanit, S.; Sippl, W.; Kokpol, S.; Homology modeling and molecular dynamics simulations of dengue virus NS2B/NS3 protease: insight into molecular interaction. *Journal of Molecular Recognition* **2010,** *23*, (3), 283-300.

[41] Erbel, P.; Schiering, N.; D'Arcy, A.; Renatus, M.; Kroemer, M.; Lim, S. P.; Yin, Z.; Keller, T. H.; Vasudevan, S. G.; Hommel, U.; Structural basis for the activation of flaviviral NS3 proteases from dengue and West Nile virus. *Nature Structural & Molecular Biology* **2006**, *13* (4), 372-373.

[42] Aleshin, A. E.; Shiryaev, S. A.; Strongin, A. Y.; Liddington, R. C.; Structural evidence for regulation and specificity of flaviviral proteases and evolution of the Flaviviridae fold. *Protein Science* **2007,** *16* (5), 795-806.

[43] Noble, C. G.; She, C. C.; Chao, A. T.; Shi, P.-Y.; Ligand-bound structures of the Dengue virus protease reveal the active conformation. *Journal of Virology* **2012**, *86* (1), 438-446.

[44] Noble, C.G.; Shi, P.; Structural biology of dengue virus enzymes: Towards rational design of therapeutics. *Antiviral Research* **2012,** *96* (2), 115-126.

[45] Schechter, I.; Berger, A.; On the size of the active site in proteases. I. Papain. Biochemical and Biophysical Research Communications 1967, 27 (2), 57-162.

[46] Chappell, K.J.; Stoermer, M.J.; Fairlie, D.P.; Young, P.R.; Insights to substrate binding and processing by West Nile virus NS3 protease through combined modeling, protease mutagenesis, and kinetic studies. *The Journal of Biological Chemistry* **2006,** *281* (50), 38448-38458.

[47] Hedstrom, L.; Serine protease mechanism and specificity. *Chemical Reviews* **2002,** *102* (12), 4501-4523.

[48] Voet, D.; Voet, J.G. *Biochemistry* **2010,** 4th Ed.

[49] Sampath, A.; Xu, T.; Chao, A.; Luo, D.; Lescar, J.; Vasudevan, S. G. Structure-Based Mutational Analysis of the NS3 Helicase from Dengue Virus. *Journal of Virology* **2006**, *80* (13), 6686-6690.

[50] Kwong, A. D.; Rao, B. G.; Jeang, K. –T. Viral and cellular RNA helicases as antiviral targets. *Nature Reviews Drug Discovery* **2005**, *4* (10), 845-853.

[51] Lim, S. P.; Sonntag, L.S.; Noble, C.; Nilar, S. H.; Ng, R. H.; Zou, G.; Monaghan, P.; Chung, K. Y.; Dong, H.; Liu, B.; Bodenreider, C.; Lee, G.; Ding, M.; Chan, W. L.; Wang, G.; Jian, Y. L.; Chao, A. T.; Lescar, J.; Yin, Z.; Vedananda, T. R.; Keller, T. H.; Shi, P. Y. Small molecule inhibitors that selectively block Dengue virus methyltransferase. *Journal of Biological Chemistry* **2011**, *286* (8), 6233-6240.

[52] Podvinec, M.; Lim, S. P.; Schmidt, T.; Scarsi, M.; Wen, D.; Sonntag, L. S.; Sanschagrin, P.; Shenkin, P. S.; Schwede, T. Novel inhibitors of Dengue virus methyltransferase: discovery by in vitro-driven virtual screening on a desktop computer grid. *Journal of Medicinal Chemistry* **2010**, *53* (4), 1483-1495.

[53] Puig-Basagoiti, F.; Qing, M.; Dong, H.; Zhang, B.; Zou, G.; Yuan, Z.; Shi, P. Y. Identification and characterization of inhibitors of West Nile virus. *Antiviral Research* **2009**, *83* (1), 71-79.

[54] Mueller, N. H.; Pattabiraman, N.; Ansarah-Sobrinho, C.; Viswanathan, P.; Pierson, T. C.; Padmanabhan, R. Identification and biochemical characterization of small-molecule inhibitors of West Nile virus serine protease by a high-throughput screen. *Antimicrobial Agents and Chemotherapy* **2008,** *52* (9), 3385-3393.

[55] Mueller, N. H.; Yon, C.; Ganesh, V. K.; Padmanabhan, R. Characterization of the West Nile virus protease substrate specificity and inhibitors. *International Journal of Biochemistry & Cell Biology* **2007**, *39* (3), 606-614.

[56] Dou, D.; Viswanathan, P.; Li, Y.; He, G.; Alliston, K. R.; Lushington, G. H.; Brown-Clay, J. D.; Padmanabhan, R.; Groutas, W. C. Design, synthesis, and in vitro evaluation of potential West Nile virus inhibitors based on the 1-oxo-1,2,3,4-tetrahydroisoquinoline and 1-oxo-1,2-dihydroisoquinoline scaffolds. *Journal of Combinatorial Chemistry* **2010**, *12* (6), 836-843.

[57] Tiew, K. C.; Dou, D.; Teramoto, T.; Lai, H.; Alliston, K. R.; Lushington, G. H.; Padmanabhan, R.; Groutas, W. C. Inhibition of Dengue virus and West Nile virus proteases by click chemistry-derived benz[d]isothiazol-3(2H)-one derivatives. *Bioorganic &. Medicinal Chemistry* **2012,** *20* (3), 1213-1221.

[58] Aravapalli, S.; Lai, H.; Teramoto, T.; Alliston, K. R.; Ferguson, E. L.; Padmanabhan, R.; Groutas, W. C. Inhibitors of Dengue virus and West Nile virus proteases based on the aminobenzamide scaffold. *Bioorganic & Medicinal Chemistry* **2012,** *20* (13), 4140-4148.

[59] Chen, Y.-L.; Yin, Z.; Duraiswamy, J.; Schul, W.; Lim, C. C.; Liu, B.; Xu, H. Y.; Qing, M.; Yip, A.; Wang, G.; Chan, W. L.; Tan, H. P.; Lo, M.; Liung, S.; Kondreddi, R. R.; Rao, R.; Gu, H.; He, H.; Keller, T. H.; Shi, P.-Y. Inhibition of Dengue Virus RNA synthesis by an adenosine nucleoside. *Antimicrobial Agents & Chemotherapy* **2010**, *54* (7), 2932-2939.

[60] Torrence, P. F.; Gupta, N.; Whitney, C.; Morrey, J. D. Evaluation of synthetic oligonucleotides as inhibitors of West Nile virus replication. *Antiviral Res.* **2006**, *70* (2), 60-65.

[61] Yang, C. C.; Hsieh, Y. C.; Lee, S. J.; Wu, S. H.; Liao, C. L.; Tsao, C. H.; Chao, Y. S.; Chern, J. H.; Wu, C. P.; Yueh, A. Novel Dengue virus-specific NS2B/NS3 protease inhibitor, BP2109, discovered by a high-throughput screening assay. *Antimicrobial Agents and Chemotherapy* **2011**, *55* (1), 229-238.

[62] Tomlinson, S. M.; Malmstrom, R. D.; Russo, A.; Mueller, N.; Pang, Y.-P.; Watowich, S. J. Structure-based discovery of Dengue virus protease inhibitors. *Antiviral Research* **2009** *82*, (3), 10-114.

[63] Julander, J. G.; Perry, S. T.; Shresta, S. Important advances in the field of anti-dengue virus research. *Antiviral Chemistry & Chemotherapy* **2011**, *21*, 105-116.

[64] Noble, C.G.; Chen, Y.; Dong, H.; Gu, F.; Lim, S.P.; Schul, W.; Wang, Q.; Shi, P.; Strategies for development of dengue virus inhibitors. *Antiviral Research* **2010,** *85* (3), 450-462.

[65] Lim, H.A.; Joy, J.; Hill, J.; Chia, C.S.B.; Novel agmatine and agmatine-like peptidomimetic inhibitors of the West Nile virus NS2B/NS3 serine protease. *European Journal of Medicinal Chemistry* **2011,** *46* (7), 3130-3134.

[66] Schuller, A; Yin, Z.; Chia, B. C. S.; Doan, D. N. P.; Kim, H-K.; Shang, L.; Loh, T. P.; Hill, J.; Vasudevan, S. G.; Tripeptide inhibitors of dengue and West Nile virus NS2B–NS3 protease. *Antiviral Research* **2011**, *92* (1) 96-101.

[67] Yin, Z.; Patel, S. J.; Wang, W. L.; Wang, G.; Chan, W. L.; Rao, K. R.; Alam, J.; Jeyaraj, D. A.; Ngew, X.; Patel, V.; Beer, D.; Lim, S. P., Vasudevan, S. G.; Keller, T. H.; Peptide inhibitors of dengue virus NS3 protease. Part 1: Warhead. *Bioorganic & Medicinal Chemistry Letters* **2006**, *16* (1), 36-39.

[68] Yin, Z.; Patel, S. J.; Wang, W. L.; Chan, W. L.; Ranga Rao, K. R.; Ngew, X.; Patel, V.; Beer, D.; Knox, J. E.; Ma, N. L.; Ehrhardt, C.; Lim, S. P., Vasudevan, S. G.; Keller, T. H.; Peptide inhibitors of dengue virus NS3 protease. Part 2: SAR study of tetrapeptide aldehyde inhibitors. *Bioorganic & Medicinal Chemistry Letters* **2006**,*16* (1), 40-43.

[69] Knox, J. E.; Ma, N. L.; Yin, Z.; Patel, S. J.; Wang, W. L.; Wang, G.; Chan, W. L.; Vanga Rao, K. R.; Wang, G.; Ngew, X.; Patel, V.; Beer, D.; Lim, S. P.;

Vasudevan, S. G.; Keller, T. H.; Peptide inhibitors of West Nile NS3 protease: SAR study of tetrapeptide aldehyde inhibitors. *Journal of Medicinal Chemistry* **2006**, *49* (22), 6585-6590.

[70] Nitsche, C.; Behnam, M.A.M.; Steuer C.; Klein, C.D.; Retro peptide-hybrids as selective inhibitors of the Dengue virus NS2B-NS3 protease. *Antiviral Research* **2012,** *94* (1), 72-79.

[71] Bodenreider, C.; Beer, D.; Keller, T. H.; Sonntag, S.; Wen, D.; Yap, L.; Yau, Y. H.; Sochat, S. G.; Huang, D.; Zhou, T.; Caflisch, A.; Su, X-C.; Ozawa, K.; Otting, G.; Vasudevan, S. G.; Lescar, J.; Lim, S. P.; A fluorescence quenching assay to discriminate between specific and nonspecific inhibitors of dengue virus protease *Analytical Biochemistry* 2009, *395*, (2), 195-204.

[72] Nitsche, C.; Steuer, C.; Klein, C.D.; Arylcyanoacrylamides as inhibitors of the Dengue an West Nile virus proteases. *Bioorganic & Medicinal Chemistry* **2011**, *19* (24), 7318-7337.

[73] Tomlinson, S.M.; Watowich, S.J.; Anthracene-based inhibitors of dengue virus NS2B-NS3 protease. *Antiviral Research* **2011,** *89* (2), 127-135.

[74] Silverman, R.B. *The organic chemistry of enzyme catalyzed reactions* **2002,** 2nd Ed.

[75] Shen, J.; Woodward, R.; Kedenburg, J.P.; Liu, X.; Chen, M.; Fang, L.; Sun, D.; Wang, P. G.; Histone Deacetylase Inhibitors through Click Chemistry**.** *Journal of Medicinal Chemistry* **2008,** *51* (23), 7417-7427.

[76] Yon, C.; Teramoto, T.; Mueller, N.; Phelan, J.; Ganesh, V. K.; Murthy, K. H.; Padmanabhan, R. Modulation of the nucleoside triphosphatase/RNA helicase and 5'-RNA triphosphatase activities of Dengue virus type 2 nonstructural protein 3 (NS3) by interaction with NS5, the RNA –dependent RNA polymerase. *Journal of Biological Chemistry* **2005**, *280* (29), 27412-27419.

[77] Systat Software Inc., San Jose, CA.

[78] Jain, A. N. Surflex: fully automatic flexible molecular docking using a molecular similarity-based search engine. *Journal of Medicinal Chemistry* **2003,** *46* (4), 499-511.

[79] Lipinski, C. A.; Lombardo, F.; Dominy, B. W.; Feeney, P. J.; Experimental and computational approaches to estimate solubility and permeability in drug discovery and development settings. *Advanced Drug Delivery Reviews* **199**7, *23* (1-3), 3-25.

[80] Keller, T. H.; Pichota, A.; Yin, Z.; A practical view of 'druggability'. *Current Opinion in Chemical Biology* **200*6,*** *10*, (4), 357-361.

[81] Johnson, T. W.; Dress, K. R.; Edwards, M.; Using the Golden Triangle to optimize clearance and oral absorption. *Bioorganic & Medicinal Chemistry Letters* **2009,** *19* (19), 5560-5564.

[82] Perola, E.; An Analysis of the Binding Efficiencies of Drugs and Their Leads in Successful Drug Discovery Programs. *Journal of Medicinal Chemistry* **2010,** *53* (7), 2986-2997.

[83] Leeson, P. D.; Empfield, J. R.; Reducing the risk of drug attrition associated with physicochemical properties. *Annual Reports in Medicinal Chemistry* **2010,** *45*, 393-407.

[84] Walters, W. P.; Green, J.; Weiss, J. R.; Murcko, M. A.; What Do Medicinal Chemists Actually Make? A 50-Year Retrospective. *Journal of Medicinal Chemistry* **2011,** *54* (19), 6405-6416.

[85] Waring, M. J.; Lipophilicity in drug discovery. *Expert Opinion on Drug Discovery* **2010,** *5* (3), 235-248.

[86] Shroot, B. US patents 4,654,354 (March 3, 1987); 4,548,942 (Oct. 22, 1985); 4,512,985 (Apr. 23, 1985).

[87] Jorgensen, W. L.; Trofimov, A.; Du, X.; Hare, A. A.; Leng, L.; Bucala, R. Benzisothiazolones as modulators of macrophage migration inhibitory factor. *Bioorganic & Medicinal Chemistry Letters* **2011**, *21* (15), 4545-4549.

[88] Matuszak, N.; Saadi, B. E.; Labar, G.; Marchand-Brynaert, J.; Lambert, D. M. Benzisothiazolinone as a useful template for the design of new monoacylglycerol lipase inhibitors: Investigation of the target residues and comparision with octhilinone. *Bioorganic & Medicinal Chemistry Letters* **2011**, *21* (24), 7321-7324.

[89] Morini, G.; Poli, E.; Comini, M.; Menozzi, A.; Possoli, C. Benzisothiazoles and β-adrenoceptors: synthesis and pharmacological investigation of novel propanolamine and oxypropanolamine derivatives in isolated rat tissues. *Archives of Pharmacal Research* **2005**, *28* (12), 1317-1323.

[90] Mahmoud, A. H.; Abouzid, K. A. M.; El Ella, D. A. El R. A.; Ismail, M. A. H. Optimization of benzoisothiazole dioxide inhibitory activity of the NS5B polymerase HCV genotype 4 using ligand-steered homological modeling, reaction-driven scaffold-hopping and E-novo workflow. *Bioinformation* **2011**, *7* (7), 328-333.

[91] Matsunaga, H.; Matsui, T.; Ohya, K.; Okino, K.; Hayashida, K.; Maebayashi, K.; Kiriike, N.; Stein, D. J. A benzisothiazole derivative and antipsychotic agent, perospirone, for augmentation of selective serotonin reuptake inhibitors (SSRIs) in refractory obsessive-compulsive disorder (OCD): two patient case series. *International Journal of Psychiatry in Clinical Practice* **2006**, *10* (2), 142-145.

[92] Wright, S. W.; Petraitis, J. J.; Abelman, M. M.; Bostrom, L. L.; Corbett, R. L.; Green, A. M.; Kindt, R. M.; Sherk, S. R.; Magolda, R. L. Inhibition of cartilage breakdown by isothiazolones. *Bioorganic & Medicinal Chemistry Letters* **1993**, *3* (12), 2875-2878.

[93] Dou, D.; Alex, D.; Du, B.; Tiew, K.-C.; Aravapalli, S.; Mandadapu, S. R.; Calderone, R.; Groutas, W. C. Antifungal activity of a series of 1,2-benzisothiazol-3(2H)-one derivatives. *Bioorganic & Medicinal Chemistry* **2011**, *19* (19), 5782-5787.

[94] Bostrom, J.; Hogner, A.; Llinas, A.; Wellner, E.; Plowright, A. T. Oxadiazoles in medicinal chemistry. *Journal of Medicinal Chemistry* **2012**, *55* (5), 1817-1830.

[95] Zoumpoulakis, P.; Camoutsis, Ch.; Pairas, G.; Soković, M.; Glamočlija, J.; Potamitis, C.; Pitsas, A. Synthesis of novel sulfonamide-1,2,4-triazoles, 1,3,4-thiadiazoles and 1,3,4-oxadiazoles, as potential antibacterial and antifungal agents. Biological evaluation and conformational analysis studies. *Bioorganic & Medicinal Chemistry* **2012**, *20* (4), 1569-1583.

[96] Stabile, P.; Lamonica, A.; Ribecai, A.; Castoldi, D.; Guercio, G.; Curcuruto, O.; Mild and convenient one-pot synthesis of 1,3,4-oxadiazoles. *Tetrahedron Letters* **2010,** *51* (37), 4801-4805.

[97] APEX2 User Manual, Bruker AXS, Madison (USA), 2005.

[98] SAINT software reference manual, Version 4, Bruker AXS, Madison (USA), 1994-1996.

[99] Sheldrick, G., SADABS (Version 2.03), University of Göttingen, Germany, 2002.

[100] SHELXTL reference manual, Version 5.1, Bruker AXS, Madison (USA), 1997.

[101] Segel, I. H. Enzyme Kinetics, John Wiley & Sons, pp 104-107, NY (1993).

[102] Ezgimen, M.; Lai, H.; Mueller, N. H.; Lee, K.; Cuny, G.; Ostrov, D. A.; Padmanabhan, R.; Characterization of the 8-hydroxyquinoline scaffold for inhibitors of West Nile virus serine protease. *Antiviral Research* **2012**, *94* (1), 18-24.

[103] Trott, O.; Olson, J.; AutoDock Vina: Improving the speed and accuracy of docking with a new scoring function, efficient optimization, and multithreading. Journal of Computational Chemistry **2010**, *31* (2), 455-461.

[104] Robin, G; Chapell, K.; Stoermer, M. J.; Hu, S-H., Young, P. R.; Fairlie, D. P. Martin, J. L.; Structure of West Nile Virus NS3 Protease: Ligand Stabilization of the Catalytic Conformation *Journal of Molecular Biology* **2009**, *385* (5), 1568-1577.

[105] De la Cruz, L.; Nguyen, T. H.; Ozawa, K.; Shin, J.; Graham, B.; Huber, T.; Ottig, G.; Binding of Low Molecular Weight Inhibitors Promotes Large Conformational Changes in the Dengue Virus NS2B-NS3 Protease: Fold Analysis by Pseudocontact Shifts. *Journal of the American Chemical Society* **2011**, *133* (47), 19205-19215.

[106] Gillespie, P.; Goodnow, R.; The hit-to-lead process in drug discovery. *Annual Reports in Medicinal Chemistry* **2004,** *39*, 293-304.

[107] Meanwell, N. A.; Improving Drug Candidates by Design: A Focus on Physicochemical Properties As a Means of Improving Compound Disposition and Safety. *Chemical Research in Toxicology* **2011**, *24* (9), 1420-1456.